2007

Free liquid jets for high speed immunoassays

Jill Marie Uhlenkamp
Iowa State University

Free liquid jets for high speed immunoassays

by

Jill Marie Uhlenkamp

A dissertation submitted to the graduate faculty

in partial fulfillment of the requirements for the degree of

DOCTOR OF PHILOSOPHY

Major: Analytical Chemistry (Chemical Instrumentation)

Program of Study Committee:
Marc D. Porter, Major Professor
Patricia A. Thiel
Robert S. Houk
Edward S. Yeung
Scott Chumbley

Iowa State University

Ames, Iowa

2007

TABLE OF CONTENTS

ACKNOWLEDGEMENTS iv

ABSTRACT vii

CHAPTER 1: GENERAL INTRODUCTION 1

Dissertation Organization 1

Literature Review 2

References 13

CHAPTER 2: HIGH SPEED HETEROGENEOUS IMMUNOASSAYS USING A FREE LIQUID JET FOR SAMPLE AND LABEL DELIVERY 17

Abstract 17

Introduction 18

Experimental Section 21

Results and Discussion 24

Conclusions 30

Acknowledgements 31

References 31

Figure Captions 35

CHAPTER 3: SURFACE-ENHANCED RAMAN SCATTERING-BASED IMMUNOASSAY FOR OVALBUMIN WITH HIGH SPEED INCUBATIONS BY FREE LIQUID JET 46

Abstract 46

Introduction 47

Theoretical Considerations 49

Experimental Section 52

Results and Discussion 56

Conclusions 62

Acknowledgements 63

References 64

Figure Captions 68

CHAPTER 4: IMMUNOASSAY INCUBATION BY FREE LIQUID JET: EFFECT OF ANTIGEN AND LABEL SIZE 81
Abstract 81
Introduction 82
Experimental Section 84
Results and Discussion 88
Conclusions 92
Acknowledgements 93
References 94
Figure Captions 96
CHAPTER 5: LOW-LEVEL DETECTION OF SHED PROTEIN FROM PATHOGENIC BACTERIA WITH FREE LIQUID JET SAMPLE INCUBATION AND SERS READOUT 103
Abstract 103
Introduction 104
Experimental Section 106
Results and Discussion 109
Conclusions 114
Acknowledgements 115
References 115
Figure Captions 118
Supplemental Information 126
CHAPTER 6: CONCLUSIONS 129

ACKNOWLEDGEMENTS

A successful scientific journey cannot be a solitary one. There are many people who are owed my gratitude for supporting me on this journey. I'd like to first thank my advisor, Marc Porter. Thank you for your support during my time in your group and for the academic freedom that really fostered my love of research. Thank you, also, for forcing me to evaluate my priorities and what I wanted to achieve at a time when it was needed. Thank you to Drs. Patricia Thiel, R. Sam Houk, Edward Yeung, Surya Mallapragada, and Scott Chumbley for serving on my committee, currently or in the past, and for their continued support.

Every member of the Porter group, past and present, has contributed to my academic growth and for that, I thank you all. I would like to especially thank Bob Lipert for his never ending patience, for always having an open door, and for "volunteering" to look at the first passes of all my chapters. Thank you also to Rachel Millen, members of the Raman sub-group (Hye-Young Park, Jeremy Driskell, Karen Kwarta, Betsy Yakes, and Radha Narayanan), and Michael and Jennifer Granger, who have all added important insights and ideas to my research. Thank you, Rachel, for also being a great friend and a source of advice and encouragement. Jeremy, thank you for showing me the ropes in the early days. I also don't know what I would have done without your willingness to answer countless questions and provide feedback during my thesis writing. Thank you to April Hill for being a great office mate and for taking such good care of Sophie when we were out of town. Thanks to Rachel, Betsy, and John Nordling for always enabling my El Azteca addiction, and for the good conversation included with lunch. Special thanks to Betsy, Karen, and Chien-Ju

"Cherry" Shih, my partners in relocation. I'm so glad we got to bond over our shared experiences in the desert. Finally, thank you to Becky Staedtler for always having a kind word, the correct form, and basically all the answers.

I would be remiss not to acknowledge those who helped me get to graduate school in the first place. Thank you to Dr. Nancy Carpenter and Dr. James Togeas, my official and unofficial advisors at UMM, respectively, for laying the foundation I have built upon and for encouraging me to seek an advanced degree.

As in my academic life, my personal life includes many people who have contributed to my success. First, thank you to my incredible parents, Steven and Merrilee Oman, for your unending love and support. You have encouraged my love of learning and believed in me every step of the way. I also need to apologize for having lived at eight different addresses since I left home, but thank you for assisting in every one of the moves, most notably the two that involved July and Arizona. Also, thank you for trying to explain to family and friends exactly why I was still in school. Thank you to my friend and brother, Jason, for teaching me everything a big brother should, for your belief in me, and for taking from our parents the "good hair", leaving for me the "brains." I'm glad we are both happy with the arrangement. Thank you to the Uhlenkamps: Roger, Cindy, Ryan, Jess, and Amy, for welcoming me to the family and for forgiving me for taking Kyle so far away from you. I promise I will try to bring us back to the Midwest someday. Thank you also to my aunt, Sue Rantala, for the support through continued letters, gifts, and fun visits.

Lastly, and most importantly, thank you to my husband, Kyle. I thank you for: agreeing to move to Arizona, nursing me back to health when unnecessary organs failed or *E. coli* attacked, believing in me even when I didn't, cheering my successes, commiserating

over my failures, laughing with me, crying with me, laughing some more, loving me, taking care of me (especially these last few months), and being my best friend. I am so blessed to have you and I look forward to our future together. I love you and from now on I promise I'll bring my share of the household duties back up to 50%.

I dedicate this thesis, in loving memory, to my grandmother Virginia Taylor, my grandfather Gayle Oman, and my uncle Jeff Rantala, all lost to cancer. It is my sincere hope that advances in science and medicine eliminate the pain and suffering such as you endured in illness, and we, your loved ones, experienced in losing you.

ABSTRACT

This dissertation explores the use of free liquid jets for high speed immunoassays. Fluorescence and surface-enhanced Raman scattering (SERS) are employed for readout. A free liquid jet was first used to speed incubations in an assay for rabbit IgG with fluorescently-tagged anti-rabbit IgG as label. Theoretical underpinnings of this method are put forward to explain the basis for the dramatic reductions in sample and label incubation times through comparisons in surface accumulation. Immunoassay incubation by free liquid jet was extended to detect a simulant for biowarfare agents with SERS detection. The theoretical model of accumulation via quiet solution and free liquid jets is extended to account for the observations in sample capture and labeling efficiency therein. The SERS-based immunoassay with free liquid jet for sample delivery was also applied to detect porcine parvovirus (PPV), an analyte with larger size than those previously used. The successful capture of PPV through jet incubation led to a study of SERS label size and its effect on labeling by jet. Finally, extremely sensitive detection of pathogenic bacteria, *E. coli* O157:H7, was demonstrated by free liquid jet. The low levels of detection achieved in this assay were attributed to an enhancement mechanism in the way of detection of protein shed from the cells. This was supported by scanning electron microscopy (SEM), used to image the immunoassay substrate surface.

CHAPTER 1: GENERAL INTRODUCTION

Dissertation Organization

The widespread use of immunoassays for analyte detection in clinical and environmental settings fuels ongoing research to develop sensitive, specific, rapid, low cost, and high throughput methods. One serious limitation of heterogeneous assays is the long incubation times often required. This dissertation seeks to overcome this challenge via the investigation of free liquid jets as a new strategy for sample and label delivery.

This dissertation is organized into five sections. The first chapter gives an overview of immunoassay methods and readout schemes. It also includes a discussion of mass transport limitations and the resulting long analysis times, and techniques developed to overcome this limitation. Four original research chapters follow the introduction, each a separate manuscript to be submitted for publication.

Chapter 2 presents results of our first exploration of free liquid jet incubation in a sandwich immunoassay for rabbit IgG with fluorescence detection. This chapter includes the investigation of parameters affecting delivery of the antigen IgG and the fluorescently-tagged anti-IgG label, as well as a comparison to an assay employing quiet solution exposures of antigen and label.

Chapters 3-5 extend the use of free liquid jets in immunoassays to the detection of a biowarfare agent simulant and viral and bacterial pathogens, respectively. The work in Chapter 3 also replaces fluorescence readout with surface-enhanced Raman scattering (SERS) and assesses an alternative means to speeding incubation times for SERS-based gold nanoparticle labels.

Chapter 4 describes an assay for porcine parvovirus (PPV) with free liquid jet incubation and SERS readout. An examination of the effect of size on antigen capture and labeling is also presented. Several sizes of gold nanoparticles were used to construct SERS-based labels, and labeling of captured IgG protein by jet was conducted.

Chapter 5 reports on the detection of *E. coli* with a comparison between incubation employing quiet solution and free liquid jets. Evidence is presented for an enhancement mechanism in the form of detection of protein shed from the bacteria, which enables extremely low levels of detection.

A final chapter gives a summary of the work presented herein.

Literature Review

Immunoassay Overview.

Immunoassays, and more generally, biosensors, are used to detect the presence and/or determine the quantity or activity of analytes in a wide range of settings. Hospitals, wastewater treatment plants, and even patients at home routinely use biosensors to make these analytical measurments.[1] An ideal biosensor would incorporate such characteristics as selectivity, sensitivity, low cost, rapidity, and high throughput and would be easy to use and/or automated. Since the earliest reports on biosensors[2] and immunoassays[3] were made, an extremely vast array of biosensors has been developed. While the existing technologies each have their strengths and weaknesses, it should be recognized that few analyte detection schemes effectively integrates all of the aforementioned attributes.

Immunoassays are biosensors that rely on the specific interaction of an antibody and its target antigen. Antibodies are immunoglobulin (Ig) proteins made up of heavy and light polypeptide chains with molecular weights of ~53 kDa and ~22.5 kDa, respectively.[4, 5] The number of heavy and light chains divides the molecules into subclasses, and IgG, with two heavy and two light chains, are used throughout the research presented in subsequent chapters. The sequence of the first 110 residues (counting from the amino terminus of the chain) of each IgG molecule is referred to as the variable region, and it is this region which confers specificity for a target antigen.[4] The antigen-antibody "bond" is made up of electrostatic, hydrogen, hydrophobic, and Van der Waals interactions. Long range forces such as hydrogen bonds and electrostatic interactions contribute to the rate of complexation at the points of contact, while the short range forces impart bond strength that reduces dissociation. Dissociation constants for antibody-antigen binding are typically greater than 10^{-9} M.[5]

Immunoassays configurations can be broadly divided into two classes: competitive and noncompetitive. As illustrated in Figure 1A, competitive assays expose analyte along with labeled analyte as a tracer. Analyte and tracer compete for a limited number of antibody binding sites on the solid phase substrate. After washing the solid phase to remove unbound analyte and tracer, the signal from the tracer is measured, which is inversely proportional to analyte concentration. Variations on this theme include using an immobilized analyte to bind a labeled antibody that has not complexed with analyte in the sample, and employing a solid phase coated with anti-immunoglobulin to capture the specific antibody, bound to either free analyte or labeled analyte (tracer).

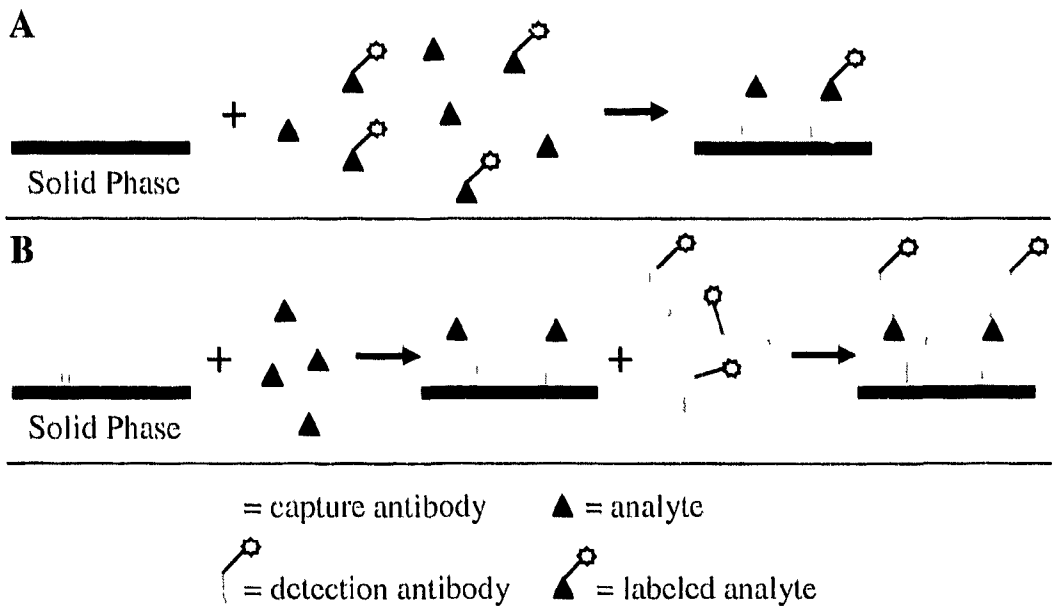

Figure 1. Schematic of (A) competitive and (B) noncompetitive immunoassays.

Noncompetitive (sandwich) assays (Figure 1B), use an antibody-coated substrate, which specifically captures analyte from the sample. After incubation and washing away the unbound analyte, labeled detection antibodies are introduced and complexed to captured analyte. The measured signal is proportional to the amount of analyte in the sample. While competitive assays have fewer steps and thus, are potentially faster than noncompetitive methods, the latter offers better specificity as it is unlikely that non-target entities will be both captured and labeled.

Similar general steps are employed in both types of assays. After immobilization of antibodies, typically by adsorption or covalent means, the remaining substrate surface is usually blocked by a solution containing proteins and/or detergents. This step limits nonspecific binding of analyte, label, and potential interfering species. The substrate is then exposed to sample for target analyte, or analyte and tracer, extraction in noncompetitive and

competitive assays, respectively. For sandwich assays, the final step exposes label to the captured analyte. Rinsing is performed following each step to remove remaining reactant.

Limitations to the use of antibodies as recognition elements in immunoassays include the loss biological activity upon surface immobilization.[6] Due to this, and the possibility that a portion of the antibodies are tethered to the surface in such a way that the antigen binding sites are unavailable, ~23% of surface-bound antibodies bind antigen from sample solution.[7] Also, the use of animals for production creates difficulty in developing antibodies against non-immunogenic species.[8] One way to overcome these challenges is through the use of aptamers, which are artificial nucleic acid sequences generated against analyte molecules. In Aptamers are isolated from libraries of multiple sequences by a technique of repeated cycles of adsorption, recovery, and amplification termed SELEX (systematic evolution of ligands by exponential enrichment). Aptamers, like antibodies, have high specificity and affinity, but offer several advantages over the latter. First, the use of animal production is eliminated and thus, aptamers against any type of molecule can potentially be developed. Moreover, aptamers can be synthesized with less variability than is sometimes observed from batch to batch in antibodies. Second, some antibodies can recognize targets only under physiological conditions, whereas aptamers can be selected under less restrictive conditions to offer more flexibility.[8]

Whether employing aptamers or antibodies, competitive or noncompetitive methods, immunoassays rely on a wide variety of readout methods. Long standing techniques include fluorescence, chemiluminescence, colorimetry, and electrometry.[5] Some of the more recently reported developments in readout include the use of quantum dots (QDs),[9-12] surface plasmon resonance (SPR),[13-16], giant magenetoresistance (GMR),[17-19] and surface-enhanced Raman

scattering (SERS).[20-29] SERS-based readout has been employed in our laboratory for the detection of IgG proteins, prostate specific antigen (PSA), and viral and bacterial pathogens.[22-24, 26, 30, 31] The theoretical origins of SERS are outlined below.

Surface-Enhanced Raman Scattering and SERS-based assays.

When light is incident on a molecule, scattering can occur. Most photons are scattered with no change in energy and this inelastic process is Rayleigh scattering. However, elastic scattering can occur when an incident photon excites an electron into a virtual state. If the electron relaxes to an electronic state with different energy from the original state, the gain or loss in energy results in Stokes and anti-Stokes scattering, respectively, with shifted frequency from that of the incident photon.[32] The evolution of Stokes and anti-Stokes lines is depicted in Figure 2.

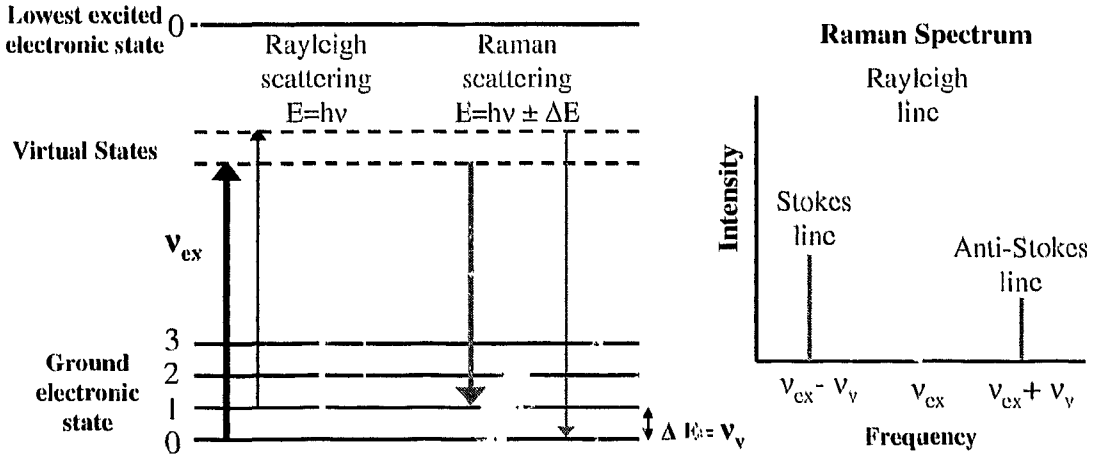

Figure 2. Photon origin of Raman scattering.

Raman scattering is an inherently weak process because, as mentioned above, most incident light is scattered inelastically. However, Fleischman and coworkers achieved Raman

intensities higher than those expected for pyridine adsorbed on silver electrodes,[33] and later Jeanmaire and Van Duyne[34] and Albrecht and Creighton[35] independently showed that the observation was not due increasing the number of adsorbates on the surface of the intentionally roughened electrodes. Jeanmaire and Van Duyne proposed that an increase in the electromagnetic field at the surface led to the enhancement.[34] While still debated today, electromagnetic enhancement is generally recognized as the major contributor to SERS, accounting for enhancements on the order of 10^5 to 10^6.[36, 37] Light incident on rough metal surfaces or small metal particles can generate a surface plasmon by exciting electrons in the conduction band. The particle or roughness feature becomes polarized and the electromagnetic field experienced by nearby molecules is much greater than that of the applied field. The magnitude of enhancement depends on the size and shape of the particle or feature and the incident wavelength.[36] A smaller contribution arises from charge transfer between the metal and adsorbate, resulting in 10- to 100-fold enhancements.[36, 38, 39]

SERS-based Immunoassay Detection.

SERS was incorporated into readout for immunoassays in our laboratory by the development of a sandwich assay employing gold nanoparticle-based labels, illustrated in Figure 3. This extrinsic Raman label, or ERL, consists of a gold nanoparticle, coated with a Raman reporter molecule (RRM). The RRM frequently used in our work is derived from 5,5'-dithiobis(succinimidyl-2-nitrobenzoate) (DSNB), shown in Figure 4.

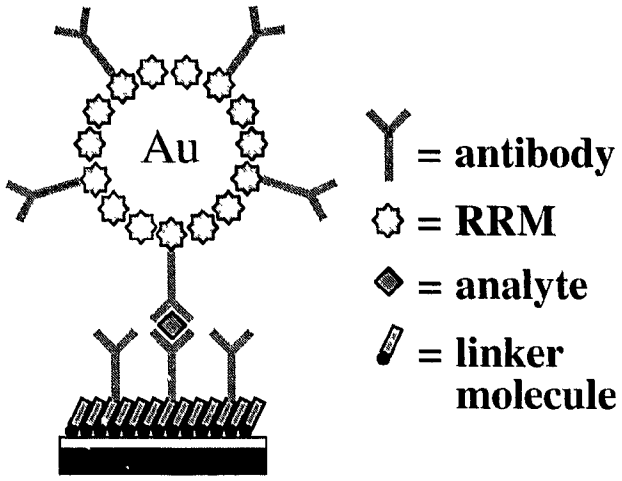

Figure 3. Extrinsic Raman Label (ERL).

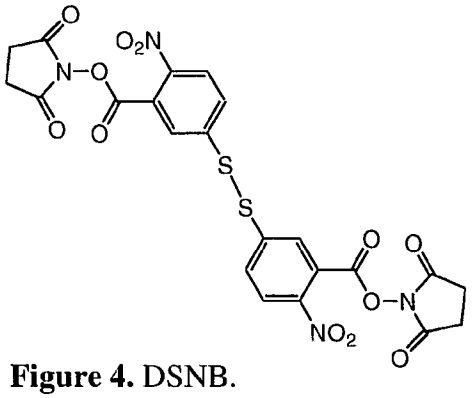

Figure 4. DSNB.

The DSNB-based adlayer provides strong Raman signals from its symmetric nitro stretch ($\nu_s(NO_2)$). It also chemisorbs to the gold nanoparticles via cleavage of the disulfide linkage and furthermore, covalently immobilizes antibodies via succinimidyl ester chemistry. Antibodies are immobilized on capture substrates through a similar reaction with the succinimidyl ester of a dithiobis(succinimidyl propionate) (DSP)-based monolayer on gold-coated glass slides. As described above, analyte and ERLs are exposed to the assay substrate

in successive steps and SERS readout is performed to quantify the concentration of analyte contained in the sample.

A sample spectrum, collected from an assay substrate with captured IgG labeled by DSNB-modified ERLs is given in Figure 5. Evident in the spectrum are characteristic features denoting the presence of DSNB. The most prominent of these is the $\nu_s(NO_2)$ at 1336 cm^{-1}. Other features include a nitro scissoring band at ~850 cm^{-1}, an aromatic ring mode at 1556 cm^{-1}, and the band at 1079 cm^{-1}, attributed to the overlap of an N-C-O stretch with an aromatic ring mode.[24] The intensity of the $\nu_s(NO_2)$ is proportional to the extent of ERL labeling, and therefore captured analyte. The intensity is measured from peak to base and is plotted against analyte concentration to give a dose-response curve.

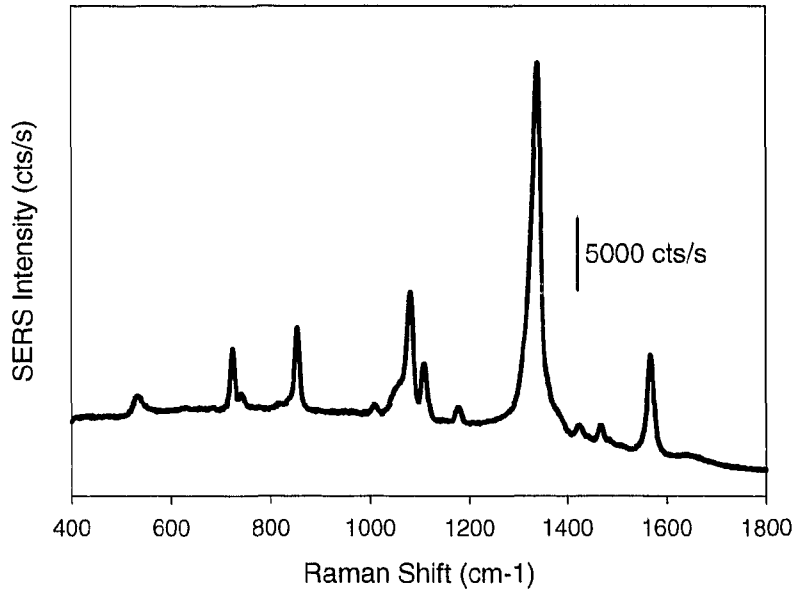

Figure 5. Representative SERS spectrum from 60-nm DSNB-based ERLs.

Overcoming long incubation times.

Immunoassays that rely on the diffusion-based delivery of analyte and label to a solid substrate often require long incubation times.[5, 40] This is exacerbated by the small diffusion

coefficients (e.g., 10^{-7} cm^2/s) of large analytes such as proteins, virus, and bacteria. Because antibody-antigen binding is often mass-transfer limited,[41-45] several approaches to overcome this limitation have been investigated.

The use of electric fields to drive charged species to substrates in microfluidic systems[46, 47] or on electronic chips[48] has resulted in total assay times of several minutes, but these methods must adjust for the differences in the charge and size of analytes and labels. Elevations in temperatures can increase diffusion coefficients and induce convection through thermal gradients, thereby shortening assay times.[30, 49, 50] However, this method can lead to decreases in binding constants, which may reduce sensitivity.

Another approach, developed in our laboratory,[23, 51] is based on rotating disk electrodes used in electrochemistry. Substrates are rotated in sample and label solutions, setting up an immobile layer of solution, or diffusion layer, at the surface. Analyte and label must diffuse through this layer to bind to their targets on the substrate.

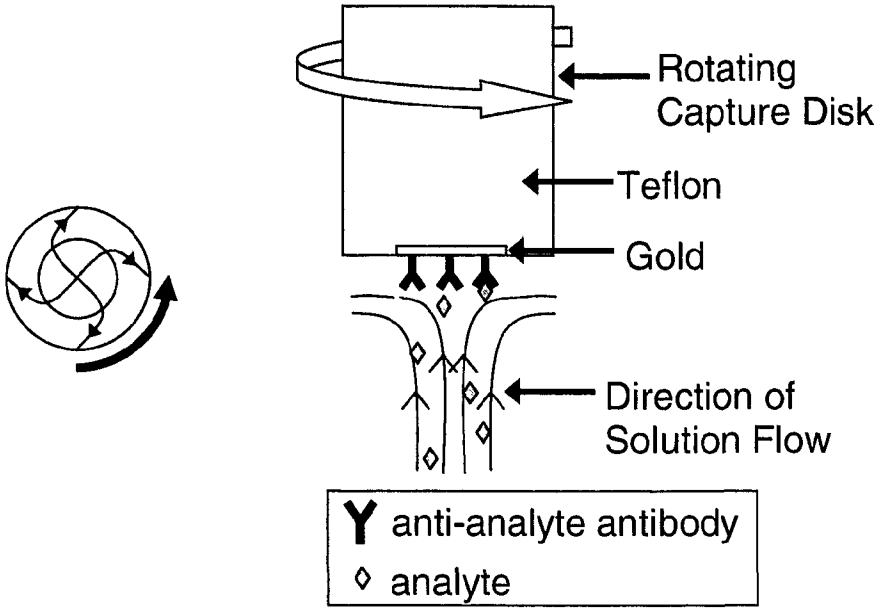

Figure 6. Capture substrate rotation for immunoassays (from reference 51).

The implementation of a rotated substrate is depicted in Figure 6. The successful incorporation of this technique in an assay for PPV with atomic force microscopy (AFM) readout resulted in a reduction in incubation time from 12 h to 10 min, with a 10-fold improvement in limit of detection when compared to an assay relying on diffusional mass transport.

Free liquid jets.

The work herein explores the use of free liquid jets for analyte and label delivery in a sandwich immunoassay. The term free liquid jet refers to a stream of liquid traveling through ambient gas. Free liquid jets were developed as a strategy to cool electronic devices. In 1986, a workshop was sponsored by the National Science Foundation to assess the need for improved techniques to meet increasing electronic cooling needs.[52] It was recognized that the trend in miniaturization of devices resulted in increased levels of power dissipation. Liquid jets are an attractive means to address this issue as large heat fluxes can be removed.[53] Since this time, liquid jets have also been employed for cooling of lasers and in metals and plastics manufacturing.[53-55]

When a jet impinges on a surface, a thin hydrodynamic boundary layer is formed. A free liquid jet and the resulting boundary layer are shown in Figure 7. The thickness of the diffusion layer depends on the thickness of the hydrodynamic layer created by the impinging jet.[56] In this way, diffusion layer thicknesses can be greatly decreased, increasing mass transport of species to the surface impinged by the jet. Submerged jets, directed through liquid, have been used to increase reactant mass transport in heterogeneous electron-transfer reactions.[57-59]

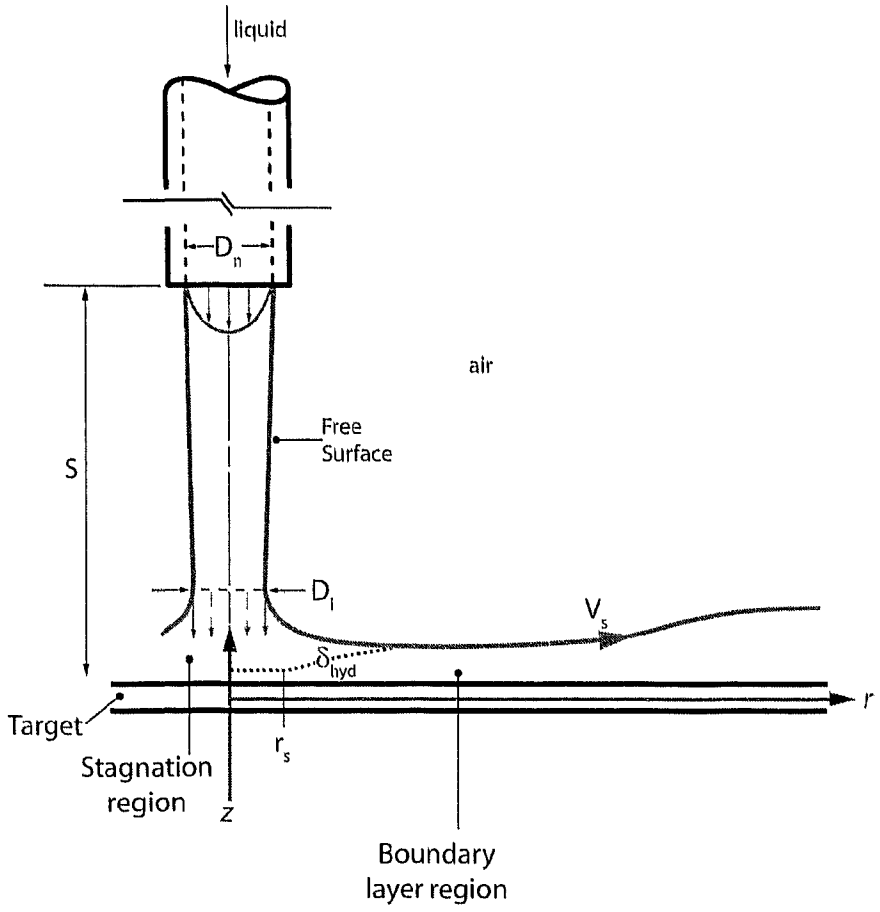

Figure 7. Schematic of a free liquid jet (from reference 52).

However, to the best of our knowledge, this dissertation describes the first use of jets for decreasing immunoassay incubation times by enhancing mass transport. This thesis reports on the detection of several classes of analytes: proteins, virus, and bacteria, via sample delivery with free liquid jet. Also, a theoretical basis for the ability to employ such rapid incubations is presented.

References

(1) D'Orazio, P. *Clin. Chim. Acta* 2003, *334*, 41-69.

(2) Clark Jr., L. C.; Lyons, C. *Ann. N Y Acad. Sci.* 1962, *102*, 29-45.

(3) Yalow, R. S.; Berson, S. A. *Nature* 1959, *184*, 1648-1649.

(4) DeLisi, C. *Antigen Antibody Interactions*; Springer-Verlag: New York, 1976.

(5) Diamandis, E. P.; Christopoulos, T. K. In *Immunoassay*; Diamandis, E. P., Christopoulos, T. K., Eds.; Academic Press: San Diego, CA, 1996, pp 1-3.

(6) Vikholm, I.; Albers, W. M. *Langmuir* 1998, *14*, 3865-3872.

(7) Dong, Y.; Shannon, C. *Anal. Chem.* 2000, *72*, 2371-2376.

(8) Van Emon, J. M. *Immunoassay and Other Bioanalytical Techniques*; CRC Press: Boca Raton, 2007.

(9) Chan, W. C. W.; Nie, S. *Science* 1998, *281*, 2016-2018.

(10) Goldman, E. R.; Clapp, A. R.; Anderson, G. P.; Uyeda, H. T.; Mauro, J. M.; Medintz, I. L.; Mattoussi, H. *Anal. Chem.* 2004, *76*, 684-688.

(11) Sun, B.; Xie, W.; Yi, G.; Chen, D.; Zhou, Y.; Cheng, J. *J. Immunol. Methods* 2001, *249*, 85-89.

(12) Tran, P. T.; Goldman, E. R.; Anderson, G. P.; Mauro, J. M.; Mattoussi, H. *Phys. Stat. Sol. B* 2002, *229*, 427-432.

(13) Lyon, L. A.; Musick, M. D.; Natan, M. J *Anal. Chem.* 1998, *70*, 5177-5183.

(14) Miyashita, M.; Shimada, T.; Miyagawa, H.; Akamatsu, M. *Anal. Bioanal. Chem.* 2005, *381*, 667-673.

(15) Nelson, B. P.; Grimsrud, T. E.; Liles, M. R.; Goodman, R. M.; Corn, R. M. *Anal. Chem.* 2001, *73*, 1-7.

(16) Smith, E. A.; Corn, R. M. *Appl. Spectrosc.* 2003, *57*, 320A-332A.

(17) Edelstein, R. L.; Tamanaha, C. R.; Sheehan, P. E.; Miller, M. M.; Baselt, D. R.; Whitman, L. J.; Colton, R. J. *Biosens. Bioelectron.* 2000, *14*, 805-813.

(18) Graham, D. L.; Ferreira, H. A.; Freitas, P. P.; Cabral, J. M. S. *Biosens. Bioelectron.* 2003, *18*, 483-488.

(19) Schotter, J.; Kamp, P. B.; Becker, A.; Puehler, A.; Brinkmann, D.; Schepper, W.; Brueckl, H.; Reiss, G. *IEEE Trans. Magn.* 2002, *38*, 3365-3367.

(20) Ansari, D. O.; Stuart, D. A.; Nie, S. *Proc. of SPIE* 2005, *5699*, 82-90.

(21) Dou, X.; Takama, T.; Yamaguchi, Y.; Yamamoto, H.; Ozaki, Y. *Anal. Chem.* 1997, *69*, 1492-1495.

(22) Driskell, J. D.; Kwarta, K. M.; Lipert, R. J.; Porter, M. D.; Neill, J. D.; Ridpath, J. F. *Anal. Chem.* 2005, *77*, 6147-6154.

(23) Driskell, J. D.; Uhlenkamp, J. M.; Lipert, R. J.; Porter, M. D. *Anal. Chem.* 2007, *79*, 4141-4148.

(24) Grubisha, D. S.; Lipert, R. J.; Park, H.-Y.; Driskell, J.; Porter, M. D. *Anal. Chem.* 2003, *75*, 5936-5943.

(25) Mulvaney, S. P.; Musick, M. D.; Keating, C. D.; Natan, M. J. *Langmuir* 2003, *19*, 4784-4790.

(26) Ni, J.; Lipert, R. J.; Dawson, G. B.; Porter, M. D. *Anal. Chem.* 1999, *71*, 4903-4908.

(27) Rohr, T. E.; Cotton, T.; Fan, N.; Tarcha, P. J. *Anal. Biochem.* 1989, *182*, 388-398.

(28) Xu, S.; Ji, X.; Xu, W.; Li, X.; Wang, L.; Bai, Y.; Zhao, B.; Ozaki, Y. *Analyst* 2004, *129*, 63-68.

(29) Zhang, C.; Zhang, Y.; Wang, S. *J. Agric. Food Chem.* 2006, *54*, 2502-2507.

(30) Kwarta, K. M., Iowa State University, Ames, 2007.

(31) Park, H.-Y.; Driskell, J. D.; Kwarta, K. M.; Lipert, R. J.; Porter, M. D.; Schoen, C.; Neill, J. D.; Ridpath, J. F. *Top. Appl. Phys.* 2006, *103*, 427-446.

(32) Ingle Jr., J. D.; Crouch, S. R. *Spectrochemical Analysis*; Prentice Hall: Upper Saddle River, NJ, 1988.

(33) Fleischmann, M.; Hendra, P. J.; McQuillan, A. J. *Chem. Phys. Lett.* 1974, *26*, 163-166.

(34) Jeanmaire, D. L.; VanDuyne, R. P. *J. Electroanal. Chem.* 1977, *84*, 1-20.

(35) Albrecht, M. G.; Creighton, J. A. *J. Am. Chem. Soc.* 1977, *99*, 5215-5217.

(36) Garrell, R. L. *Anal. Chem.* 1989, *61*, 401A-411A.

(37) Moskovits, M. *J. Chem. Phys.* 1978, *69*, 4159-4161.

(38) Otto, A.; Timper, J.; Billmann, J.; Kovacs, G.; Pockrand, I. *Surf. Sci.* 1980, *92*, L55-L57.

(39) Schatz, G. C. *Acc. Chem. Res.* 1984, *17*, 370-376.

(40) Ekins, R. P.; Chu, F. W. *Clin. Chem.* 1991, *37*, 1955-1967.

(41) Frackelton, A. R., Jr.; Weltman, J. K. *J. Immunol.* 1980, *124*, 2048-2054.

(42) Myszka, D. G.; Morton, T. A.; Doyle, M. L.; Chaiken, I. M. *Biophys. Chem.* 1997, *64*, 127-137.

(43) Nygren, H.; Kaartinen, M.; Stenberg, M. *J. Immunol. Methods* 1986, *92*, 219-225.

(44) Nygren, H.; Werthen, M.; Stenberg, M. *J. Immunol. Methods* 1987, *101*, 63-71.

(45) Stenberg, M.; Nygren, H. *J. Theor. Biol.* 1985, *113*, 589-597.

(46) Dodge, A.; Fluri, K.; Verpoorte, E.; de Rooij, N. F. *Anal. Chem.* 2001, *73*, 3400-3409.

(47) Hu, G.; Gao, Y.; Sherman, P. M.; Li, D. *Microfluid. Nanofluid.* 2005, *1*, 346-355.

(48) Ewalt, K. L.; Haigis, R. W.; Rooney, R.; Ackley, D.; Krihak, M. *Anal. Biochem.* 2001, *289*, 162-172.

(49) Bora, U.; Kannan, K.; Nahar, P. *J. Immunol. Methods* 2004, *293*, 43-50.

(50) Johnstone, R. W.; Andrew, S. M.; Hogarth, M. P.; Pietersz, G. A.; McKenzie, I. F. *Mol. Immunol.* 1990, *27*, 327-333.

(51) Driskell, J. D.; Kwarta, K. M.; Lipert, R. J.; Vorwald, A.; Neill, J. D.; Ridpath, J. F.; Porter, M. D. *J. Virol. Methods* 2006, *138*, 160-169.

(52) Incropera, F. P. *Liquid Cooling of Electronic Devices By Single-Phase Convection*; John Wiley & Sons, Inc.: New York, 1999.

(53) Lienhard, J. H. V. *Annu. Rev. Heat Transfer* 1995, *6*, 199-270.

(54) Baonga, J. B.; Louahlia-Gualous, H.; Imbert, M. *Appl. Therm. Eng.* 2006, *26*, 1125-1138.

(55) Fabbri, M.; Dhir, V. K. *J. Heat Transfer* 2005, *127*, 760-769.

(56) Levich, V. G. *Physicochemical Hydrodynamics*; Prentice-Hall: Englewood Cliffs, 1962.

(57) Gunasingham, H.; Fleet, B. *Anal. Chem.* 1983, *55*, 1409-1414.

(58) Huang, Y. L.; Khoo, S. B.; Yap, M. G. *Am. Biotechnol. Lab.* 1993, *11*, 18-20.

(59) Laevers, P.; Hubin, A.; Terryn, H.; Vereecken, J. *J. Appl. Electrochem.* 1995, *25*, 1017-1022.

CHAPTER 2: HIGH SPEED HETEROGENEOUS IMMUNOASSAYS USING A FREE LIQUID JET FOR SAMPLE AND LABEL DELIVERY

A manuscript in preparation for submission to *Analytical Chemistry*

Jill M. Uhlenkamp,[1,2] Robert J. Lipert,[2] and Marc D. Porter[1]*

[1]Center for Combinatorial Sciences, the Biodesign Institute, and the Department of Chemistry and Biochemistry, Arizona State University, Tempe, AZ 85287-6401

[2]Institute for Combinatorial Discovery, Departments of Chemistry and of Chemical and Biological Engineering, Ames Laboratory-U.S. DOE, Iowa State University, Ames, Iowa 50011-3020

Abstract

Long incubation times are often an impediment to the application of heterogeneous immunoassays in disease profiling and biowarfare agent detection. This situation is usually a consequence of the slow, diffusion-based delivery of antigen to the capture solid phase, and is magnified further by the need for a labeling step in the case of sandwich assays. The work reported herein sought to enhance the flux of both antigen and label to the capture surface by use of a free liquid jet, thereby reducing assay time. To this end, the impact of the conditions for jet operation (e.g., sample volume, flow rate, and label concentration) were examined

with respect to the rapid delivery of antigen and label. These tests employed rabbit IgG as the test antigen, immobilized goat anti-rabbit IgG in the formation of the capture substrate, and Cy5-tagged goat anti-rabbit IgG as a fluorescent label. Based on these findings, comparison of performance (e.g., limit of detection (LOD)) was then made between assays carried out in stagnant solution (20.0-μL sample and label volumes and 24-h total incubation time) and those conducted with a free liquid jet (500-μL sample and label volumes and 6-s total incubation time) via a sandwich-type heterogeneous assay. The results showed that while using a 25-times larger sample volume, the overall assay time was decreased by more than 14,000 times with no loss in LOD. The potential to widely apply this technique for the creation of near "real time" immunoassays is briefly discussed, along with a qualitative modeling assessment in how the two approaches differ in the rate of reactant delivery.

Introduction

Techniques such as enzyme-linked immunosorbent assays (ELISA), fluorescence immunoassays (FIA), and DNA arrays play increasingly important roles in the diagnosis of human and animal disease and the detection of biowarfare agents.[1-6] Examples of recent developments include advancements in throughput, ease-of-use, and limits of detection,[7-14] along with a growing focus on miniaturization[15-20] and simultaneous multianalyte detection.[21-25] However, the lengthy incubation times often associated with heterogeneous immunoassays remains a long-standing challenge, especially in instances that demand both rapid sample turnaround and low limits of detection.

Heterogeneous assays involve the delivery of antigen to a capture substrate, and in the case of sandwich immunoassays, the capture step is followed by a labeling step. Both steps

are frequently carried out in quiet solution through which both antigen and label are delivered by diffusional mass transfer. However, the large sizes of biological targets (e.g., proteins, viruses, and bacteria) translates to small diffusion coefficients (e.g., 10^{-7} cm^2/s), and, as a consequence, potentially lengthy incubation times. The development of methodologies to reduce incubation times without degradation in other analytical figures of merit (e.g., sensitivity and limit of detection) are therefore of fundamental and technological importance.

As detailed in earlier reports,[26-30] one pathway to lowering incubation times arises from the fact that the rate of antigen-antibody binding is generally limited by mass transport rather than protein-protein recognition, i.e., binding kinetics. For this reason, a wide range of strategies have been examined as approaches to increase the delivery (i.e., flux) of the antigen or label to the capture substrate and, thus, decrease incubation times.[31-39] These techniques include the use of electric fields to enhance the transport of charged antigens and/or labels, and the application of magnetic fields to drive the movement of superparamagnetic labels. Approaches relying on elevations in temperature and rotation of the capture substrate, both of which result in increases in flux of antigen and/or labels, have also been reported.

The use of electric fields has resulted in total assay times of several minutes, and has been implemented with microfluidic systems[32, 36] or active electronic chips[33] in order to precisely deliver and localize antigens and/or labels at a given address. These methods, nonetheless, must be adjusted to account for differences in the charge and size of the target. Magnetic labels and substrates have also been employed to lower times to a few minutes.[34, 38, 39] Other techniques to shorten assay times, such as elevations in temperature[13, 31, 37] and fluidic confinement of reagents to small volumes,[35] have been reported. Elevated

temperatures, though, may lead to decreased sensitivity because the dissociation rate of the antigen-antibody complex often undergoes a larger increase with temperature than the corresponding association rate, resulting in a decrease in the binding constant.[37] Microfluidic systems have a propensity for clogging, especially in the analysis of complex sample media. Our laboratory has recently described an assay format that utilized capture substrate rotation as a means to achieve incubation times of ~25 min, while also lowering the LOD with respect to assays that were carried out in quiet solution and required ~24 h of total incubation time.[8, 9]

In building on our work, this paper describes a novel method to decrease the overall incubation time for heterogeneous immunoassays by application of a free liquid jet to both analyte and label delivery. Free liquid jets have been used for cooling in metal and plastics manufacturing, lasers, and electronic equipment.[40-42] Liquid jets have also found important applications in electrochemistry in which a wall-jet electrode is employed to increase reactant mass transport in, for example, studies of heterogeneous electron-transfer reactions .[43-45] The wall-jet is, however, conceptually different from the free liquid jet. The free liquid jet drives a stream of fluid through air, whereas that from a wall-jet is directed through a stagnant liquid. To our knowledge, this work represents the first extension of free liquid jets to heterogeneous immunoassays for the explicit purpose of decreasing incubation times by increasing the flux of the antigen and/or label to the surface of a capture substrate.

We show herein that a free liquid jet is easily adapted to heterogeneous immunoassays, can dramatically reduce the time required for sample and label incubation, and has the potential to simultaneously lower limits of detection. The following sections support these claims by using a sandwich immunoassay for rabbit IgG and Cy5-tagged goat

anti-rabbit IgG as a fluorescence label. We therefore examined the effect of a variety of experimental parameters (e.g., sample volume, fluid flow rate, and label concentration) on the speed and detection limits for the assay. We also performed a direct comparison to an assay with stagnant capture and labeling incubations, and carried out a qualitative modeling assessment on how the two approaches differ in the rate of reactant delivery. The potential to widely apply this technique for the creation of near "real time" immunoassays is briefly discussed.

Experimental Section

Reagents. Octadecanethiol (ODT), dithiobis(succinimidyl propionate) (DSP), and phosphate buffered saline (PBS) packs (10 mM, pH 7.2) were acquired from Sigma. SuperBlock and BupH Borate Buffer Packs (50 mM, pH 8.5) were obtained from Pierce. All buffers were passed through a Steri-Cup GP Filter Unit (Millipore). Glass substrates were cleaned with Contrad 70 (Decon Labs) prior to coating with chromium and gold. Poly(dimethyl siloxane) (PDMS, Dow Corning) was used to prepare microcontact printing stamps. Polyclonal goat anti-rabbit IgG antibody, polyclonal Cy5-labeled goat anti-rabbit IgG, and whole molecule rabbit IgG were purchased from US Biological. Polyclonal goat anti-rabbit IgG and polyclonal Cy5-labeled goat anti-rabbit IgG were purified prior to receipt by immunoaffinity chromatography, and received as 0.5 mg/mL solutions in PBS (pH 7.2); both solutions contained 0.01% (w/v) sodium azide and 40% (v/v) glycerol; the Cy5-labeled antibody solution also included 10 mg/mL bovine serum albumin (BSA). Whole molecule rabbit IgG, 10 mg/mL in PBS (pH 7.2), was purified prior to receipt by Protein A affinity chromatography. The as-received rabbit IgG was diluted with 10 mM PBS.

Capture Substrate Preparation. Gold-coated glass slides served as the substrate for assembling the capture surface. First, ~10 nm of chromium was resistively evaporated onto glass squares (1 x 1 cm) at 0.1 nm/s using an Edwards 306A resistive evaporator. Next, ~300 nm of 99.9% pure gold was deposited at the same rate.

The gold-coated glass substrates were exposed for 20 s to an octadecanethiol (ODT)-saturated PDMS stamp, with a 3-mm hole cut in its center.[46-48] The substrates were then rinsed with ethanol, dried under a stream of high purity nitrogen, and immersed in a 0.1 mM ethanolic solution of dithiobis(succinimidyl propionate) (DSP) for 12 h. These steps created an ODT-derived monolayer that acted as a hydrophobic barrier in order to localize reagents on the DSP-coated portion of the substrate. The DSP-derived monolayer served as a coupling agent for tethering the polyclonal capture antibodies via the amide linkage that forms from the reaction of its succinimidyl terminus with the primary amines of the protein. Next, 20.0 μL of goat anti-rabbit IgG, diluted to 100 μg/mL with 50 mM aqueous borate buffer (pH 8.5), was pipetted onto the substrate and allowed to react for 8-12 h in a humidity chamber at room temperature. The substrate was next washed three times by brief immersions (~5 s) in 2 mL of 10 mM PBS to remove unreacted antibody. After rinsing, 20 μL of SuperBlock buffer was pipetted onto the capture surface to block any unreacted succinimidyl terminal groups. After 12 h, the substrate was rinsed using the above procedure.

Protocol for Quiet Assay. For assays carried out in quiet solution, 20.0-μL aliquots of varied concentrations of rabbit IgG, diluted in PBS, were exposed to separate capture substrates for 8-12 h, as noted. Next, the substrates were rinsed by three imersions in 2 mL of fresh 10 mM PBS. Finally, 20.0 μL of 10 μg/mL Cy5-labeled goat anti-rabbit IgG was

pipetted onto each substrate. Following incubation, the rinsing procedure described above was repeated.

Protocol for Jet Assay. For assays conducted with free liquid jet delivery, rabbit IgG solutions in PBS were delivered by a syringe pump. The same procedure was used for exposure to Cy5-labeled goat anti-rabbit IgG. The above rinsing protocol was employed after both the antigen delivery and labeling steps.

For delivery of the antigen and label, a 3-mm distance between the jet nozzle and capture surface was used. The jet nozzle was defined by 0.5-mm internal diameter PEEK tubing (Upchurch Scientific) that was attached to the end of a syringe by standard fluidic adapters. As depicted in Scheme 1 (not to scale), the jet was directed normal to the substrate surface (arrows indicate flow in radial direction). The flow was driven by a PHD2000 Programmable syringe pump from Harvard Apparatus.

Instrumentation. Fluorescence images were collected with a Nikon Eclipse TE200 inverted microscope mounted on a Prairie Technologies epifluorescent system, which consisted of a UNIBLITZ shutter, a mercury lamp with a Prairie Technologies filter wheel, and a Hamamatsu C4742-95 CCD camera (6.7 x 6.7 μm pixels in a 1280 x 1024 pixel format). An XF110-2 filter cube set from Omega Optical was used to match the fluorescence wavelength of the Cy5-labeled antibody. Each sample was imaged at three different locations with 1-s exposures or less. Image analysis was accomplished with MetaMorph Version 6.3 software (Universal Imaging Corporation). The average intensity per pixel was measured from each image and the overall average from all pixels is reported. After correction for background, measured from a gold-coated slide, all fluorescence intensities were normalized to 1 s and are reported with arbitrary units (AU).

Results and Discussion

Preliminary Findings. (a). Development of quiet solution assay. A sandwich-type immunoassay for rabbit IgG that used quiet solution exposures of both antigen and label antibody was performed to serve as a basis of comparison to those carried out with delivery of antigen and label by free liquid jet. In past work, we typically conducted protein assays with 8-12 h incubation times for the antigen capture step and 12-16 h for the antigen labeling step.[14, 49-51] However, the latter step employed labels based on 30-60 nm gold particles. Since the nanoparticles are much larger in size than the Cy5-tagged antibodies, a study was carried out to ascertain the appropriate label incubation time for a quiet assay, i.e., an assay relying on diffusion for the mass transport delivery of the fluorescently-tagged tracer antibody. These tests therefore entailed a stagnant, 8-h exposure to either 20.0 μL of a 1000 ng/mL solution of rabbit IgG or 20.0 μL of a blank solution (i.e., 10 mM PBS). These samples were then incubated for varying times (4, 6, 8, and 12 h) with 20.0 μL of 10 μg/mL of Cy5-labeled goat anti-rabbit IgG.

Figure 1 shows the fluorescence intensities measured from each experiment. In the case of the incubations with the rabbit IgG solutions, the fluorescence signal increases with increasing labeling time. Using 4 h as a reference point, the signal increases in strength by 21, 125, and 210% with the 6-, 8-, and 12-h incubations, respectively. Moreover, the signal evolution for the blank exposures also undergoes an increase with time. The increases in the blank signals are 268, 329, and 483% for the 6-, 8-, and 12-h incubations with respect to that performed in 4 h. These data signify that the labeling equilibrium has not been reached for the 8-h incubation, and probably not at 12 h. While not fully optimized, all the comparative

stagnant solution experiments that are detailed later will be carried out with an 8-h capture step and a 12-h label step.

(b). Jet assay optimization. Several parameters were studied in an effort to determine the key operational conditions for the free liquid jet assay, including sample volume, flow rate, and label concentration. First, the effect of flow rate on the amount of antigen captured was examined. Flow rates of 10.0, 20.0, 30.0 and 40.0 mL/min were used to deliver 10.0 mL of 1000 ng/mL rabbit IgG, followed by labeling with 20.0 μL of Cy5-tagged anti-rabbit IgG (10 μg/mL) in quiet solution for 12 h. There was, however, no statistical difference between the measured signals and therefore in the amount of captured rabbit IgG (results not shown). We attribute these findings to saturation of the capture surface. A comparison of the capture surface area (7.07×10^{12} nm^2) to the footprint of a single IgG protein (78.5 nm^2) indicates that the amount of IgG in each 10.0 mL sample is in huge excess (~4000 fold) of that required to theoretically saturate the surface if we assume a 100% capture efficiency. From these data, we opted to employ a flow rate of 10.0 mL/min in all subsequent experiments.

Second, the effect of sample volume on the resulting fluorescence signal was investigated. Volumes of 100, 500, 1000, and 2000 μL of rabbit IgG (1000 ng/mL) were delivered by jet, followed by stagnant labeling with 20.0 μL of 10 μg/mL of the Cy5-tagged antibody for 8 h. The results, given in Figure 2, indicate that the amount of labeling antibody, and therefore captured rabbit IgG, approximates a linear increase with sample volume. We therefore selected a sample volume of 500 μL for the subsequent investigations, which represents a balance between signal strength and sample. However, the signal obtained using a 100-μL sample is much higher (~30 times) than that expected from a blank (see data from

Figure 6, which shows that the intensity of the blank from the assay performed with free liquid jet delivery of antigen and quiet solution labeling was ~0.3 AU). These results therefore point to the potential use of smaller sample volumes, albeit at the expense of the LOD.

Next, the concentration of the Cy5-tagged antibody was varied to determine if a solution more dilute than the 10 μg/mL level used thus far could be employed. This concentration, along with a series of dilutions from 1 to 0.001 μg/mL, was investigated for labeling the captured rabbit IgG with the jet. The substrates were first exposed to 20.0 μL samples of rabbit IgG (1000 ng/mL) via quiet solution for 8 h, followed by labeling by the jet delivery of 1.0 mL of Cy5 anti-rabbit IgG of varied concentration. The results are shown in Figure 3. As is evident, there was virtually no detectable signal from the samples labeled at the two lowest concentrations of Cy5 anti-rabbit IgG. A relatively weak signal, slightly greater than that expected from a blank sample collected under similar conditions (~0.06 AU, see Figure 6), was achieved from the sample labeled with the 0.1 μg/mL solution. The use of 1 μg/mL Cy5 anti-rabbit IgG resulted in a much higher level of labeling, but because roughly twice as much fluorescence was detected with the 10 μg/mL labeling solution, that concentration was adopted for the following comparison studies.

Comparison of quiet and jet assays. With operational conditions selected, assays for both types of delivery pathways were carried out for comparison. The quiet exposure assay was completed with 12-h incubations for 20.0-μL volumes of both rabbit IgG and Cy5 anti-rabbit IgG, translating to an overall time of 24 h. The jet assay was performed with 500-μL samples of rabbit IgG and Cy5 anti-rabbit IgG, both delivered at 10 mL/min, for a total

exposure time of 6 s. The jet assay, while employing a sample volume 25 times that of the quiet assay, was therefore over 14,000 times faster than the stagnant assay.

The results for the quiet and jet assays are shown by the representative fluorescence micrographs for each assay in Figure 4 and the dose-response curves in Figure 5. The first notable observation is the difference in fluorescence intensities for the two experiments. The stagnant assays generally had much stronger signals than the jet assays. The intensity, for example, of the quiet assay for the 500 ng/mL sample of rabbit IgG is ~23 times that of the jet assay. Additionally, the sensitivity (i.e., the change in intensity with respect to concentration) of the quiet assay is also greater than that of the jet assay for concentrations near 3000 ng/mL. Furthermore, the blank for the quiet assay is much stronger (~100 times) than that for the jet assay. The result of the extremely low signal for the blank in the jet assay is that the LOD is comparable to that of the jet assay. If LOD is defined by the concentration that would yield an intensity equal to the intensity of the blank plus three times the standard deviation of the blank intensity, an analysis of the data for the quiet assay and the jet assay yields LODs of 60 ng/mL (400 pM) and 50 ng/mL (330 pM), respectively. Thus, a free liquid jet assay was performed with an increase in sample size of ~25, but with a dramatic decrease in incubation time and no loss in detection limit.

How, then, do the two delivery mechanisms translate to the observed differences in Figure 5? Two approaches were taken to gain a qualitative perspective of the basis for the differences, recognizing that the lower signal strength found for the jet assay arises could be a consequence of the antigen incubation step, the label incubation step, or a combination of both steps. To determine the impact of each step, two sets of experiments were performed. The first set used a quiet incubation for the capture of rabbit IgG, but jet incubation for

fluorescence labeling. The second set reversed the conditions, with rabbit IgG and Cy5 anti-rabbit IgG incubations performed with jet and quiet delivery, respectively. Figure 6 plots the results.

Of the two experiments, the set that applied jet incubation to rabbit IgG capture and quiet incubation for labeling the captured IgG yielded stronger signals at IgG concentrations well above background levels. This result argues that jet incubation is more effective when applied to the antigen capture step than the labeling step.

We next applied models from the electrochemical arena to gain qualitative insights into differences in the rates of mass transfer, and therefore, the accumulation of antigen and label at the capture surface. In both models, we assume that: (1) the bulk concentration of reactant is invariant over the course of the experiment; (2) the rate of the reaction at the surface of the capture substrate is mass transport limited; and (3) the surface concentration of free binding sites is not changed as a consequence of binding/labeling. Therefore, the diffusion layer thickness in quiet solution ($\delta_{diff,q}$) is given by:[52]

$$\delta_{diff,q} = \sqrt{2Dt} \tag{1}$$

where D is the diffusion coefficient of antigen or label in cm^2/s ($D = 4.9 \times 10^{-7}$ for IgG[53]), and t is time in s. Furthermore, the accumulated surface concentration of antigen or label (particles/cm^2) under quiet solution conditions, Γ_q, can be expressed by Equation 2,[8]

$$\Gamma_q = 2n\left(\frac{Dt}{\pi}\right)^{1/2} \tag{2}$$

where n is the bulk antigen or label concentration with units of, for example, particles/cm^3.

A parallel treatment of the situation for the free liquid jet delivery of antigen and label starts with a calculation of the thickness of the hydrodynamic layer, δ_{hyd}, created by the jet at the substrate surface. For a free liquid jet:[54]

$$\delta_{hyd} = 2.04\left(\frac{2a\nu}{V_i}\right)^{1/2} \tag{3}$$

and a is the radius of the jet, ν is the kinematic viscosity (1.0×10^{-2} cm^2/s), and V_i is the jet impingement velocity in cm/s. Then, for flow past a flat plate, δ_{diff} is related to δ_{hyd} according to Levich by:[55]

$$\delta_{diff} \cong \left(\frac{D}{\nu}\right)^{1/3} \delta_{hyd} \tag{4}$$

Substitution of Equation 4 into Equation 3 gives:

$$\delta_{diff,j} = 2.88 D^{1/3} \nu^{1/6} \left(\frac{a}{V_i}\right)^{1/2} \tag{5}$$

Finally, if we apply the Nernst diffusion layer treatment to determine the flux of reactant across the diffusion layer, the accumulated surface concentration can be approximated as:[52]

$$\Gamma_j = \frac{nDt}{\delta_{diff,j}} \tag{6}$$

Equations 5 and 6 can be used to approximate the difference in antigen and label accumulation for the two modes of reactant delivery under our experimental conditions.

These results are shown in Table 1. As is evident, the values under our experimental setup for Γ_q are ~20 times those for Γ_j. These data begin to explain the basis for the differences in plots in both Figures 5 and 6, noting that the labeling efficiency by jet is compounded by the lower level of antigen accumulation by jet. Furthermore, the lower level

of potential accumulation, which can also be viewed as the number of collisions for the reactant with the surface, suggests a possible explanation for the lower blank response with jet delivery. If the binding constant for nonspecific adsorption in either the capture or labeling steps is lower than that for specific binding or proceeds at a rate below the mass transfer limit, then the level of nonspecific adsorption would be lower than that observed for the stagnant solution experiments.

Conclusions

This paper has demonstrated the incredible potential of assays using free liquid jets to deliver antigen and label in heterogeneous assays. Our results showed that high speed assays could be realized with total incubation times of only a few seconds. At a more quantitative level, we were able to decrease the assay incubation time by 14,400 times from 24 h to just 6 s with no compromise in limit of detection. However, our free liquid jet setup employed 500-μL sample volumes, whereas our earlier work with a stagnant solution format called for 20-μL samples. Experiments are currently being designed for hardware that can be readily adapted to work with smaller sample volumes, and span a wider range of flow rates. This method for assay incubation has potential applicability to all assays that require the delivery of antigen and/or label to a substrate surface. Furthermore, the lower signal from blank with the jet assay, which signals lower non-specific binding, is an intriguing consequence of the use of jets for label delivery. Work to gain insight into the origins of this observation is also underway, and could lead to a new pathway to further lower LODs.

Acknowledgements

This work was supported by CEROS-DARPA, the Institute for Combinatorial Discovery at Iowa State University, and the Biodesign Institute at Arizona State University. The Ames Laboratory is operated for the US Department of Energy through Iowa State University under contract No.W7405-eng-82.

References

(1) Ekins, R. P. *J. Chem. Educ.* **1999**, *76*, 769-780.

(2) George, S. *Clin. Chem. Lab. Med.* **2004**, *42*, 1288-1309.

(3) Hage, D. S. *Anal. Chem.* **1999**, *71*, 294R-304R.

(4) Kricka, L. J. *Pure Appl. Chem.* **1996**, *68*, 1825-1830.

(5) Soper, S. A.; Brown, K.; Ellington, A.; Frazier, B.; Garcia-Manero, G.; Gau, V.; Gutman, S. I.; Hayes, D. F.; Korte, B.; Landers, J. L.; Larson, D.; Ligler, F.; Majumdar, A.; Mascini, M.; Nolte, D.; Rosenzweig, Z.; Wang, J.; Wilson, D. *Biosens. Bioelectron.* **2006**, *21*, 1932-1942.

(6) Wu, A. H. B. *Clin. Chim. Acta* **2006**, *369*, 119-124.

(7) Cao, Y. C.; Jin, R.; Mirkin, C. A. *Science* **2002**, *297*, 1536-1540.

(8) Driskell, J. D.; Kwarta, K. M.; Lipert, R. J.; Vorwald, A.; Neill, J. D.; Ridpath, J. F.; Porter, M. D. *J. Virol. Methods* **2006**, *138*, 160-169.

(9) Driskell, J. D.; Uhlenkamp, J. M.; Lipert, R. J.; Porter, M. D. *Anal. Chem.* **2007**, *79*, 4141-4148.

(10) Ferguson, J. A.; Steemers, F. J.; Walt, D. R. *Anal. Chem.* **2000**, *72*, 5618-5624.

(11) Ihara, T.; Mori, Y.; Imamura, T.; Mukae, M.; Tanaka, S.; Jyo, A. *Anal. Chim. Acta* **2006**, *578*, 11-18.

(12) Kerman, K.; Nagatani, N.; Chikae, M.; Yuhi, T.; Takamura, Y.; Tamiya, E. *Anal. Chem.* **2006**, *78*, 5612-5616.

(13) Kwarta, K. M., Iowa State University, Ames, 2007.

(14) Park, H.-Y.; Driskell, J. D.; Kwarta, K. M.; Lipert, R. J.; Porter, M. D.; Schoen, C.; Neill, J. D.; Ridpath, J. F. *Top. Appl. Phys.* **2006**, *103*, 427-446.

(15) Bacarese-Hamilton, T.; Gray, J.; Ardizzoni, A.; Crisanti, A. *Methods Mol. Med.* **2005**, *114*, 195-207.

(16) Ekins, R. P.; Chu, F. W. *Clin. Chem.* **1991**, *37*, 1955-1967.

(17) Joos, T. O.; Schrenk, M.; Hopfl, P.; Kroger, K.; Chowdhury, U.; Stoll, D.; Schorner, D.; Durr, M.; Herick, K.; Rupp, S.; Sohn, K.; Hammerle, H. *Electrophoresis* **2000**, *21*, 2641-2650.

(18) Knight, P. R.; Sreekumar, A.; Siddiqui, J.; Laxman, B.; Copeland, S.; Chinnaiyan, A.; Remick, D. G. *Shock* **2004**, *21*, 26-30.

(19) MacBeath, G. *Nat. Genet.* **2002**, *32*, 526-532.

(20) Yuk, C.-S.; Lee, H. K.; Kim, H. T.; Choi, Y. K.; Lee, B. C.; Chun, B.-H.; Chung, N. *Biotechnol. Lett.* **2004**, *26*, 1563-1568.

(21) Caslavska, J.; Allemann, D.; Thormann, W. *J. Chromatogr., A* **1999**, *838*, 197-211.

(22) Christodoulides, N.; Tran, M.; Floriano, P. N.; Rodriguez, M.; Goodey, A.; Ali, M.; Neikirk, D.; McDevitt, J. T. *Anal. Chem.* **2002**, *74*, 3030-3036.

(23) Ekins, R. P.; Chu, F. *Trends Biotechnol.* **1994**, *12*, 89-94.

(24) Wilson, M. S.; Nie, W. *Anal. Chem.* **2006**, *78*, 2507-2513.

(25) Zhang, C.; Zhang, Y.; Wang, S. *J. Agric. Food Chem.* **2006**, *54*, 2502-2507.

(26) Frackelton, A. R., Jr.; Weltman, J. K. *J. Immunol.* **1980**, *124*, 2048-2054.

(27) Myszka, D. G.; Morton, T. A.; Doyle, M. L.; Chaiken, I. M. *Biophys. Chem.* **1997**, *64*, 127-137.

(28) Nygren, H.; Kaartinen, M.; Stenberg, M. *J. Immunol. Methods* **1986**, *92*, 219-225.

(29) Nygren, H.; Werthen, M.; Stenberg, M. *J. Immunol. Methods* **1987**, *101*, 63-71.

(30) Stenberg, M.; Nygren, H. *J. Theor. Biol.* **1985**, *113*, 589-597.

(31) Bora, U.; Kannan, K.; Nahar, P. *J. Immunol. Methods* **2004**, *293*, 43-50.

(32) Dodge, A.; Fluri, K.; Verpoorte, E.; de Rooij, N. F. *Anal. Chem.* **2001**, *73*, 3400-3409.

(33) Ewalt, K. L.; Haigis, R. W.; Rooney, R.; Ackley, D.; Krihak, M. *Anal. Biochem.* **2001**, *289*, 162-172.

(34) Hahn, Y. K.; Jin, Z.; Kang, J. H.; Oh, E.; Han, M.-K.; Kim, H.-S.; Jang, J.-T.; Lee, J.-H.; Cheon, J.; Kim, S. H.; Park, H.-S.; Park, J.-K. *Anal. Chem.* **2007**, *79*, 2214-2220.

(35) Hofmann, O.; Voirin, G.; Niedermann, P.; Manz, A. *Anal. Chem.* **2002**, *74*, 5243-5250.

(36) Hu, G.; Gao, Y.; Sherman, P. M.; Li, D. *Microfluid. Nanofluid.* **2005**, *1*, 346-355.

(37) Johnstone, R. W.; Andrew, S. M.; Hogarth, M. P.; Pietersz, G. A.; McKenzie, I. F. *Mol. Immunol.* **1990**, *27*, 327-333.

(38) Luxton, R.; Badesha, J.; Kiely, J.; Hawkins, P. *Anal. Chem.* **2004**, *76*, 1715-1719.

(39) Wellman, A. D.; Sepaniak, M. J. *Anal. Chem.* **2006**, *78*, 4450-4456.

(40) Baonga, J. B.; Louahlia-Gualous, H.; Imbert, M. *Appl. Therm. Eng.* **2006**, *26*, 1125-1138.

(41) Fabbri, M.; Dhir, V. K. *J. Heat Transfer* **2005**, *127*, 760-769.

(42) Lienhard, J. H. V. *Annu. Rev. Heat Transfer* **1995**, *6*, 199-270.

(43) Gunasingham, H.; Fleet, B. *Anal. Chem.* **1983**, *55*, 1409-1414.

(44) Huang, Y. L.; Khoo, S. B.; Yap, M. G. *Am. Biotechnol. Lab.* **1993**, *11*, 18-20.

(45) Laevers, P.; Hubin, A.; Terryn, H.; Vereecken, J. *J. Appl. Electrochem.* **1995**, *25*, 1017-1022.

(46) Chen, C. S.; Mrksich, M.; Huang, S.; Whitesides, G. M.; Ingber, D. E. *Biotech. Prog.* **1998**, *14*, 356-363.

(47) Kumar, A.; Whitesides, G. M. *Appl. Phys. Lett.* **1993**, *63*, 2002-2004.

(48) Libioulle, L.; Bietsch, A.; Schmid, H.; Michel, B ; Delamarche, E. *Langmuir* **1999**, *15*, 300-304.

(49) Driskell, J. D.; Kwarta, K. M.; Lipert, R. J.; Porter, M. D.; Neill, J. D.; Ridpath, J. F. *Anal. Chem.* **2005**, *77*, 6147-6154.

(50) Grubisha, D. S.; Lipert, R. J.; Park, H.-Y.; Driskell, J.; Porter, M. D. *Anal. Chem.* **2003**, *75*, 5936-5943.

(51) Ni, J.; Lipert, R. J.; Dawson, G. B.; Porter, M. D. *Anal. Chem.* **1999**, *71*, 4903-4908.

(52) Bard, A. J.; Faulkner, L. R. *Electrochemical Methods: Fundamentals and Applications*, 2 ed.; John Wiley & Sons, Inc.: New York, 2001.

(53) Starr, T. E.; Thompson, N. L. *J. Phys. Chem. B* **2002**, *106*, 2365-2371.

(54) Incropera, F. P. *Liquid Cooling of Electronic Devices By Single-Phase Convection*; John Wiley & Sons, Inc.: New York, 1999.

(55) Levich, V. G. *Physicochemical Hydrodynamics*; Prentice-Hall: Englewood Cliffs, 1962.

Figure Captions

Figure 1. The fluorescence intensity measured with 25-ms integrations, normalized to 1 s, for each 1000 ng/mL rabbit IgG and blank sample as a function of labeling time. Both the antigen (20.0 μL, 8 h) and label incubation steps (20.0 μL, 10 μg/mL Cy5 goat anti-rabbit IgG) were carried out in quiet solution. The error bars represent the standard deviation of three measurements taken at different locations on each sample. The standard deviations for the blanks with 4, 6, 8, and 12 h binding were 0.01, 0.05, 0.03, and 0.09 AU, respectively; those for the 1000 ng/mL rabbit IgG samples with 4, 6, 8, and 12 h binding were 0.12, 0.02, 0.16, and 0.06 AU, respectively.

Figure 2. The fluorescence intensity measured with 100-ms integrations, normalized to 1 s, for each 1000 ng/mL rabbit IgG sample of varied volume delivered at 10.0 mL/min by jet. Labeling was completed via an 8-h quiet incubation (20.0-μL of 10 μg/mL Cy5 goat anti-rabbit IgG). The error bars represent the standard deviation of three measurements taken at different locations on the sample. These signals are attributed to specific binding, with the signal from the corresponding blank sample below 0.3 AU. The gray, dashed line is a linear fit to the data and has an r^2 value of 0.97.

Figure 3. The fluorescence intensity measured with 1-s integrations for 1000 ng/mL rabbit IgG samples (20.0-μL aliquots with 8-h incubation) labeled by 1.0 mL of varied concentrations of Cy5-tagged goat anti-rabbit IgG. The error bars represent the standard deviation of three measurements taken at different locations on the sample. The inset shows the lowest three label concentrations along with a dashed line, which represents an expected

value for a blank sample (based on the data from Figure 6 with quiet sample exposure, followed by free liquid jet label incubation).

Figure 4. Representative fluorescence micrographs (4 x 10^5 μm^2) for assays in quiet solution (A-D, 50-ms integration) and with free liquid jet assays (E-H, 500-ms integration). (A) 500, (B) 250, (C) 100, (D) 0, (E) 5000, (F) 1000, (G) 500, and (H) 0 ng/mL rabbit IgG.

Figure 5. Dose-response curves for assays performed with either 12-h quiet (20.0-µL samples) or 3-s jet (500-µL samples) exposures for both rabbit IgG and Cy5-labeled goat anti-rabbit IgG (10 µg/mL). Intensities are normalized to 1 s integration, from 50 ms and 500 ms for quiet and jet assays, respectively. The error bars represent the standard deviation of fluorescence intensity measurements from three locations on the surface. The black and gray dashed lines represent the lowest detectable signal of the quiet and jet assays, respectively (i.e., the blank signal plus three times its standard deviation) and are at 2.00 and 0.02 AU, respectively.

Figure 6. Dose-response curves for assays performed with either 12-h quiet exposure for rabbit IgG (20.0-µL samples) and a 3-s jet exposure for Cy5-labeled goat anti-rabbit IgG (500 µL, 10 µg/mL) (400-ms integrations normalized to 1 s), or 3-s jet exposure for rabbit IgG (500-µL samples) and 12-h quiet exposure for Cy5-labeled goat anti-rabbit IgG (20.0 µL, 10 µg/mL) (150-ms integrations normalized to 1 s). The error bars represent the standard deviation of fluorescence intensity measurements from three locations on the surface. The dashed lines represent the lowest detectable signal (i.e., the blank signal plus three times its

standard deviation) and are at 0.06 AU for the quiet/jet assay and at 0.27 AU for the jet/quiet assay.

Table 1. Γ_q as a function of incubation time and Γ_j as a function of sample volume, flow rate, and delivery time; each for conditions employed experimentally and other hypothetical parameters.

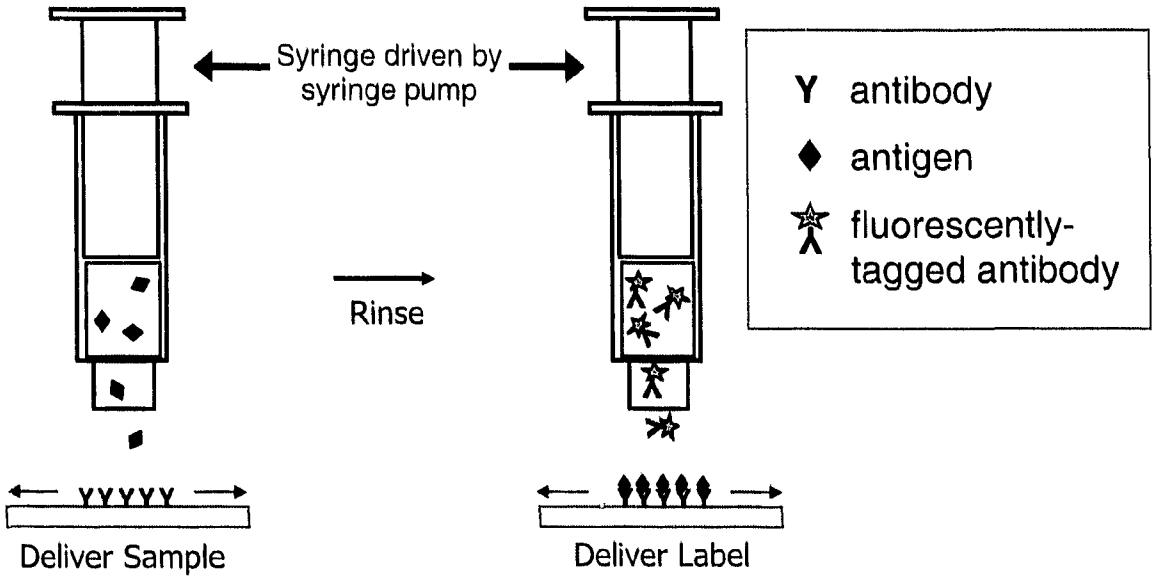
Syringe driven by
syringe pump
Rinse
Y antibody
antigen
fluorescently-
tagged antibody
Deliver Sample
Deliver Label

Scheme 1

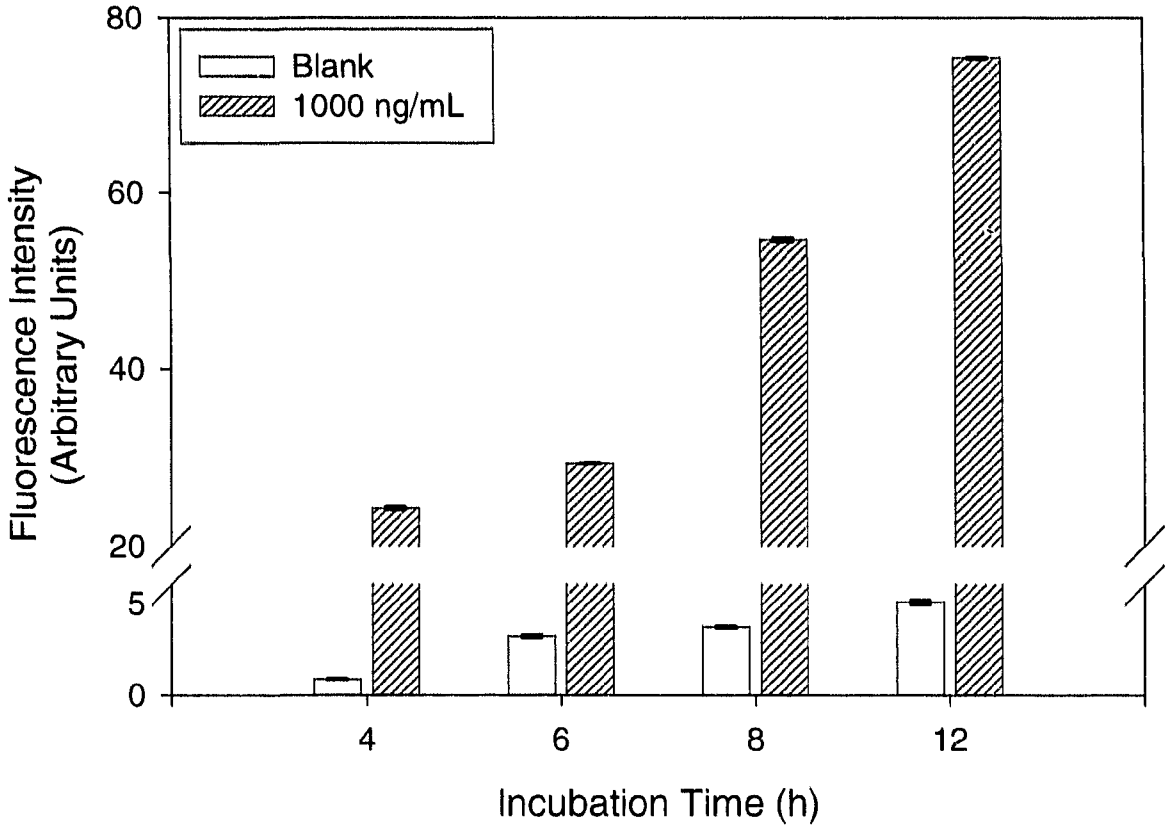
80
60
40
20
5
0
Blank
1000 ng/mL
Fluorescence Intensity
(Arbitrary Units)
4
6
8
12
Incubation Time (h)

Figure 1

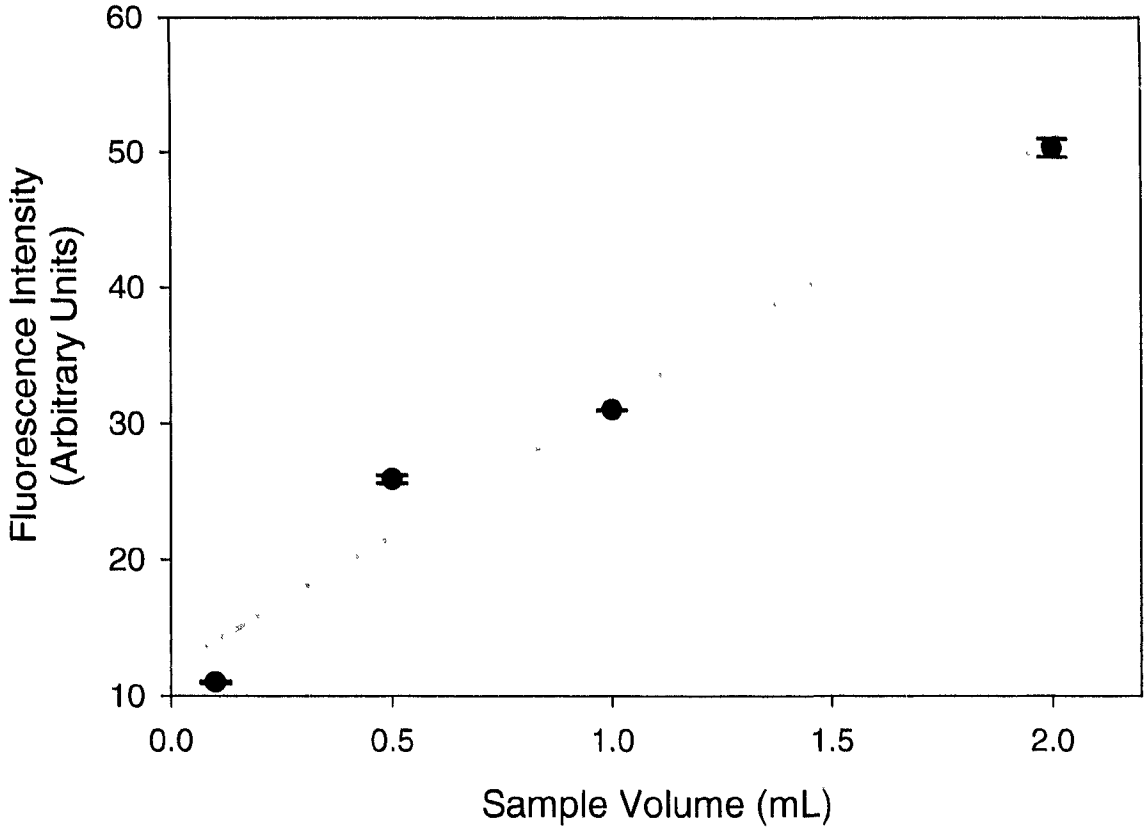
60
50
40
30
20
10
Fluorescence Intensity
(Arbitrary Units)
0.0
0.5
1.0
1.5
2.0
Sample Volume (mL)

Figure 2

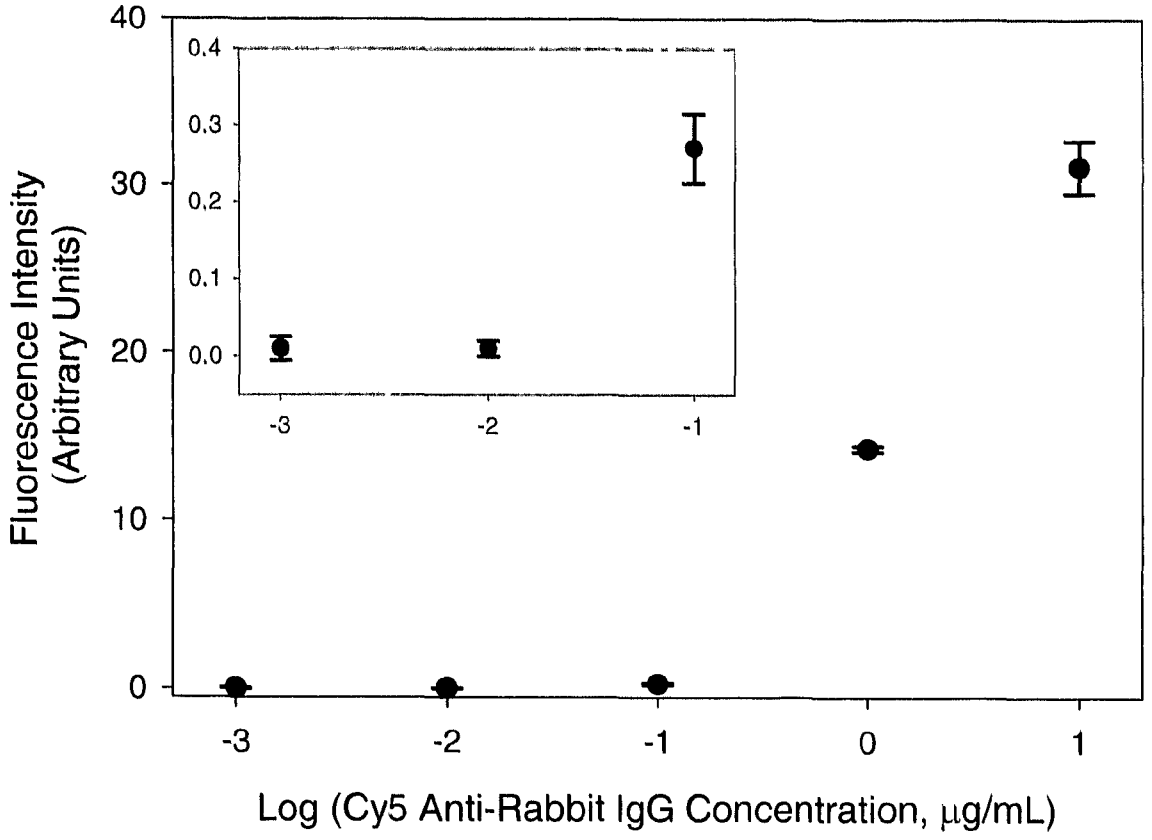
Fluorescence Intensity
(Arbitrary Units)
40
30
20
10
0
-3
-2
-1
0
1
Log (Cy5 Anti-Rabbit IgG Concentration, μg/mL)
0.4
0.3
0.2
0.1
0.0
-3
-2
-1

Figure 3

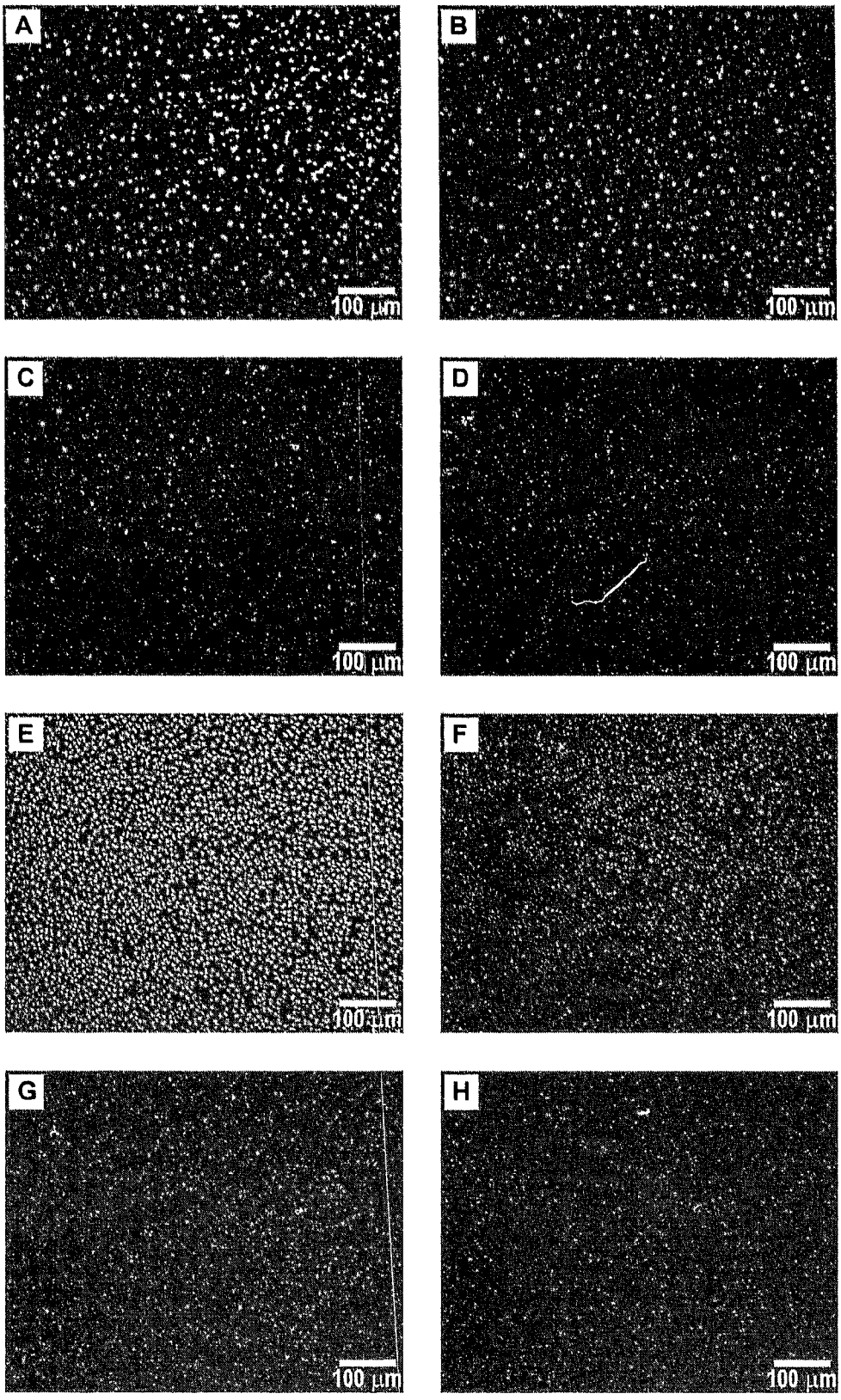

Figure 4

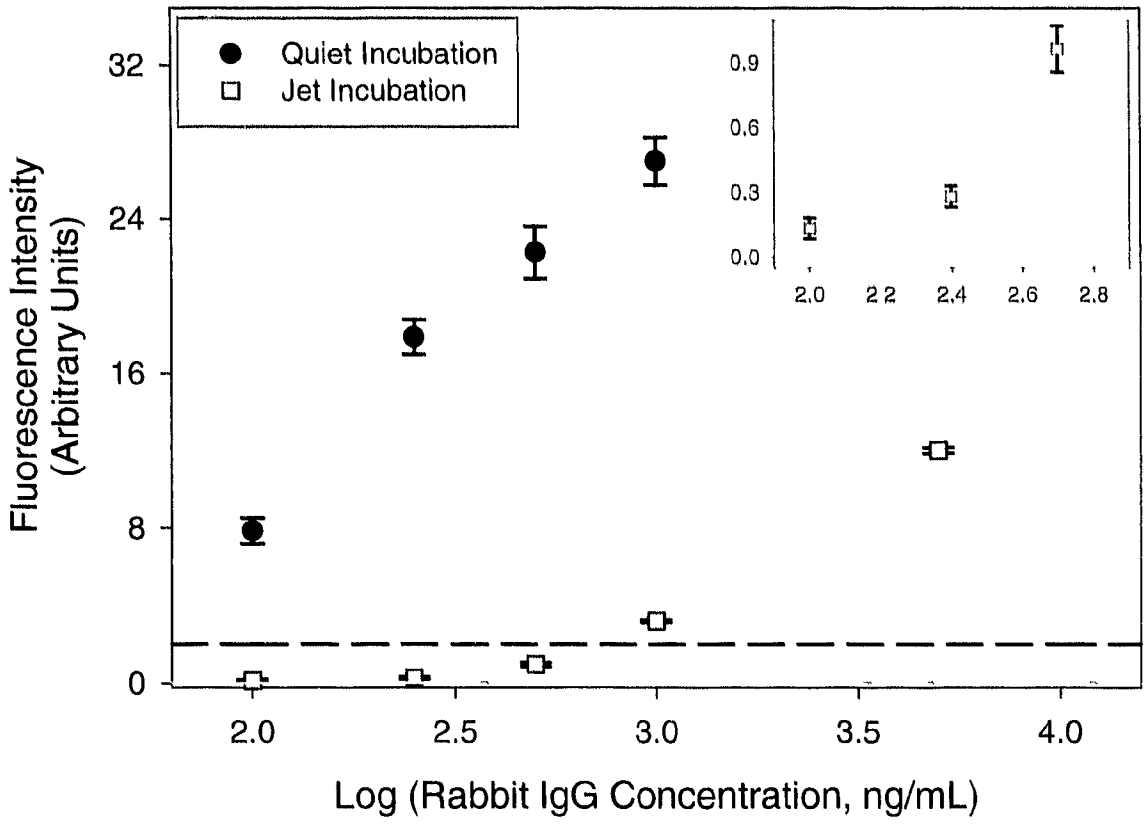
Quiet Incubation
Jet Incubation
Fluorescence Intensity
(Arbitrary Units)
32
24
16
8
0
2.0
2.5
3.0
3.5
4.0
Log (Rabbit IgG Concentration, ng/mL)
0.9
0.6
0.3
0.0
2.0
2.2
2.4
2.6
2.8

Figure 5

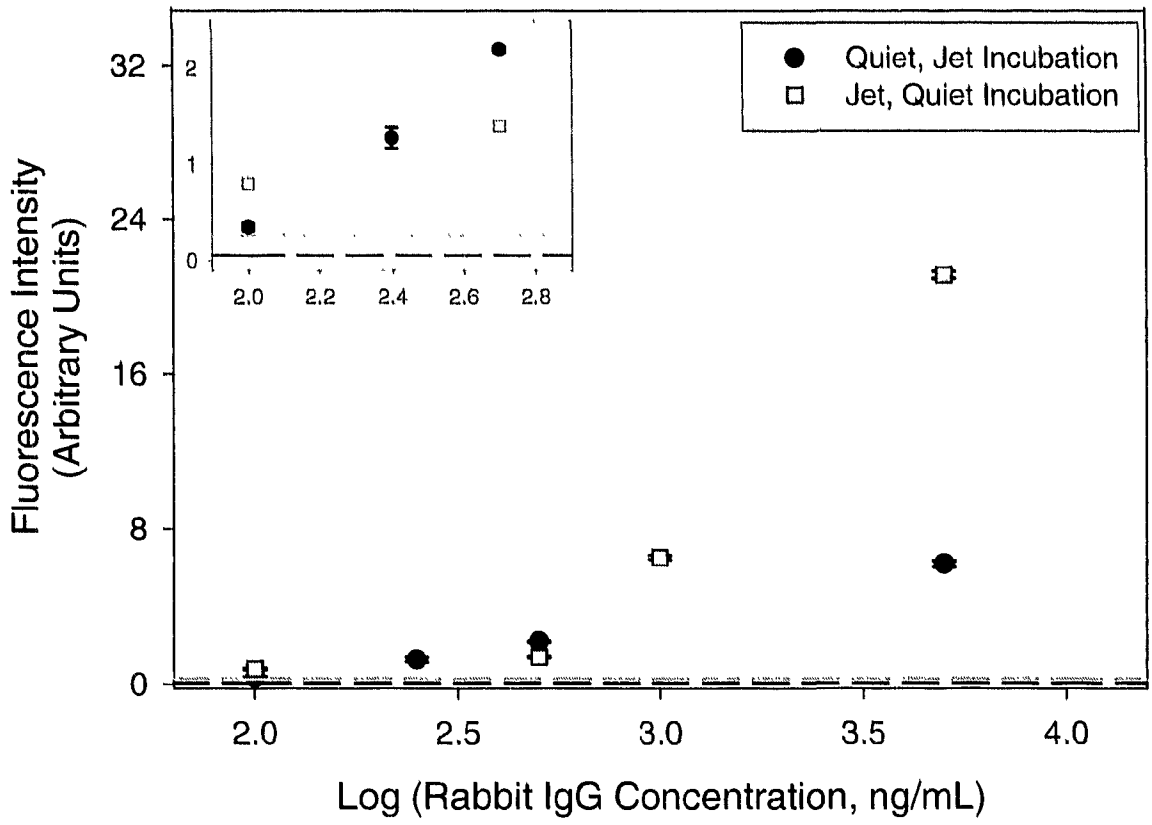
Quiet, Jet Incubation
Jet, Quiet Incubation
Fluorescence Intensity
(Arbitrary Units)
32
24
16
8
0
2.0
2.5
3.0
3.5
4.0
Log (Rabbit IgG Concentration, ng/mL)
2
1
0
2.0
2.2
2.4
2.6
2.8

Figure 6

Reagent	Concentration ng/mL	Concentration IgG/mL	Γ_q^a 12 h	Γ_j^a 3 s
Rabbit IgG	100	4.0×10^{11}	6.6×10^{10}	3.3×10^{9}
	250	1.0×10^{12}	1.6×10^{11}	8.1×10^{9}
	500	2.0×10^{12}	3.3×10^{11}	1.6×10^{10}
	1000	4.0×10^{12}	6.6×10^{11}	3.3×10^{10}
	5000	2.0×10^{13}	3.3×10^{12}	1.6×10^{11}
Cy5 anti-rabbit IgG	10,000	4.0×10^{13}	6.6×10^{12}	3.3×10^{11}

Table 1

a) Based on packing density and binding activity analysis, the surface concentration of active capture IgG antibodies is 6.7×10^{-13} mol/cm^2 (4.0×10^{12} molecules/cm^2).

CHAPTER 3: SURFACE-ENHANCED RAMAN SCATTERING-BASED IMMUNOASSAY FOR OVALBUMIN WITH HIGH SPEED INCUBATIONS BY FREE LIQUID JET

A manuscript in preparation for submission to *Analytical Chemistry*

Jill M. Uhlenkamp,[1,2] Robert J. Lipert,[2] Michael C. Granger,[1] and Marc D. Porter[1]*

[1]Center for Combinatorial Sciences, the Biodesign Institute, and the Department of Chemistry and Biochemistry, Arizona State University, Tempe, AZ 85287-6401

[2]Institute for Combinatorial Discovery, Departments of Chemistry and of Chemical and Biological Engineering, Ames Laboratory-U.S. DOE, Iowa State University, Ames, Iowa 50011-3020

Abstract

An extremely rapid and sensitive immunoassay for ovalbumin has been developed. Ovalbumin is a simulant for ricin and botulinum toxins. The assay employs a free liquid jet for enhanced mass transfer of antigen, which decreased the antigen incubation time from 8 h to 6 s or less. The labeling step, performed via incubation with quiet solution, was shortened from 12-16 h to 35 min by increasing the label concentration from our earlier SERS-based assays. Assay readout was performed with surface-enhanced Raman scattering (SERS)

detection. This assay was first optimized for rabbit IgG and was then extended to the detection of ovalbumin in phosphate buffered saline (PBS) and non-fat milk. The limits of detection achieved for ovalbumin in PBS and milk were 34 ng/mL (790 pM) and 12 ng/mL (280 pM), respectively.

Introduction

The detection of biowarfare agents (BWAs) is an increasingly important issue in public safety.[1] There are, however, a wide range of challenges to realizing this capability. Some of these challenges include the necessity of large sample volumes, low throughput, and the performance of existing labeling methods for the detection of multiple biomarkers.

Two examples of possible BWAs are ricin and botulinum toxins, which could potentially be aerosolized or introduced into food or water supplies. These agents have median lethal doses (LD_{50}) of 30 μg/kg for ricin and 1 ng/kg for botulinum toxin. While accidental exposure to ricin is highly unlikely, botulinum toxin poisoning, or botulism, readily occurs through exposure to contaminated food products.[2,3]

The Centers for Disease Control (CDC) currently specifies the use of time-resolved fluorescence as the immunoassay for the detection of ricin in suspect samples.[4] There are, however, several other reported approaches,[1] including enzyme-linked immunosorbent assays (ELISA),[5,6] a colorimetric assay,[7] fluorescence-based assay,[8-10] immunochromatographic assay,[11] and a planar array immunosensor.[12] These methods have limits of detection (LOD) ranging from 1.5 to 400 pM. These assays were typically performed in clean buffer; however, one test was carried out in river water with an LOD of 15 pM.[10] The best LOD (1.5 pM) was achieved with an enhanced colorimetric and

chemiluminescence ELISA,[6] a fluorescence-based fiber optic immunoassay,[10] and an immunochromatographic sandwich assay format employing two monoclonal antibodies and silver enhancement.[11] The main drawback of many of these detection methods is a long incubation time, often on the order of several hours.

Methods for the detection of botulinum toxin are less well developed. The CDC lists a mouse assay as the currently accepted method.[2] Several groups have developed alternative techniques for this toxin, but none appear to have yet gained widespread adoption.[13-15] Tests based on polymerase chain reaction (PCR) have also been reported, but that can detect *Clostridium botulinum*, the bacterium that produces botulinum toxin, not the toxin itself.[16-18]These detection modes have a similar set of strengths and weaknesses as those outlined above for assays.

We propose to surmount several of the difficulties in BWA detection by employing a rapid, sensitive sandwich immunoassay with free liquid jet incubation and SERS readout. Previously, we reported on an assay for rabbit IgG that required an incubation time of 6 s with free liquid jet delivery of antigen and fluorescently-tagged antibody labels.[19] The work described herein examines the replacement of fluorescence readout with SERS. SERS is a new addition to the techniques used for readout in immunoassays.[20-27] Our laboratory has reported on the use of SERS readout for the simultaneous detection of several IgGs with extrinsic Raman labels (ERLs).[24] ERLs consist of gold nanoparticles which are modified by a layer of chemisorbed Raman scatterers, followed by a coating of antibodies. This construction places the scatterer near the nanoparticle surface, to maximize the Raman signal intensity,[28] and imparts specificity for the target analyte. SERS-based detection has several advantages over fluorescence. One of these advantages is that SERS bands are 10-100 times

narrower than those of fluorescence, potentially simplifying multiplexed detection. Very low LODs are also achievable with SERS, and we have demonstrated femtomolar detection for prostate specific antigen[22] and single-digit binding event recognition.[29]

We therefore show that by integrating SERS detection with free liquid jet incubation in a heterogeneous assay, a rapid and sensitive assay for ovalbumin, a simulant for ricin and botulinum toxin, can be developed. The effects of several assay parameters (e.g., flow rate and sample volume) were first explored with the detection of rabbit IgG as a model system. Then, by drawing on the insights gained from that study, an assay for ovalbumin was designed and carried out. We also investigated an alternative means to speed label incubation via ERL concentration. The extension of this method to real-world matrixes was also demonstrated by the detection of ovalbumin in milk.

Theoretical Considerations

In earlier work, we described the use of a rotating capture substrate to increase the flux of antigen and label to a capture surface,[30, 31] which led to a reduction in the total incubation time from ~24 h when employing quiet incubations to 25 min. This method, heavily used in electrochemistry to control the flux of reactant to a rotating disk electrode (RDE), creates a thin diffusion layer adjacent to the rotating surface, the thickness (δ_{diff}) of which is inversely proportional to the rotation rate (ω). Analyte from the bulk solution is therefore continuously presented to the outer boundary of the diffusion layer through convective transport. As a result, the flux of analyte to the surface is defined by the rate of its diffusive mass transport through the diffusion layer, and is inversely proportional to δ_{diff}, and directly proportional to $\omega^{1/2}$.

An alternate means to increase the flux of an analyte to a surface is through the use of a free liquid jet, which is the focus of this paper. By directing a stream of solution normal toward a surface, a hydrodynamic layer is created adjacent to the surface which has properties similar to that with the rotating disk system. A schematic of the hydrodynamics involved in a free liquid jet system is shown in Figure 1. The thickness of the hydrodynamic layer (δ_{hyd}) is nearly uniform across the stagnation zone and is given by:[32]

$$\delta_{hyd} = 2.04\left(\frac{2a\nu}{V_i}\right)^{1/2} \tag{1}$$

where a is the radius of the jet, ν is the kinematic viscosity (ν=0.010 cm^2/s), and V_i is the jet impingement velocity in cm/s. The radius of the stagnation zone, r_s, can be reasonably approximated as $0.7D_i$,[32] giving a stagnation zone with a diameter of 0.7 mm for the 0.5-mm diameter jet employed in our experiments. As depicted in Figure 1, the hydrodynamic boundary layer, and therefore diffusion layer, increases as the radial distance from the stagnation zone increases.

According to Levich,[33] the thickness of the diffusion layer for flow past a flat plate is related to δ_{hyd} by:

$$\delta_{diff} \cong \left(\frac{D}{\nu}\right)^{1/3}\delta_{hyd} \tag{2}$$

where D is the diffusion coefficient of the reactant (D = 4.9 x 10^{-7} for IgG[34] and 7.6 x 10^{-7} for ovalbumin[35]). It follows then, that

$$\delta_{diff,J} = 2.88D^{1/3}\nu^{1/6}\left(\frac{a}{V_i}\right)^{1/2} \tag{3}$$

The Nernst diffusion layer model can be used to determine the flux of reactant across the diffusion layer and the accumulated surface concentration, Γ_j (particles/cm^2), can then be approximated as:

$$\Gamma_j = \frac{nDt}{\delta_{diff,j}} \tag{4}$$

where n is the bulk antigen or label concentration with units of particles/cm^3 and t is time in s. Expressions for δ and Γ in quiet solution assays similarly evolve from models from the electrochemical field. In quiet solution, the diffusion layer thickness, ($\delta_{diff,q}$) is:[36]

$$\delta_{diff,q} = \sqrt{2Dt} \tag{5}$$

Moreover, Γ under quiet solution conditions can be expressed by:[30]

$$\Gamma_q = 2n\left(\frac{Dt}{\pi}\right)^{1/2} \tag{6}$$

These formulations assume that: (1) the bulk concentration of reactant does not change over the course of the experiment; (2) the rate of reaction at the surface of the capture substrate is mass transport limited; and (3) the surface concentration of available binding sites is not changed as a consequence of binding/labeling.

Figures 2A plots $\delta_{diff,q}$ for IgG (D = 4.9 x 10^{-7} cm^2/s) and ovalbumin (D = 6.7 x 10^{-7} cm^2/s) as a function of incubation time. As expected, $\delta_{diff,q}$ increases with time. Figures 2B and 2C plot the resulting Γ_q for IgG and ovalbumin, respectively. As is evident, the predicted accumulation for ovalbumin, a smaller protein, is close to ten times higher than that for IgG. These data highlight the significance of incubation times and demonstrate the need for enhanced mass transport in order to achieve high speed assays without increasing LOD.

Figure 3A gives $\delta_{diff,j}$ for IgG and ovalbumin as a function of jet flow rate. At higher flow rates, $\delta_{diff,j}$ becomes increasingly smaller. However, as is seen in Figures 3B and C, a smaller $\delta_{diff,j}$ does not translate to increased antigen or label accumulation. This is because at a given flow rate, incubation time is determined by the sample volume used. Therefore, at higher flow rates, increasingly smaller exposure times result in lower accumulation of antigen or label. The application of free liquid jet delivery for our heterogeneous immunoassay therefore accomplishes very short incubations because δ_{diff} is dramatically smaller than in quiet solution.

Experimental Section

Reagents. Gold nanoparticles with a diameter of 60 nm (<8% variation) and a concentration of 2.6 x 10^{10} particles/mL were acquired from Ted Pella. Octadecanethiol (ODT), dithiobis(succinimidyl propionate) (DSP), bovine serum albumin (BSA) and phosphate buffered saline (PBS) packs (10 mM, pH 7.2) were obtained from Sigma. SuperBlock and BupH Borate Buffer Packs (50 mM, pH 8.5) were purchased from Pierce. DSNB [5,5'-dithiobis(succinimidyl-2-nitrobenzoate)] was synthesized in house following a previously published method.[22] All buffers were passed through a 0.22-μm pore size Steri-Cup GP Filter Unit (Millipore). Prior to coating with chromium and gold, glass substrates were cleaned with Contrad 70 (Decon Labs). Microcontact printing stamps were fabricated from poly(dimethyl siloxane) (PDMS, Dow Corning).

Polyclonal goat anti-rabbit IgG antibody, whole molecule rabbit IgG, polyclonal rabbit anti-chicken ovalbumin, and ovalbumin were obtained from US Biological. Polyclonal goat anti-rabbit IgG was purified prior to receipt by immunoaffinity chromatography, and

supplied as 0.5 mg/mL in PBS (pH 7.2). The solution contained 0.01% (w/v) sodium azide and 40% (v/v) glycerol. Whole molecule rabbit IgG was purified by Protein A affinity chromatography and provided at 10 mg/mL in PBS (pH 7.2). Rabbit IgG was diluted with 10 mM PBS. Polyclonal rabbit anti-chicken ovalbumin was purified by delipidation, fractionation, and ion-exchange chromatography and supplied at 10 mg/mL in PBS (pH 7.2) with 0.01% (w/v) sodium azide and 40% (v/v) glycerol. Ovalbumin (99% purity, determined by SDS-PAGE) was shipped as a neat, lyophilized powder. Rabbit IgG solutions were prepared in PBS. Ovalbumin solutions were made using either PBS or milk. Non-fat milk (Shamrock Farms) was purchased and used as a biological matrix.

Capture Substrate Preparation. Immunoassay capture substrates were prepared on glass slides coated with a thin layer of evaporated gold. First, ~10 nm of chromium were resistively deposited onto glass squares (1 x 1 cm) at a rate of 0.1 nm/s using an Edwards 306A resistive evaporator, followed by ~300 nm of 99.9% pure gold in the same manner.

A PDMS stamp with a 3-mm diameter hole cut in its center was soaked in 1 mM ODT, dried under a stream of high purity nitrogen, and exposed to the gold-coated glass squares for 20 s.[37-39] This procedure created a hydrophobic barrier at the edges of the circular address for localization of samples and reagents within the address. The substrates were then rinsed with ethanol, dried under a stream of high purity nitrogen, and immersed in a 0.1 mM ethanolic solution of DSP for ~12 h. The last step creates a DSP-derived monolayer in the unstamped center of the substrate. The terminal succinimidyl ester of the resulting monolayer served to covalently couple to primary amines of capture polyclonal antibodies.

Next, 20.0 μL of antibody, diluted to 100 μg/mL in 50 mM aqueous borate buffer (pH 8.5), was pipetted onto the substrate and allowed to react for 8-12 h in a humidity chamber at

room temperature. The substrate was then immersed three times in 2 mL of fresh 10 mM PBS to remove unreacted antibody. After rinsing, 20.0 μL of blocking solution was pipetted onto the capture surface to block any remaining succinimidyl ester. Finally, the substrate was rinsed as described above after an 8-12 h exposure to the blocking solution.

SERS Label Preparation. ERLs are designed to provide large Raman signals and immunospecificity.[22, 24] The former is attained by using a DSNB-derived Raman reporter, which has an intrinsically strong Raman scattering cross-section from its symmetric nitro stretch ($\nu_s(NO_2)$). DSNB also has the ability to chemisorb to gold nanoparticles. The latter is realized by the immobilization of the trace antibody at the terminus of the DSNB-based adlayer, which acts to covalently immobilize antibodies onto the particles. Overall, this design minimizes the distance between the $\nu_s(NO_2)$ and the surface of the gold nanoparticle in order to maximize the surface enhancement, and provides a basis for molecular recognition by the polyclonal antibody coating.

ERLs are constructed by first adding 40.0 μL of 50 mM borate buffer to a 1.0-mL suspension of 60-nm gold nanoparticles to adjust the pH to 8.5. At this pH, the amine functionalities of the antibody are deprotonated, facilitating reaction with the succinimidyl ester of DSNB. Next, 10.0 μL of 1.0-mM DSNB in acetonitrile was added to the nanoparticle suspension. After ~8 hours, 20 μg of antibody was added to the suspension, and incubated for ~12 h. To block any unreacted succinimidyl ester groups, 100.0 μL of 10% BSA in 2 mM aqueous borate buffer was added and allowed to react for ~8 h. The nanoparticle suspension was then centrifuged at 2000*g* for 10 min to remove unreacted DSNB and antibody. The supernatant was decanted and the nanoparticles were resuspended in 1.0 mL of 2 mM aqueous borate buffer with 1% (w/v) BSA. This process was repeated two more times

and the final resuspension volume was adjusted to give the desired concentration. Next, 1.5 M NaCl was added to bring the final salt concentration to 150 mM, imitating physiological conditions. Finally, the suspension was passed through a 0.22-μm syringe tip filter (Costar) to remove aggregates.

Immunoassay Protocol for Quiet Assay. Assays in quiet solution exposed 20.0 μL aliquots of varied concentrations of antigen to the capture substrates for a controlled amount of time. The antigenic solutions were either rabbit IgG diluted in PBS or ovalbumin diluted in PBS or in non-fat milk. After antigen capture, the substrates were rinsed by immersion three times in 2 mL of fresh aqueous 2 mM borate (150 mM NaCl). Next, 20.0 μL of ERLs, constructed with either goat anti-rabbit IgG or rabbit anti-chicken ovalbumin, was pipetted onto the substrates. After label incubation, the rinsing procedure described above was repeated.

Immunoassay Protocol for Jet Assay. A syringe pump delivered 500 μL antigen samples for assays conducted with free liquid jet incubation. Labeling was achieved in quiet solution as described above. The same rinsing protocol was used after the antigen delivery and labeling steps.

The jet nozzle was offset from the surface of the capture substrate by 3 mm. The jet nozzle was defined by 0.5-mm (internal diameter) PEEK tubing (Upchurch Scientific), which was attached to the end of a syringe by standard fluidic adapters. The flow was driven by a PHD2000 Programmable syringe pump from Harvard Apparatus. Figure 1 again illustrates the delivery of antigen to the capture surface by jet.

Instrumentation. Raman spectra were collected with a NanoRaman I (Concurrent Analytical) employing a 30 mW, 632.8-nm He-Ne laser. The spectrograph is comprised of a

modified f/2.0 Czerny-Turner imaging spectrometer and has a resolution of 6-8 cm^{-1}. The laser light is focused to a 25-μm diameter spot on the surface using an objective with a numerical aperture of 0.68. The scattered light is collected with the same objective and detected with a thermo-electrically cooled (0°C) Kodak 0401E CCD. All spectra were collected with an integration time of 1 s.

Results and Discussion

Assay optimization for antigen delivery by jet. Based on our first report on assays with free liquid jet delivery,[19] the amount of antigen captured will increase with sample volume, potentially until reaching equilibrium. Therefore, the effect of sample volume for the SERS-based jet assay was investigated. Samples of 1000 ng/mL rabbit IgG in PBS with volumes ranging from 0.1 and 5 mL were exposed to an anti-rabbit capture substrate by jet at 10 mL/min. These samples were then labeled with 20.0 μL of 5.2×10^{10} ERL/mL anti-rabbit ERLs via quiet solution for 16 h.

These data are presented in Figure 4. Representative SERS spectra are shown in Figure 4A, and exhibit features diagnostic of the presence of DSNB-labeled ERLs. The most prominent band is the $\nu_s(NO_2)$ at 1336 cm^{-1}.[22] Figure 4 shows the average SERS intensity of the $\nu_s(NO_2)$ from five locations on the substrate versus sample volume. The results are similar to those we reported previously for a fluorescence-based assay[19] in that the amount of captured rabbit IgG initially increased as the sample volume increased and then leveled off at volumes greater than 1.0 mL. We believe the leveling off in signal is because of capture substrate saturation. That is, the number of IgG proteins delivered in a 1-mL volume (i.e., 4×10^{12}) is much greater than the theoretical number that would cover the capture surface (i.e., 9

x 10^{10}) based on IgG footprint. A sample volume of 500 µL was chosen for use in most of the subsequent studies as a compromise between volume and signal strength. The sample volume is therefore half of that which resulted in the highest intensity (i.e., 1.0 mL), while still obtaining 78% of the maximum signal.

There is another interesting observation from these data. The standard deviations of the SERS intensity measurements from five different locations on the capture surface are similar to those of our previous work on SERS readout. These results represent measurements taken beyond the 0.7-mm diameter of the stagnation zone (Figure 1). The data therefore indicate that sampling beyond the stagnation zone does not appear to have an impact on the measurement, possibly because any differences in δ_{diff} are marginally small.

In order to assess the ability of the jet-based assay to employ smaller volumes, an assay using 100-µL samples was conducted. Solutions of rabbit IgG in PBS, ranging in concentration from 50 ng/mL to 10 µg/mL, were used. These samples were delivered by jet at 10 mL/min for a total exposure time of 0.6 s. The substrates were then exposed to ERLs via quiet solution for 16 h.

The dose-response curve is given in Figure 5. For comparison, data from an assay for rabbit IgG carried out with an 8-h quiet solution exposure of 20.0 µL samples and a 16-h exposure of ERLs are also shown in Figure 5. Interestingly, the intensities for the quiet assay are very similar to those for the jet assay; however, the blank for the quiet assay has a lower intensity than that for the jet assay, highlighting the importance of controlling and minimizing non-specific binding. This situation translates to a slightly better LOD for the quiet assay than for the jet assay. The LOD is defined by the concentration that would yield a signal equal to that of the blank plus three times the standard deviation of the blank signal.

Thus, the LOD for the jet assay was 35 ng/mL (230 pM), while that for the quiet solution assay was 10 ng/mL (70 pM). Nonetheless, with only five times more sample used in the assay with jet incubation, the LOD was only 3.5 times higher and the capture time was reduced by 48,000 times to less than 1 s. We note that the assay also demonstrates specificity as exposures to antigen other than rabbit IgG (e.g., human IgG) resulted in signals not exceeding those of a blank sample (data not shown).

Extension of jet delivery to ERLs. Next, jet delivery of ERLs was explored to further decrease assay time. Two capture substrates were exposed to 20.0 μL of 100 ng/mL of rabbit IgG diluted in PBS and two were incubated with 20.0 μL of PBS, all for 9 h. Each set (sample and blank) was then exposed to 20.0 μL of ERLs via quiet solution for 16 h or 500 μL of ERLs via jet at 10 mL/min. Figure 6 presents the results. While the intensity of the sample labeled via quiet solution was ~29,000 cts/s, that labeled via jet was only ~460 cts/s. A similar trend was found for the blanks; the signal for the blank in quiet solution was 1055 cts/s and there was no measurable SERS intensity for the blank treated by jet exposure. These data show that the conditions used to successfully capture antigen via jet are not directly applicable to labeling with ERLs by jet.

Several other experiments were performed in an effort to achieve more effective labeling with ERLs by jet, including increasing ERL concentration and volume, adjusting the ERL solution composition (e.g., BSA concentration), and increasing the surface concentration of captured antigen. All these investigations yielded very low levels of labeling (data not shown). One possible explanation for this limitation is that the ERLs delivered by jet dislodge the captured antigen. To test this hypothesis, a capture substrate was exposed to 20.0 μL of 100 ng/mL rabbit IgG for 9 h in quiet solution and then to 0.5 mL of ERLs by jet

at a rate of 10 mL/min. A 20.0 μL aliquot of ERLs was then added to the substrate for 16 h of quiet solution labeling. If the ERL delivery by jet is dislodging bound antigen, we would expect to see a lower SERS intensity than that observed for the sample in the previous experiment, which employed only quiet ERL binding.

These data are also presented in Figure 6. Since the SERS intensity for the sample exposed to ERLs delivered by jet followed by quiet solution ERLs is not statistically different from that of the sample labeled with ERLs by quiet solution alone, it is apparent that captured antigen is not being removed by the jet exposure of the ERLs. Similarly, an experiment was performed to determine whether the jet exposure of ERLs displaces previously bound ERLs. Substrates with captured rabbit IgG labeled via quiet solution with ERLs were therefore exposed to additional ERLs by jet. Again there was no statistical difference in SERS intensity was measured for these samples and those labeled with ERLs via quiet solution (data not shown).

Assay for ovalbumin by jet. The SERS-based assay with jet delivery of antigen was next extended to the detection of ovalbumin, a simulant for bacterial toxins. When an assay for ovalbumin was first attempted, abnormally high signals were observed for the blank samples when our typical protocol using SuperBlock as a blocking solution was employed (data not shown). In order to address this, the performance of an alternative blocking solution, 1% BSA in aqueous 2 mM borate buffer, was studied. Two capture substrates were prepared with SuperBlock as the blocking solution and two substrates used 1% (w/v) BSA. Each type of capture substrate was then exposed to 20.0 μL aliquots of blank PBS solution or 1000 ng/mL ovalbumin in PBS for 9 h via quiet solution. After rinsing, the substrates were labeled with 20.0 μL of 5.2×10^{10} ERL/mL ERLs for 14 h. The results, shown in Figure 7,

reveal that the 1% BSA solution is a more effective blocking agent. The signal from the blank with 1% BSA blocking is lower than that of the blank employing SuperBlock, whereas the signals from both of the 1000 ng/mL samples are not statistically different. These data show that the 1% BSA solution more effectively reduces non-specific binding and, importantly, does not inhibit specific binding. Since this blank signal level is on par with that usually observed with our other SERS-based assays,[22,40] 1% BSA was employed in the subsequent ovalbumin assays.

Free liquid jet incubation of 0.5 mL samples of ovalbumin spiked in PBS, ranging in concentration from 1 to 5000 ng/mL was performed to construct a dose-response curve. Labeling was completed with an 8-h quiet solution exposure of anti-ovalbumin ERLs (5.2 x 10^{10} ERLs/mL). The results are shown in Figure 8. The LOD for this assay was 3 ng/mL (60 pM). An assay with 8-h quiet solution incubation of ovalbumin and 8-h incubation of ERLs yielded an LOD of 1 ng/mL (20 pM) (data not shown). The use of jet exposure of ovalbumin therefore decreases the assay time from 16 to ~8 h with only a small sacrifice in LOD. Furthermore, the jet-based assay for ovalbumin was shown to be specific for only ovalbumin when challenged with rabbit and human IgG.

Since several experiments aimed at labeling with ERLs by jet had proven ineffective, an alternative method to speed the labeling step for the SERS-based assay was explored, recognizing that the number of label impingements on a surface is directly proportional to the concentration of those gold particles in solution (Equation 6) This relationship indicates that the label incubation may be enhanced by increasing the label concentration. To test this hypothesis, the ERL concentration was increased five-fold to 2.6 x 10^{11} ERLs/mL and 20.0 µL aliquots of these ERLs were then used to label four separate sets of samples; each set

consisted of two substrates with antigen incubation by jet: one exposed to 500 µL of 1000 ng/mL of ovalbumin in PBS and one to 500 µL of PBS buffer as a blank. ERL incubation times of 15, 25, 35, and 45 min were investigated.

The resulting SERS intensities from each sample are plotted in Figure 9. As ERL incubation time increased, the SERS intensity of the 1000 ng/mL samples initially increased, but begins to level off at ~35 min. This situation reflects that the amount of captured ERLs has reached closest packed saturation (i.e., 2.5 x 10^9 ERLs at 100% coverage on a 3-mm diameter substrate), or that equilibrium labeling has been reached. The SERS intensity of the blank samples also increased as the incubation time increased. Based on these data and the tradeoffs between gains in the signal strength for specific binding relative to the small increases in non-specific binding, 35-min ERL incubations will be used in the next experiments. We add that these results support the potential use of even shorter ERL incubation times, but no test have yet been performed along these lines.

Finally, a series of assays at several concentrations of ovalbumin with jet exposure of ovalbumin and shortened ERL incubation with increased ERL concentration were performed. These tests also included assays for ovalbumin spiked in non-fat milk, which acted to simulate a real-world matrix. As before, 500-µL samples of ovalbumin were delivered by jet. Labeling was achieved by 35 min quiet solution exposure to 20.0 µL of ERLs (2.6 x 10^{11} ERL/mL). Figure 10 displays both sets of results.

There are two notable differences in these results. First, the assay in milk has a lower blank signal. Second, the responses from most of the spiked milk samples are stronger than their analogs in PBS. As a consequence, the assay in milk has a slightly lower LOD and a larger linear dynamic range. The LOD for the assay in milk was 12 ng/mL (280 pM), while

that for the assay in PBS was 34 ng/mL (790 pM). The lower signal for the milk assay blank is attributable to the fact that milk is often used as a blocking agent in immunoassays and appears to function similarly in these experiments.

Conclusions

This work combined free liquid jet delivery of antigen in a sandwich-type immunoassay with SERS readout. This technique yielded an assay for rabbit IgG with a reduction in antigen incubation time requirement from 8 h to just 600 ms. This jet-based assay had an LOD of 35 ng/mL which was only a little higher than 10 ng/mL achieved with an assay performed with an 8-h incubation of rabbit IgG. The antigen incubation time was therefore reduced by 48,000 times with a loss of LOD of a factor of about three.

An assay for ovalbumin, a simulant for ricin and botulinum toxins, was also performed with free liquid jet. The LOD of 3 ng/mL was again only slightly higher than that of an assay completed with quiet solution incubation (1ng/mL). Ovalbumin was also detected in milk via free liquid jet, which represents a real-world sample matrix and demonstrates the applicability of free liquid jet delivery to real samples.

Total assay incubation times were further reduced by increasing the concentration of ERLs by 5 times that of our previously reported protocol. This increase enabled a reduction in label incubation times from 8-12 h to only 35 min. Further reductions in label incubation times could be achieved with a higher concentration but may come with an increased cost of reagents (e.g., protein and gold colloids).

We believe that the inability to label with ERLs by jet with the conditions employed here may be due to several factors. The most important factor is the difference in

impingement values for ERLs incubated in quiet solution and those delivered by jet. Γ for the former is 3.7 x 10^9 ERLs/cm^2 while the latter is only 1.1 x 10^4 ERLs/cm^2.

Another contributing factor may be that the ERLs experience a shear force greater than those of the initial interactions with captured antigen. Studies to probe this challenge are underway. One possible way to increase the likelihood of ERL labeling by jet is to orient the surface-bound antibodies in such a way that interaction with captured antigen is more favored. ERL size will also be varied in a future work to determine if labeling is enhanced with smaller ERLs, which have larger diffusion coefficients.

Experiments are planned with assays employing quiet solution incubation and free liquid jet delivery, which will seek to make comparisons to the models presented herein with respect to sample size, incubation times, and flow rates. These investigations may offer additional insight into the most effective means with which to apply free liquid jets for sample and label delivery, potentially leading to even lower LODs.

Acknowledgements

This work was supported through grants from CEROS-DARPA and the NADC and by the Institute for Combinatorial Discovery of Iowa State University and the Biodesign Institute at Arizona State University. The Ames Laboratory is operated for the US Department of Energy through Iowa State University under contract No.W7405-eng-82.

References

(1) Lee, S. G.; Lee, F. K.; Gopalakrishnakone, P. *J. Chromatogr., A* **2006**, *1133*, 1-12.

(2) http://www.cdc.gov/ncidod/dbmd/diseaseinfo/files/botulism_manual.htm, Centers for Disease Control and Prevention, Atlanta, 1998. Accessed on July 7, 2007.

(3) http://www.bt.cdc.gov/agent/ricin/facts.asp, Centers for Disease Control and Prevention, 2006. Accessed on July 8, 2007.

(4) http://www.bt.cdc.gov/agent/ricin/labtesting.asp, Centers for Disease Control and Prevention, Atlanta, 2006. Accessed on July 8, 2007.

(5) Koja, N.; Shibata, T.; Mochida, K. *Toxicon* **1980**, *18*, 611-618.

(6) Poli, M. A.; Rivera, V. R.; Hewetson, J. F.; Merrill, G. A. *Toxicon* **1994**, *32*, 1371-1377.

(7) Shyu, H.-F.; Chiao, D.-J.; Liu, H.-W.; Tang, S.-S. *Hybrid. Hybridomics* **2002**, *21*, 69-73.

(8) Delehanty, J. B.; Ligler, F. S. *Anal. Chem.* **2002**, *74*, 5681-5687.

(9) Goldman, E. R.; Clapp, A. R.; Anderson, G. P.; Uyeda, H. T.; Mauro, J. M.; Medintz, I. L.; Mattoussi, H. *Anal. Chem.* **2004**, *76*, 684-688.

(10) Narang, U.; Anderson, G. P.; Ligler, F. S.; Buranst, J. *Biosens. Bioelectron.* **1997**, *12*, 937-945.

(11) Shyu, R.-H.; Shyu, H.-F.; Liu, H.-W.; Tang, S.-S. *Toxicon* **2001**, *40*, 255-258.

(12) Wadkins, R. M.; Golden, J. P.; Pritsiolas, L. M.; Ligler, F. S. *Biosens. Bioelectron.* **1998**, *13*, 407-415.

(13) Fach, P.; Perelle, S.; Dilasser, F.; Grout, J.; Dargaignaratz, C.; Botella, L.; Gourreau, J.-M.; Carlin, F.; Popoff, M. R.; Broussolle, V. *Appl. Environ. Microbiol.* **2002**, *68*, 5870-5876.

(14) Kumar, P.; Colston, J. T.; Chambers, J. P.; Rael, E. D.; Valdes, J. J. *Biosens. Bioelectron.* **1994**, *9*, 57-63.

(15) Wictome, M.; Newton, K. A.; Jameson, K.; Dunnigan, P.; Clarke, S.; Gaze, J.; Tauk, A.; Foster, K. A.; Shone, C. C. *FEMS Immunol. Med. Microbiol.* **1999**, *24*, 319-323.

(16) Aranda, E.; Rodriguez, M. M.; Asensio, M. A.· Cordoba, J. J. *Lett. Appl. Microbiol.* **1997**, *25*, 186-190.

(17) Braconnier, A.; Broussolle, V.; Perelle, S.; Fach, P.; Nguyen-The, C.; Carlin, F. *J. Food Prot.* **2001**, *64*, 201-207.

(18) Ferreira, J. L.; Baumstark, B. R.; Hamdy, M. K.; McCay, S. G. *J. Food Prot.* **1993**, *56*, 18-20.

(19) Uhlenkamp, J. M.; Lipert, R. J.; Porter, M. D. *Manuscript in preparation.*

(20) Ansari, D. O.; Stuart, D. A.; Nie, S. *Proc. of SPIE* **2005**, *5699*, 82-90.

(21) Dou, X.; Takama, T.; Yamaguchi, Y.; Yamamoto, H.; Ozaki, Y. *Anal. Chem.* **1997**, *69*, 1492-1495.

(22) Grubisha, D. S.; Lipert, R. J.; Park, H.-Y.; Driskell, J.; Porter, M. D. *Anal. Chem.* **2003**, *75*, 5936-5943.

(23) Mulvaney, S. P.; Musick, M. D.; Keating, C. D.; Natan, M. J. *Langmuir* **2003**, *19*, 4784-4790.

(24) Ni, J.; Lipert, R. J.; Dawson, G. B.; Porter, M. D. *Anal. Chem.* **1999**, *71*, 4903-4908.

(25) Rohr, T. E.; Cotton, T.; Fan, N.; Tarcha, P. J. *Anal. Biochem.* **1989**, *182*, 388-398.

(26) Xu, S.; Ji, X.; Xu, W.; Li, X.; Wang, L.; Bai, Y.; Zhao, B.; Ozaki, Y. *Analyst* **2004**, *129*, 63-68.

(27) Zhang, X.; Young, M. A.; Lyandres, O.; Van Duyne, R. P. *J. Am. Chem. Soc.* **2005**, *127*, 4484-4489.

(28) Kneipp, K.; Kneipp, H.; Itzkan, I.; Dasari, R. R.; Feld, M. S. *J. Phys.: Condens. Matter* **2002**, *14*, R597-R624.

(29) Park, H.-Y.; Lipert, R. J.; Porter, M. D. *Proc. of SPIE* **2004**, 464-477.

(30) Driskell, J. D.; Kwarta, K. M.; Lipert, R. J.; Vorwald, A.; Neill, J. D.; Ridpath, J. F.; Porter, M. D. *J. Virol. Methods* **2006**, *138*, 160-169.

(31) Driskell, J. D.; Uhlenkamp, J. M.; Lipert, R. J.; Porter, M. D. *Anal. Chem.* **2007**, *79*, 4141-4148.

(32) Incropera, F. P. *Liquid Cooling of Electronic Devices By Single-Phase Convection*; John Wiley and Sons, Inc.: New York, 1999.

(33) Levich, V. G. *Physicochemical Hydrodynamics*; Prentice-Hall: Englewood Cliffs, 1962.

(34) Starr, T. E.; Thompson, N. L. *J. Phys. Chem. B* **2002**, *106*, 2365-2371.

(35) Bello, M. S.; Rezzonico, R.; Righetti, P. G. *Science* **1994**, *266*, 773-776.

(36) Bard, A. J.; Faulkner, L. R. *Electrochemical Methods: Fundamentals and Applications*, 2 ed.; John Wiley & Sons, Inc.: New York, 2001.

(37) Chen, C. S.; Mrksich, M.; Huang, S.; Whitesides, G. M.; Ingber, D. E. *Biotech. Prog.* **1998**, *14*, 356-363.

(38) Kumar, A.; Whitesides, G. M. *Appl. Phys. Lett.* **1993**, *63*, 2002-2004.

(39) Libioulle, L.; Bietsch, A.; Schmid, H.; Michel, B.; Delamarche, E. *Langmuir* **1999**, *15*, 300-304.

(40) Driskell, J. D.; Kwarta, K. M.; Lipert, R. J.; Porter, M. D.; Neill, J. D.; Ridpath, J. F. *Anal. Chem.* **2005**, *77*, 6147-6154.

Figure Captions

Figure 1. Schematic of a free liquid jet depicting the hydrodynamic properties of the jet and resulting stagnation and boundary layer regions, adapted from reference 32.

Figure 2. (A) Predicted values of $\delta_{diff,q}$ as a function of incubation time for IgG ($D = 4.9 \times 10^{-7}$ cm^2/s) and ovalbumin ($D = 7.6 \times 10^{-7}$ cm^2/s). (B-C) Γ_q as a function of V_i for experimental concentrations employed in quiet incubation of (B) IgG and (C) ovalbumin.

Figure 3. (A) Predicted values of $\delta_{diff,j}$, as a function of V_i for IgG and ovalbumin. (B-C) Γ_j as a function of V_i for experimental concentrations employed in free liquid jet incubation of (B) IgG and (C) ovalbumin.

Figure 4. (A) Representative SERS spectra for the delivery of samples of rabbit IgG (1000 ng/mL), ranging in volume from 100-μL to 1.0-mL, by free liquid jet at a flow rate of 10.0 mL/min, and then labeled by ERLs in quiet solution for 16 h. (B) The SERS intensity of $\nu_s(NO_2)$ for each sample as a function of sample volume. The error bars represent the standard deviation of five measurements taken at different locations on each sample.

Figure 5. Dose-response plot of $\nu_s(NO_2)$ intensity as a function of sample concentration for an assay with free liquid jet delivery of 100-μL samples and an assay with 8-h quiet solution incubation of 20.0-μL samples, both with 16-h quiet solution labeling with ERLs. The error bars represent the standard deviation of five measurements taken at different locations on

each sample. The dashed lines are the LODs (the blank signal plus three times its standard deviation).

Figure 6. Comparison of ERL binding by jet (0.5 mL at 10 mL/min), by quiet solution (20.0 μL for 16 h), and by jet followed by quiet solution, for rabbit IgG (100 ng/mL) and blank samples. SERS intensity is that of $\nu_s(NO_2)$. The error bars represent the standard deviation of five measurements taken at different locations on each sample. There was no detectable signal from the blank labeled with ERLs by free liquid jet.

Figure 7. Comparison of the performance of SuperBlock and a 1% BSA solution used for blocking in an assay for ovalbumin. SERS intensities are those of $\nu_s(NO_2)$. The error bars represent the standard deviation of five measurements taken at different locations on each sample.

Figure 8. Dose-response curve for an assay performed with 3-s free liquid jet exposure of 500-μL samples of ovalbumin in PBS at 10.0 mL/min and 8-h quiet exposure for anti-ovalbumin ERLs. The error bars represent the standard deviation of five SERS intensity measurements made at different locations on each sample. The dashed line represents the LOD.

Figure 9. The SERS intensities of $\nu_s(NO_2)$ as a function of ERL (1.6×10^{10} ERL/mL) quiet solution labeling time of substrates exposed to 500-μL samples of ovalbumin (1000 ng/mL) and blank delivered by free liquid jet at 10.0 mL/min.

Figure 10. Dose-response curves for assays carried out with 3-s jet exposure (10.0 mL/min) of 500-μL samples of ovalbumin in either PBS or non-fat milk; each with 35-min quiet solution exposure of 20.0 μL of ERLs (2.6×10^{10} ERL/mL). The error bars represent the standard deviation of five SERS intensity measurements made at different locations on each sample. The dashed line is indicative of the LOD.

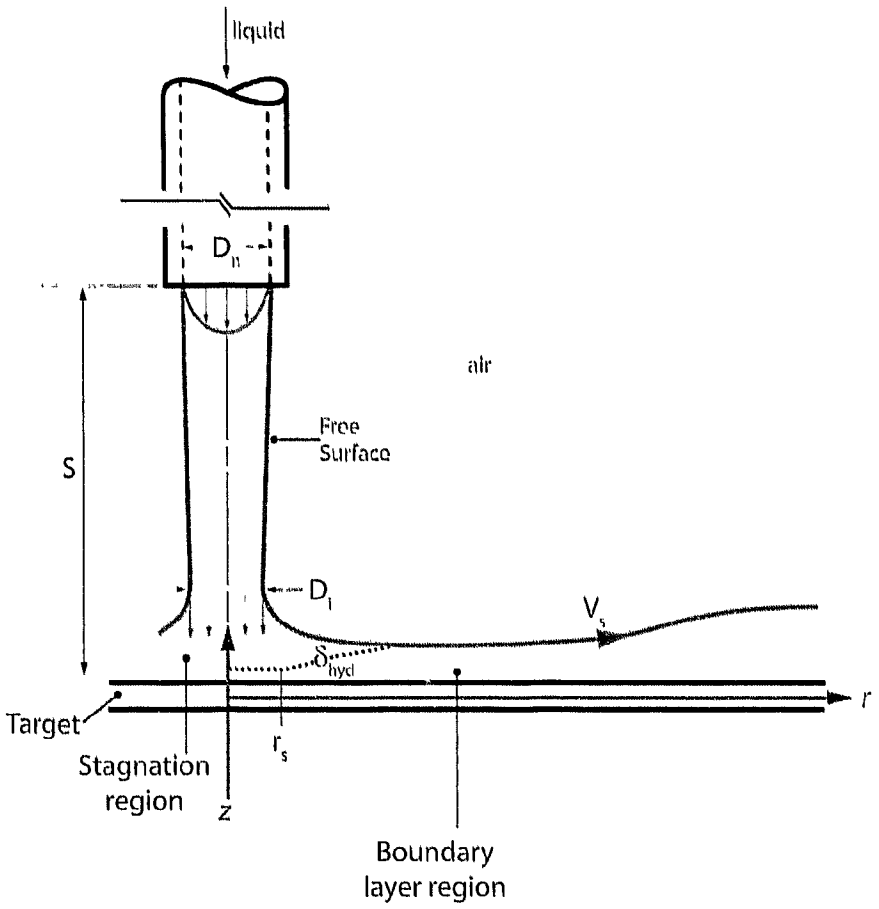
liquid
D_n
air
S
Free
Surface
D_j
V_s
δ_{hyd}
r
Target
Stagnation
region
r_s
z
Boundary
layer region

Figure 1

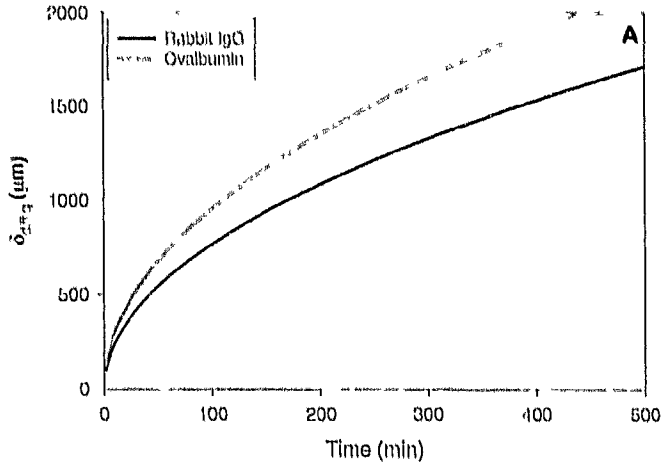
2000
1500
1000
500
0
Rabbit IgG
Ovalbumin
A
0
100
200
300
400
500
Time (min)

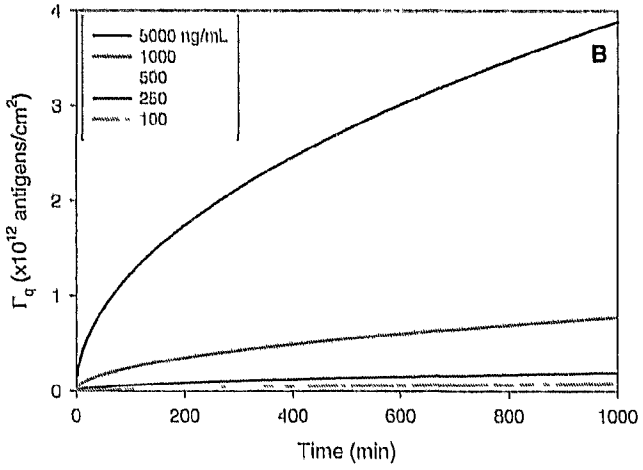
5000 ng/mL
1000
500
250
100
B
Γq (x10^12 antigens/cm^2)
0
1
2
3
4
0
200
400
600
800
1000
Time (min)

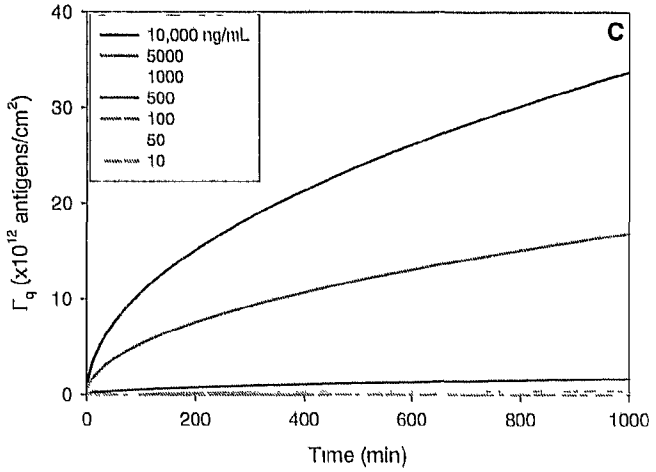
10,000 ng/mL
5000
1000
500
100
50
10
C
Γq (x10^12 antigens/cm^2)
0
10
20
30
40
0
200
400
600
800
1000
Time (min)

Figure 2

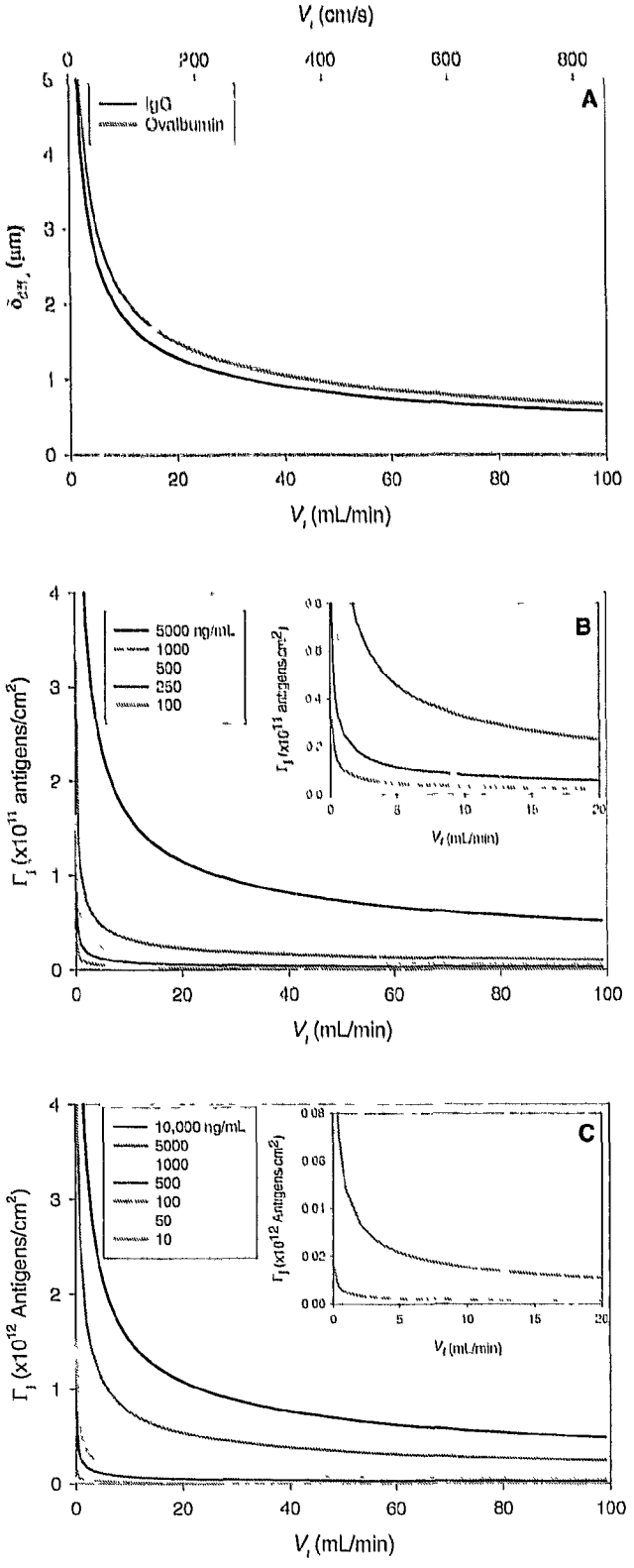
V_t (cm/s)
0
200
400
600
800
IgG
Ovalbumin
A
δ_{eff} (μm)
V_t (mL/min)
5000 ng/mL
1000
500
250
100
B
Γ_1 (x10^{11} antigens/cm^2)
10,000 ng/mL
5000
1000
500
100
50
10
C
Γ_1 (x10^{12} Antigens/cm^2)

Figure 3

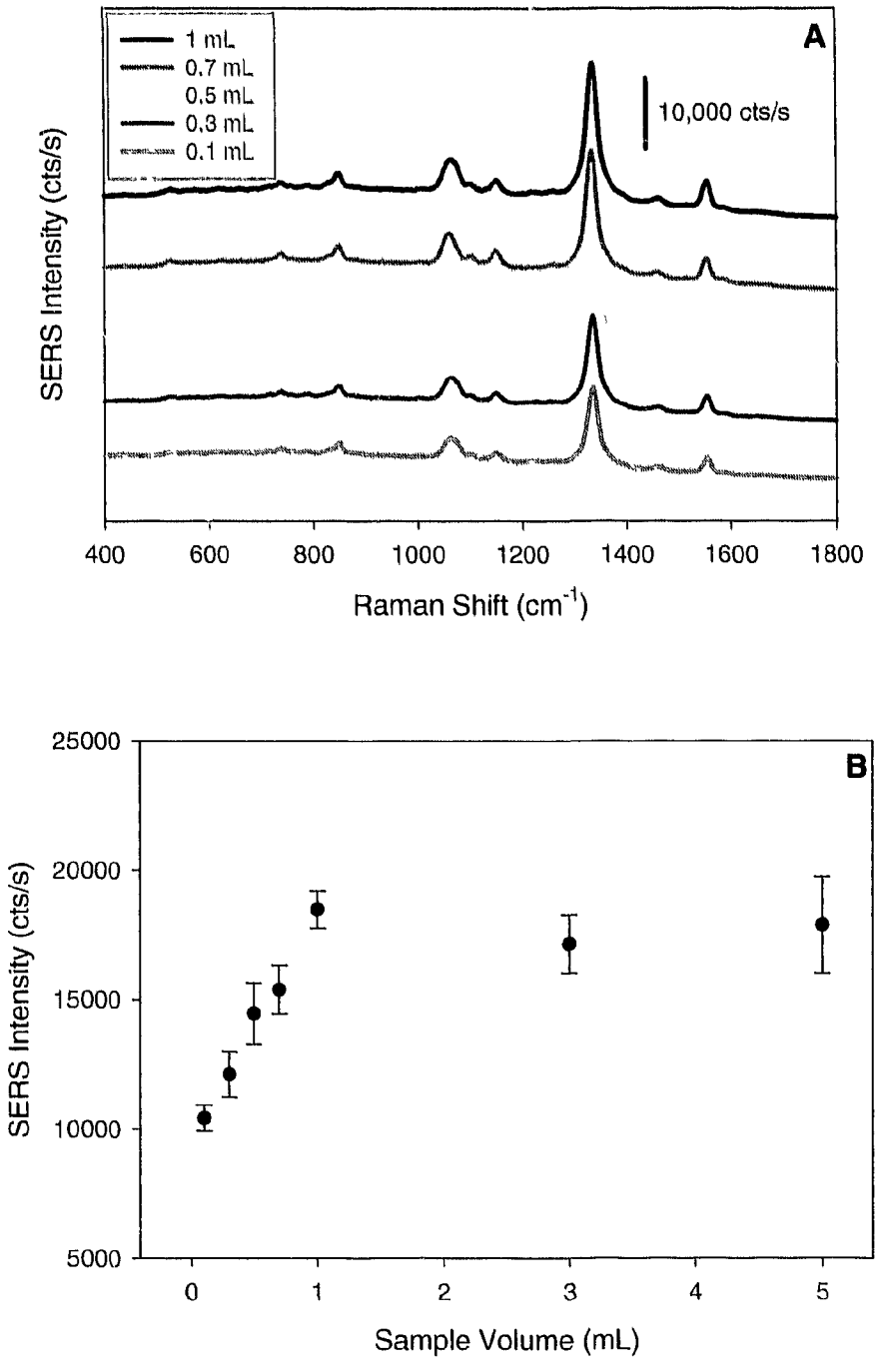
A
1 mL
0.7 mL
0.5 mL
0.3 mL
0.1 mL
10,000 cts/s
SERS Intensity (cts/s)
400
600
800
1000
1200
1400
1600
1800
Raman Shift (cm-1)
B
25000
20000
15000
10000
5000
SERS Intensity (cts/s)
0
1
2
3
4
5
Sample Volume (mL)

Figure 4

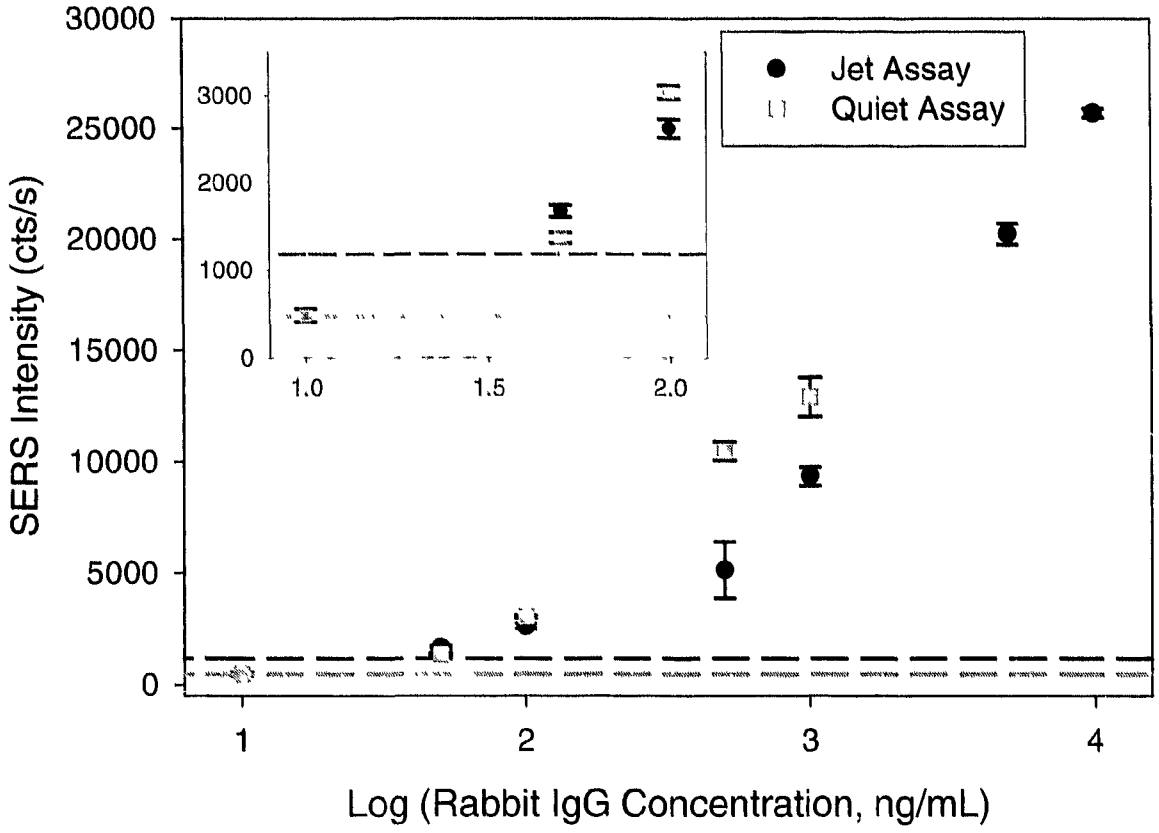
30000
25000
20000
15000
10000
5000
0
SERS Intensity (cts/s)
1
2
3
4
Log (Rabbit IgG Concentration, ng/mL)
Jet Assay
Quiet Assay
3000
2000
1000
0
1.0
1.5
2.0

Figure 5

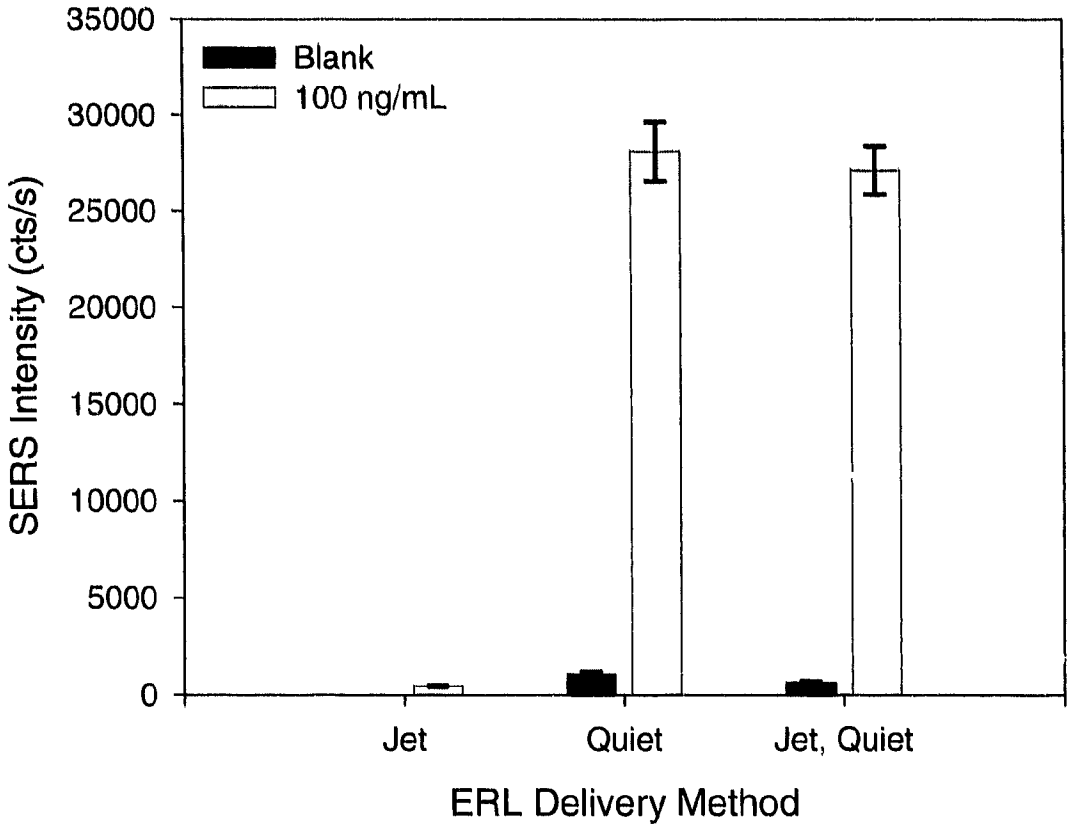
35000
30000
25000
20000
15000
10000
5000
0
SERS Intensity (cts/s)
Blank
100 ng/mL
Jet
Quiet
Jet, Quiet
ERL Delivery Method

Figure 6

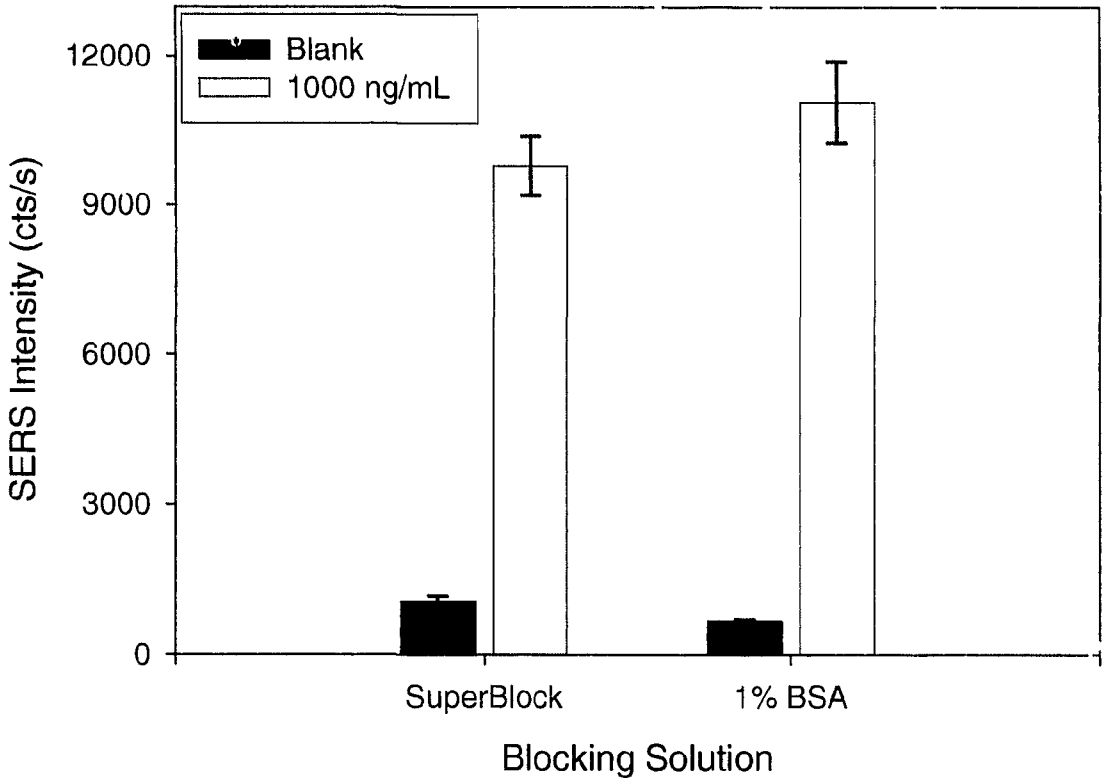
Blank
1000 ng/mL
12000
9000
6000
3000
0
SERS Intensity (cts/s)
SuperBlock
1% BSA
Blocking Solution

Figure 7

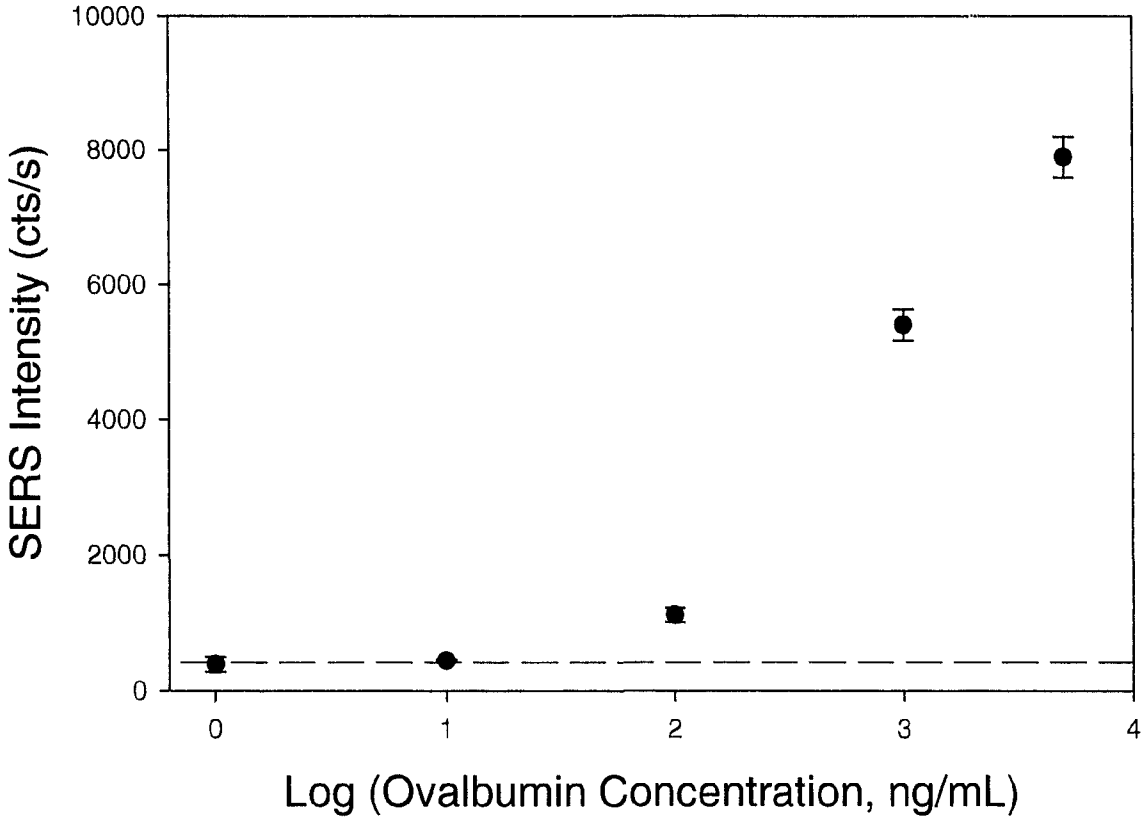
10000
8000
6000
4000
2000
0
SERS Intensity (cts/s)
0
1
2
3
4
Log (Ovalbumin Concentration, ng/mL)

Figure 8

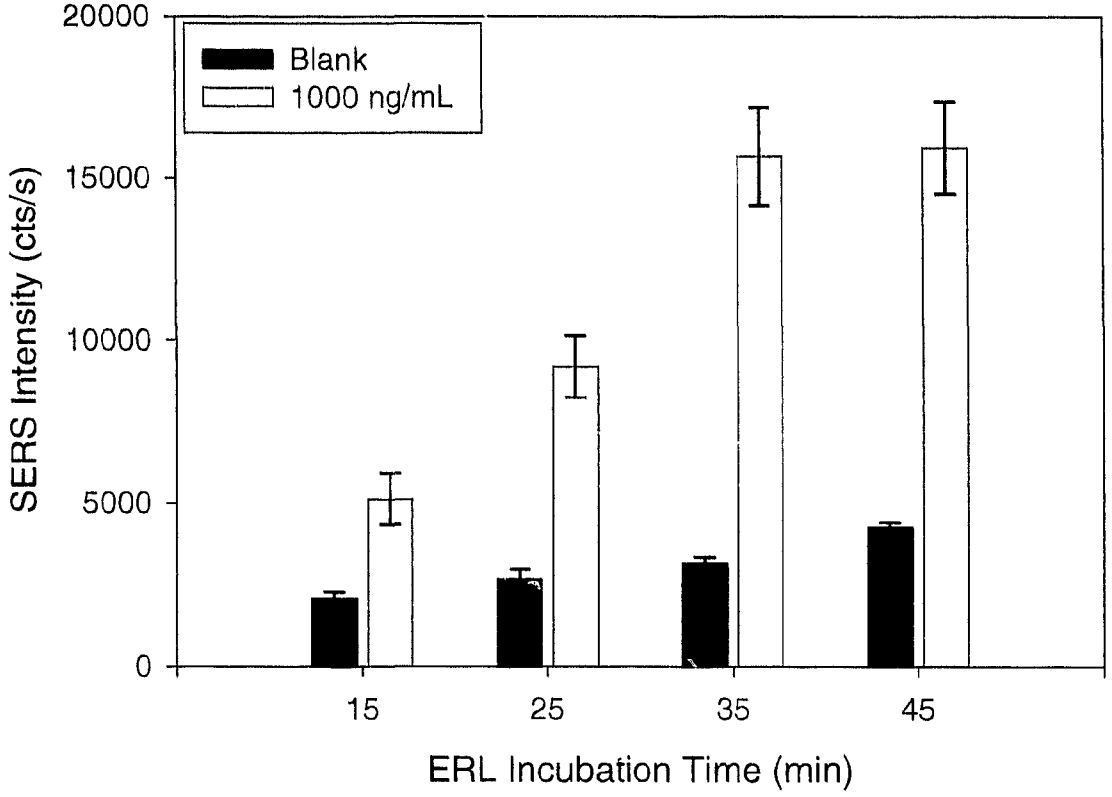
20000
15000
10000
5000
0
SERS Intensity (cts/s)
Blank
1000 ng/mL
15
25
35
45
ERL Incubation Time (min)

Figure 9

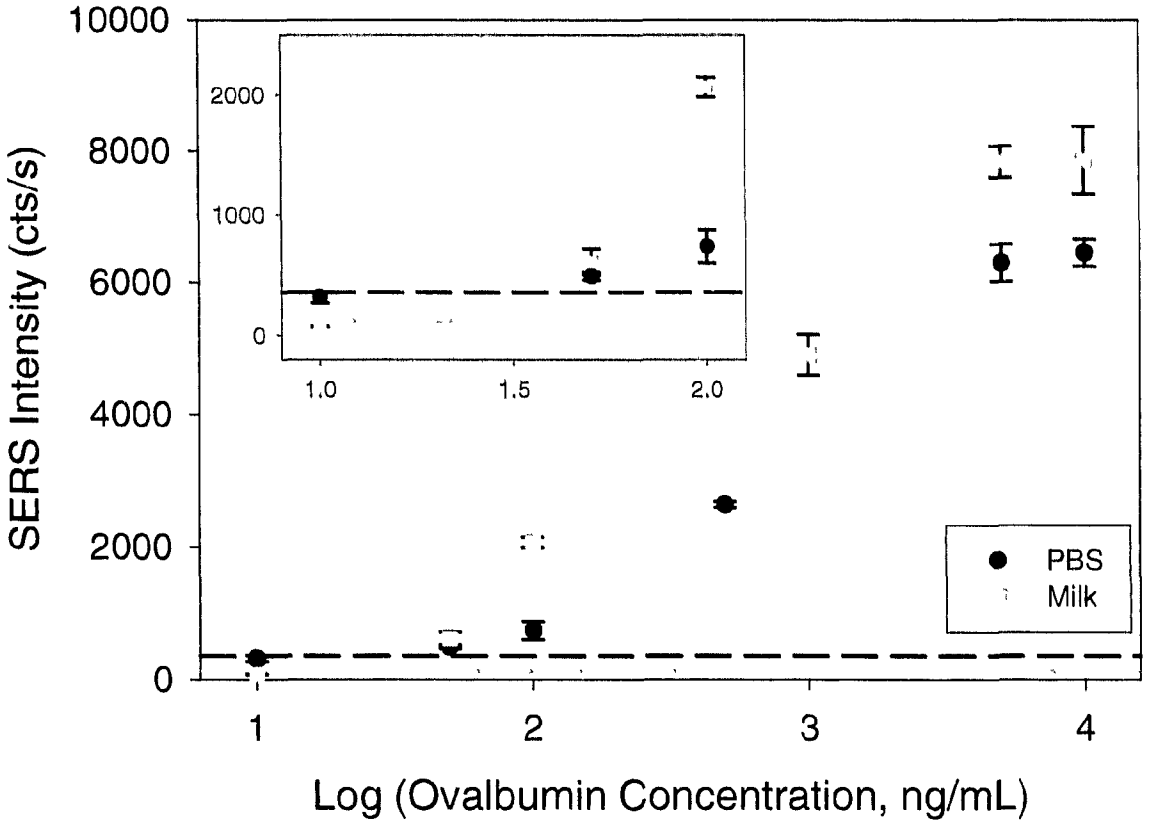
10000
8000
6000
4000
2000
0
SERS Intensity (cts/s)
1
2
3
4
Log (Ovalbumin Concentration, ng/mL)
2000
1000
0
1.0
1.5
2.0
PBS
Milk

Figure 10

CHAPTER 4: IMMUNOASSAY INCUBATION BY FREE LIQUID JET: EFFECT OF ANTIGEN AND LABEL SIZE

A manuscript in preparation for submission to *Langmuir*

Jill M. Uhlenkamp[1,2] and Marc D. Porter[1]*

[1]Center for Combinatorial Sciences, the Biodesign Institute, and the Department of Chemistry and Biochemistry, Arizona State University, Tempe, AZ 85287-6401

[2]Institute for Combinatorial Discovery, Departments of Chemistry and Chemical and Biological Engineering, Ames Laboratory-U.S. DOE, Iowa State University, Ames, Iowa 50011-3020

Abstract

Current methods employed for viral pathogen detection often lack the full complement of characteristics (e.g., specificity, sensitivity, speed, simplicity, and low cost) needed for widespread applicability to early disease diagnosis and detection of agents of bioterrorism. Immunoassays have many of these traits but frequently suffer from long incubation times by reliance on diffusional mass transport to deliver antigen and label to a solid substrate. The effect of antigen size will be investigated as we extend the use of a free liquid jet, reported previously for the delivery of proteins such as IgG and ovalbumin in a

sandwich assay, to virus delivery. Label delivery by jet will also be explore by varying gold nanoparticle size used for the construction of immunoassay labels employed in surface-enhanced Raman scattering (SERS)-based readout.

Introduction

Immunoassays are an important tool in the diagnosis of human and animal disease and for the detection of agents of biowarfare.[1,2] As such, improvements in speed, cost, sensitivity, accuracy, and portability are continually sought. The methods most often applied to viral pathogen detection, however, often do not meet all of these needs. These techniques include enzyme-linked immunosorbent assay (ELISA), polymerase chain reaction (PCR), electron microscopy, virus isolation, and serologic testing.[3,4] One serious drawback of many of these modes of detection is lengthy incubation steps required due to reliance on diffusional mass transport to solid substrates in heterogeneous assays. This problem is exacerbated as diffusion coefficients for large biological targets such as viruses, bacteria, and proteins are relatively small (e.g., 10^{-7} cm^2/s).

We have recently described detection of viral pathogens with a label-free heterogeneous immunoassay and atomic force microscopy (AFM) readout.[5] This method employed capture substrate rotation to increase flux of antigen, thereby decreasing incubation times from 12-24 h employed in quiet solution assays to 10 min. While this result was a dramatic improvement over assays employing static conditions, additional reductions in incubation times could further increase the utility of these assays.

Another avenue to incubation time reduction that we have reported on is the use of a free liquid jet for the delivery of antigen and label in heterogeneous, sandwich-type

immunoassays. [7] Free liquid jets are frequently used in the cooling of electronic equipment, lasers, and metal and plastics manufacturing to achieve a very thin, immobile layer of liquid on a surface (i.e., hydrodynamic boundary layer) which offers very low resistance to heat flow.[8-11] Similarly, applying free liquid jets to immunoassays decreases the thickness of the diffusion layer (δ_{diff}) compared to that of stagnant solution and increases the flux of analyte and label to the substrate. Figure 1 depicts the hydrodynamic boundary layer resulting from free liquid jet impingement. In our studies with proteins, the use of free liquid jet for analyte and label delivery led to the reduction in incubation times from 8-12 h to just 3 s or less.[6, 7]

We have now used free liquid jet delivery for capture of a virus to extend the usefulness of this technique beyond capture and labeling with protein. Porcine parvovirus (PPV) was used as a model virus for capture via free liquid jet delivery in a sandwich immunoassay. PPV is a 25-nm diameter spherical virus with a capsid consisting of 60 copies of a viral protein.[12] Labeling of captured PPV was accomplished with extrinsic Raman labels (ERLs), described in previous works with SERS-based readout.[13-17] Thus, an assay employing capture of PPV by jet was compared to that from quiet solution.

Additionally, the effect of delivery by jet of several sizes of ERLs was also explored. Past work with jet delivery of 60-nm diameter ERLs did not accomplish levels of labeling comparable to those employing stagnant solution incubations. Since the successful capture of PPV demonstrates that jet delivery can be applied to analytes larger than proteins, ERLs constructed of different sized nanoparticles (i.e., 20, 40, 60, and 80 nm) were tested for labeling captured rabbit IgG to investigate a means for SERS-based labeling by jet.

Experimental Section

Reagents. PPV (titer: 3.2 x 10^9 $TCID_{50}$/mL) was obtained from the National Animal Disease Center (NADC). In previous work, we determined the conversion factor from $TCID_{50}$/mL to number of virus particles/mL to be ~1400 virus particles/$TCID_{50}$.[5] Monoclonal anti-PPV antibodies, also provided by the NADC, were purified to 99.9% with a protein G column (Bio-Rad) and stored in 10 mM PBS.

Gold nanoparticles with diameters of 20, 40, 60 and 80 nm (<8% variation) and concentrations of 7.0 x 10^{11}, 9.0 x 10^{10}, 2.6 x 10^{10}, and 1.1 x 10^{10} particles/mL, respectively, were acquired from Ted Pella. Octadecanethiol (ODT), dithiobis(succinimidyl propionate) (DSP), bovine serum albumin (BSA) and PBS packs (10 mM, pH 7.2) were purchased from Sigma. SuperBlock and BupH Borate Buffer Packs (50 mM, pH 8.5) were obtained from Pierce. DSNB [5,5'-dithiobis(succinimidyl-2-nitrobenzoate)] was synthesized according to a previously published procedure.[15] Buffer solutions were passed through a Steri-Cup GP Filter Unit (Millipore) with a 0.22-μm pore size.

Polyclonal goat anti-rabbit IgG antibody, purified prior to receipt by immunoaffinity chromatography, and whole molecule rabbit IgG were acquired from US Biological. The solution of polyclonal goat anti-rabbit IgG was provided as 0.5 mg/mL in PBS (pH 7.2) and contained 0.01% (w/v) sodium azide and 40% (v/v) glycerol. Whole molecule rabbit IgG was supplied purified by Protein A affinity chromatography and purchased at 10 mg/mL in PBS (pH 7.2). All rabbit IgG and PPV solutions were prepared by dilution with 10 mM PBS, which was also used as sample blanks.

Capture Substrate Preparation. Gold-coated glass slides (1 cm x 1 cm) were used to construct immunoassay capture substrates. These slides were prepared by the resistive evaporation of first, a ~10-nm layer of chromium at 0.1 nm/s and, next, a ~300-nm layer of 99.9% pure gold at 0.1-0.2 nm/s using an Edwards 306A resistive evaporator. Prior to the deposition of chromium and gold, the glass squares were cleaned with Contrad 70 (Decon Labs).

Poly(dimethyl siloxane) (PDMS, Dow Corning) was used to create microcontact printing stamps for depositing a hydrophobic barrier for reagent localization. A PDMS stamp with a 3-mm diameter hole cut in its center was soaked in 1-mM ODT in ethanol and dried with high purity nitrogen.[18-20] The gold-coated glass squares were then "stamped" for 20 s, rinsed with ethanol, and dried under a stream of high purity nitrogen. Next, a DSP-derived monolayer was formed in the uncoated gold address by immersion in a 0.1-mM ethanolic solution of DSP for ~12 h followed by rinsing with ethanol and drying with high purity nitrogen.

Next, 20.0 μL of antibody, diluted to 100 μg/mL with 50 mM aqueous borate buffer (pH 8.5), was pipetted onto the center of the substrate and allowed to react for 8-12 h in a humidity chamber at room temperature. The free amines of the antibody covalently couple to the terminal succinimidyl ester of the DSP-based monolayer. The substrate was then briefly immersed three times in 2 mL of fresh 10 mM PBS to remove unreacted antibody. After rinsing, 20.0 μL of SuperBlock was pipetted onto the capture surface. Finally, the substrates were rinsed as described above after an 8-12 h exposure to the blocking solution.

SERS Label Preparation. ERLs are designed to package immunospecificity and large Raman signals. The latter entails use of a DSNB-derived Raman reporter, which has an

intrinsically strong Raman scattering cross-section from its symmetric nitro stretch, ($\nu_s(NO_2)$). DSNB also has the ability to chemisorb to gold nanoparticles and subsequently covalently immobilize antibodies via succinimidyl ester chemistry, which achieves the former. Moreover, this design maximizes the surface enhancement as it minimizes the distance between the Raman scattering mode and the gold nanoparticle.

To create ERLs, the pH of a 1.0 mL suspension of gold nanoparticles is first adjusted to 8.5 by the addition of 40.0 μL of 50 mM aqueous borate buffer. This pH encourages the deprotonation of the free amines of antibodies added later for coupling to the succinimidyl esters of DSNB. Next, 10.0 μL of 1.0-mM DSNB in acetonitrile was added to the nanoparticle suspension. After ~8-12 h of reaction, 20 μg of antibody was added and the suspension was allowed to incubate overnight. To block unreacted succinimidyl ester groups, 100.0 μL of 10% BSA in 2 mM aqueous borate buffer was added and allowed to react for 3-8 h. Following incubation with BSA, centrifugation was performed to remove unreacted DSNB and antibody. Centrifugation was performed at 2000*g* for 10 min for 60- and 80-nm particles and at 10,000*g* for 20 min for 20 and 40 nm particles. The supernatant was removed and the nanoparticles were resuspended in 1.0 mL of 2 mM aqueous borate buffer with 1% BSA. This process was repeated two more times and the final volume was adjusted to give the desired concentration. Next, concentrated NaCl was added to bring the final salt concentration to 150 mM, imitating physiological conditions. Finally, the suspension was passed through a 0.22-μm syringe tip filter (Costar) to remove aggregates.

Assay Protocol. Samples of PPV were delivered by a syringe pump (PHD2000, Harvard Apparatus). The jet nozzle was defined by PEEK tubing (Upchurch Scientific) with 0.5-mm internal diameter that was attached to a syringe by standard fluidic adapters and

positioned 3 mm from the sample surface. All PPV samples delivered by jet were 0.5 mL. Following PPV delivery, substrates were rinsed by three successive immersions in 2.0 mL of fresh 10 mM PBS. Labeling was achieved in quiet solution with 20.0-μL aliquots of ERLs (5.2×10^{10} ERL/mL) exposed for the times indicated. These samples were then rinsed with 2 mM aqueous borate buffer with 150 mM NaCl as described above. The rabbit IgG and PPV samples used in quiet solution assays were 20.0-μL aliquots with exposure times noted. Rinsing for these substrates was performed as described above.

Prior to delivery of ERLs of varied size by jet, substrates were exposed to 20.0 μL samples of 1000 ng/mL via stagnant solutions for 8 h. Quiet solution and jet-based delivery of various sizes of ERLs were completed as described above for PPV samples with 20.0-μL and 0.5-mL samples of ERLs used for quiet and jet exposures, respectively. To facilitate SEM imaging, the samples were chemically fixed with glutaraldehyde, which forms cross-links between neighboring proteins by formation of methylene bridges via the free amine groups.[21] Fixation was necessary in order to allow for rinsing with water, to remove salt residues left by buffer rinses. To this end, samples to be imaged were rinsed as described above and then exposed to 20.0 μL of 10% (v/v) glutaraldehyde in water for 30 min after ERL exposure. The substrates were then rinsed by two successive immersions in 2 mL of fresh 2 mM aqueous borate buffer with 150 mM NaCl, and finally with a gentle stream of deionized water.

Instrumentation. (i) SERS Measurements. Raman spectra were collected with a NanoRaman I (Concurrent Analytical) employing a 30-mW, 632.8-nm He-Ne laser with incident power of 2-3 mW. The spectrograph is comprised of a modified f/2.0 Czerny-Turner imaging spectrometer and has a resolution of 6-8 cm^{-1}. The laser light is focused on the

surface to a 25-μm spot using an objective with a numerical aperture of 0.68, and the scattered light is collected with the same objective. A thermo-electrically cooled (0°C) Kodak 0401E CCD was used. All spectra were collected with an integration time of 1 s unless otherwise noted.

(ii) Scanning Electron Microscopy (SEM). SEM images were acquired using a Philips FEI XL30 ESEM FEG Environmental scanning electron microscope. Samples were sputter coated with ~100 Å of gold prior to imaging. An accelerating voltage of 25 kV was used. The images were collected from secondary electrons.

Results and Discussion

PPV assay by jet. Free liquid jet delivery was first compared to quiet solution exposure for PPV incubation at a single concentration, 3.2×10^7 $TCID_{50}$/mL. A 0.5-mL sample of PPV in PBS and a 0.5-mL blank sample were each delivered to a capture substrate at 10.0 mL/min. Since ERL delivery by jet proved only partially effective in work with IgGs,[6] and we subsequently found a similar problem with anti-PPV ERLs (data not shown), these samples were labeled with a 20.0-μL aliquot of anti-PPV ERLs for 16 h via quiet solution. For comparison, 20.0-μL samples of the PPV and blank solutions were exposed to capture substrates for 9 h, followed by labeling with 20.0 μL of ERLs for 16 h, both via quiet solution. These data are shown in Figure 2. Representative spectra for each of the four samples are shown in Figure 2a with SERS intensity plotted versus Raman shift. Spectral features characteristic of the DSNB-based Raman reporter molecule are clearly evident.[15] The most prominent band is at 1336 cm^{-1}, which arises from $\nu_s(NO_2)$. The intensities of this feature for the 3.2×10^7 $TCID_{50}$/mL PPV samples, delivered by jet and in quiet solution, are

plotted in Figure 2b. The responses for the blank samples are not discernable from the measurement noise. While lower than that from quiet solution, the signal for the sample with jet delivery is significantly higher than that of the blank, indicating that PPV incubation can be accomplished by jet delivery. We note that the signals result from the specific capture of PPV since substrates exposed to other species (e.g., feline calicivirus) did not result in intensities greater than those of blank samples.

Next, an assay for PPV in PBS at a range of concentrations was performed in order to construct a dose-response curve. Five samples, ranging from 6.4×10^5 to 6.4×10^7 $TCID_{50}$/mL, and a PBS blank were used. Each 0.5-mL sample was delivered by jet at 10.0 mL/min. Labeling was achieved by 16-h quiet solution exposure of 20.0 μL aliquots of anti-PPV ERLs. The resulting dose-response curve is shown in Figure 3. Each point represents the average signal of five spectra collected with 1-s integrations at different locations on the capture substrate and the error bars correspond to the standard deviation of the measurements. The average signal measured for the blank sample was 92±8 cts/s. If we define the LOD by the concentration that would yield a signal equal to that of the blank plus three times its standard deviation (116 cts/s), these results yield an LOD of 4×10^5 $TCID_{50}$/mL. In comparison, the LOD achieved with quiet solution assays utilizing 12-h exposures of 20.0-μL each of PPV and ERLs was 2×10^7 $TCID_{50}$/mL (data not shown).[22] Jet-based delivery of PPV therefore results in lower LODs than those for quiet solution assays while simultaneously decreasing the incubation time by a factor of 14,400.

ERL delivery by jet. The success of PPV capture shows that incubation by jet delivery can be realized for objects larger than proteins (e.g., IgG and ovalbumin). In a previous work, 60-nm diameter ERLs were delivered by jet to label captured rabbit IgG, with

very low levels of ERL binding observed.[6] The level of bound ERLs was comparable to that which is seen due to non-specific binding (i.e., the signal from a blank sample) when quiet exposure of ERLs is employed.

One factor considered that could prevent the binding of ERLs by jet is the large size (60 nm diameter) compared to the size of an IgG protein (14.5 nm x 8.5 nm x 4.0 nm).[23] The force experienced by an object in flowing liquid is proportional to its diameter.[24] At issue then is whether the impact of a 60-nm diameter ERL is large enough to overcome the binding force of the interaction with captured antigen. Since the success of PPV (25 nm diameter) capture by jet shows that objects larger than 10 nm can be used with this technique, ERLs of a comparable size (i.e., 20-nm diameter) were studied with respect to delivery by jet and compared to the performance of larger ERLs (40-, 60-, and 80-nm diameter).

To explore the effect of ERL size on labeling efficiency via jet delivery, gold nanoparticles with diameters of 20, 40, 60, and 80 nm were used to construct anti-rabbit-coated ERLs, all at a final concentration of 5.2×10^{10} ERL/mL. Anti-rabbit IgG capture substrates were exposed to 20.0-μL aliquots of 1000 ng/mL rabbit IgG in PBS for 8 h. After rinsing, half of the capture substrates were exposed to ERLs by jet and half were exposed to ERLs via quiet solution. Quiet solution studies employed 20.0 μL of ERLs and incubations of 16 h. The jet studies delivered 0.5 mL of ERLs at 10.0 mL/min for an incubation time of 3 s. Fixing with glutaraldehyde, as outlined above, was used to allow for rinsing with water to facilitate SEM. SEM images were collected at five locations on each substrate and representative images for each ERL size are shown for both cases in Figure 4. For all exposures of ERLs via quiet solution (Figures 4A-D), a large number of objects, with dimensions characteristic of the ERLs employed, bound to the captured IgG. In contrast, the

micrographs in Figures 4E-H reveal that very few ERLs label bound IgG when delivered by jet. It appears evident that, regardless of size, jet-based ERL exposure cannot equal the level of labeling acquired via quiet solution.

The ERLs in each image were enumerated and the number was extrapolated to the number bound per 3-mm diameter capture area. Those data are shown in Figure 5 in which the average number of ERLs per capture area from five images is plotted and the error bars represent the standard deviation. There were no detectable 20-nm ERLs in the images for jet delivery. The number of ERLs captured in the jet experiments are roughly equal for 40-, 60-, and 80-nm diameter ERLs. Like that for jet delivery, the number of ERLs per capture area is roughly equivalent for all sizes tested with the exception of the 40-nm ERLs. The reason for this in unknown but may relate to poor performance of fixing for this sample, resulting in loss of bound ERLs upon water rinsing.

Nonetheless, the results indicate that delivery by jet is only marginally effective for any of the investigated anti-rabbit ERL concentrations and sizes. Additionally, 60-nm anti-PPV ERLs did not successfully label captured PPV when delivered by jet (results not shown). Because capture of PPV via jet was achieved while labeling with 20-nm ERLs proved difficult, it is apparent that the size of the object, has only a small (if any) impact on the ability of an object to bind to its target through jet exposure.

There are, however, important differences in the surface characteristics of the viruses and the ERLs. As mentioned above, PPV has a capsid consisting of 60 copies of a viral protein, and the antibody used in these studies is a monoclonal antibody against that protein. In contrast, ERLs are constructed with polyclonal goat anti-rabbit IgG antibodies and these antibodies are in various orientations on the surface of the gold nanoparticle. It is possible

that PPV successfully binds by jet because the correct orientation for binding to anti-PPV (assuming the anti-PPV antibody is tethered to the surface in such a way that it is active) is more probable. The anti-rabbit ERLs, on the other hand, may have only a portion of surface bound antibodies in active orientations and these antibodies may come into contact with epitopes on surface bound rabbit IgG against which they are not specific. Furthermore, PPV is exposed to a capture substrate, whereas ERLs target captured analyte, which would only occupy a portion of the original capture sites on the substrate. There are therefore fewer binding sites available to ERLs than PPV. Further studies are needed to investigate these hypotheses to understand the reason for the lack of ERL labeling by jet.

As mentioned above, the drag force on an ERL may be enough to overcome the initial interactions between the antibodies on the ERL and the captured IgG protein. This could be less of a factor for the PPV assay because the interaction between anti-PPV and PPV may be stronger. This stronger interaction, however, may be overcome in the case of anti-PPV ERL labeling captured PPV as the force would be greater on the larger ERL. Further studies are needed to understand whether the force on the object delivered by jet is a factor in binding, and to what extent. Also, studies with ERLs of different sizes constructed with anti-PPV may clarify the roles of size and antibody-antigen interaction strength on the success of binding with jet delivery.

Conclusions

We have demonstrated the use of a free liquid jet for incubation of PPV in a sandwich immunoassay. This technique allowed for the capture of PPV from 0.5-mL samples in 3 s, which represents a reduction of over 14,000-fold in incubation time from an assay relying on

diffusional mass transport. SERS readout was employed for an immunoassay for PPV with jet incubation, resulting in an LOD of 4 x 10^5 $TCID_{50}$/mL which betters LODs achieved in quiet solution assays. As we have shown in previous work, readout for an assay for PPV can also be achieved by atomic force microscopy (AFM) without a labeling step,[5] therefore a total incubation time of only 3 s could potentially be realized in an assay for PPV.

We have also determined that size is not the only factor precluding the use of jet delivery for ERLs. This result may lead to an improved design for ERLs, allowing for delivery by jet and for the completion of SERS-based sandwich-type immunoassays in under 1 minute. One possible way to increase the likelihood for ERL binding by jet may be to use antibody fragments to raise the probability that a favorable interaction will occur when delivered to the substrate surface.

Acknowledgements

This work was supported through grants from CEROS-DARPA and the NADC and by the Institute for Combinatorial Discovery of Iowa State University and the Biodesign Institute at Arizona State University. The Ames Laboratory is operated for the US Department of Energy through Iowa State University under contract No. W7405-eng-82. We gratefully acknowledge the use of facilities within the Center for Solid State Science at Arizona State University.

References

(1) Diamandis, E. P.; Christopoulos, T. K. In *Immunoassay*; Diamandis, E. P., Christopoulos, T. K., Eds.; Academic Press: San Diego, CA, 1996, pp 1-3.

(2) Sokoll, L. J.; Chan, D. W. *Anal. Chem.* 1999, *71*, 356R-362R.

(3) Elnifro, E. M.; Ashshi, A. M.; Cooper, R. J.; Klapper, P. E. *Clin. Microbiol. Rev.* 2000, *13*, 559-570.

(4) Storch, G. A. *Essentials of Diagnostic Virology*; Churchill Livingstone: New York, 2000.

(5) Driskell, J. D.; Kwarta, K. M.; Lipert, R. J.; Vorwald, A.; Neill, J. D.; Ridpath, J. F.; Porter, M. D. *J. Virol. Methods* 2006, *138*, 160-169.

(6) Uhlenkamp, J. M.; Lipert, R. J.; Granger, M. C ; Porter, M. D. *Manuscript in preparation.*

(7) Uhlenkamp, J. M.; Lipert, R. J.; Porter, M. D. *Manuscript in preparation.*

(8) Baonga, J. B.; Louahlia-Gualous, H.; Imbert, M. *Appl. Therm. Eng.* 2006, *26*, 1125-1138.

(9) Fabbri, M.; Dhir, V. K. *J. Heat Transfer* 2005, *127*, 760-769.

(10) Incropera, F. P. *Liquid Cooling of Electronic Devices By Single-Phase Convection*; John Wiley and Sons, Inc.: New York, 1999.

(11) Lienhard, J. H. V. *Annu. Rev. Heat Transfer* 1995, *6*, 199-270.

(12) Simpson, A. A.; Hebert, B.; Sullivan, G. M.; Parrish, C. R.; Zadori, Z.; Tijssen, P.; Rossmann, M. G. *J. Mol. Biol.* 2002, *315*, 1189-1198.

(13) Driskell, J. D.; Kwarta, K. M.; Lipert, R. J.; Porter, M. D.; Neill, J. D.; Ridpath, J. F. *Anal. Chem.* 2005, *77*, 6147-6154.

(14) Driskell, J. D.; Uhlenkamp, J. M.; Lipert, R. J.; Porter, M. D. *Anal. Chem.* 2007, *79*, 4141-4148.

(15) Grubisha, D. S.; Lipert, R. J.; Park, H.-Y.; Driskell, J.; Porter, M. D. *Anal. Chem.* 2003, *75*, 5936-5943.

(16) Ni, J.; Lipert, R. J.; Dawson, G. B.; Porter, M. D. *Anal. Chem.* 1999, *71*, 4903-4908.

(17) Park, H.-Y.; Driskell, J. D.; Kwarta, K. M.; Lipert, R. J.; Porter, M. D.; Schoen, C.; Neill, J. D.; Ridpath, J. F. *Top. Appl. Phys.* 2006, *103*, 427-446.

(18) Chen, C. S.; Mrksich, M.; Huang, S.; Whitesides, G. M.; Ingber, D. E. *Biotech. Prog.* 1998, *14*, 356-363.

(19) Kumar, A.; Whitesides, G. M. *Appl. Phys. Lett.* 1993, *63*, 2002-2004.

(20) Libioulle, L.; Bietsch, A.; Schmid, H.; Michel, B.; Delamarche, E. *Langmuir* 1999, *15*, 300-304.

(21) Lopez, O.; Lopez-Iglesias, C.; Cocera, M.; Walther, P.; Parra, J. L.; de la Maza, A. *J. Struct. Biol.* 2004, *146*, 302-309.

(22) Kwarta, K. M., Iowa State University, Ames, 2007.

(23) Silverton, E. W.; Navia, M. A.; Davies, D. R. *Proc. Natl. Acad. Sci. U. S. A.* 1977, *74*, 5140-5144.

(24) Batchelor, G. K. *An Introduction to Fluid Dynamics*; Cambridge University Press: Cambridge, 2000.

Figure Captions

Figure 1. Schematic of a free liquid jet depicting the hydrodynamic properties of the jet and resulting stagnation and boundary layer regions. Adapted from reference 10.

Figure 2. (A) Representative spectra for each sample, offset for clarity. The top two spectra are from the PPV samples with concentration of 3.2 x 10^7 $TCID_{50}$/mL, and the bottom two are from the blank samples. (B) The SERS intensity of the $\nu_s(NO_2)$ measured for each 3.2 x 10^7 $TCID_{50}$/mL PPV sample. The error bars represent the standard deviation of five measurements taken at different locations on the sample. The signals due to the blank samples are not shown as they were not discernable from the peak-to-peak noise.

Figure 3. Dose-response curve for 0.5-mL samples of PPV in PBS delivered by jet at 10.0 mL/min. Labeling was achieved via 16-h quiet solution exposure of ERLs. The SERS intensity of the $\nu_s(NO_2)$ was measured for each sample at five locations on the capture surface and the average is plotted. The error bars represent the standard deviation of five measurements taken at different locations on the sample. The dashed line represents the limit of detection, defined by the signal of the blank plus three times the standard deviation of the blank signal.

Figure 4. Representative scanning electron micrographs for substrates with captured rabbit IgG labeled by quiet solution for 16 h with 20.0 μL of ERLs (A-D) and by jet at 10.0 mL/min with 0.5 mL of ERLs (E-H); ERLs made with nanoparticles of diameter (A) 80 nm, (B) 60

nm, (C) 40 nm, (D) 20 nm, (E) 80 nm, (F) 60 nm, (G) 40 nm, and (H) 20 nm. The scale bars in each image are 500 nm.

Figure 5. Number of ERLs bound in the capture area by size, for quiet exposure and jet delivery. The error bars represent the standard deviation from five measurements.

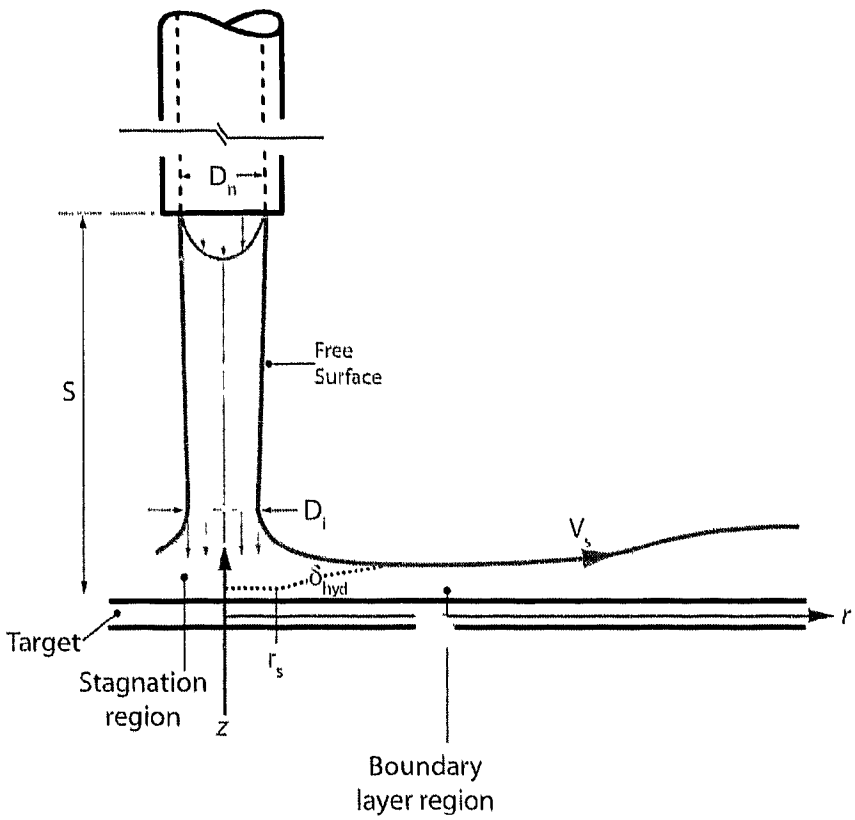
D_n
S
Free
Surface
D_j
V_s
δ_hyd
r
Target
Stagnation
region
r_s
z
Boundary
layer region

Figure 1

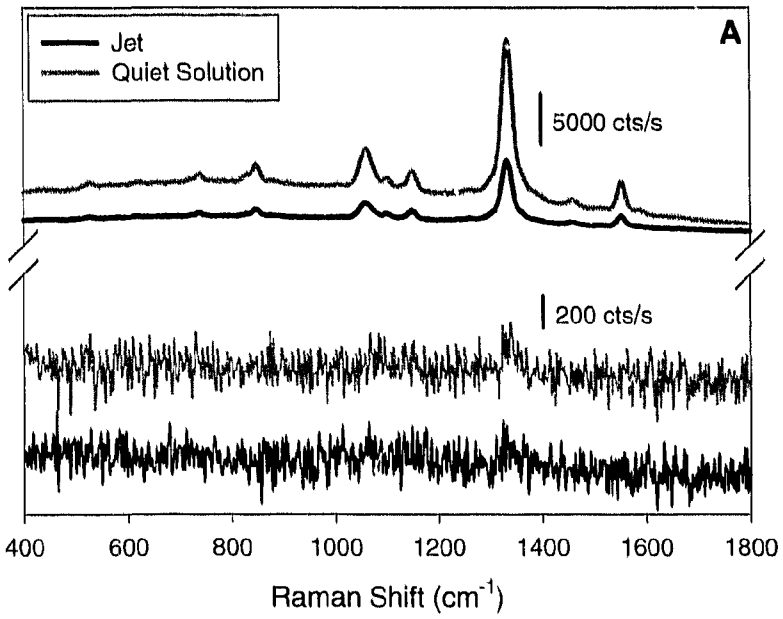
Jet
Quiet Solution
A
5000 cts/s
200 cts/s
400
600
800
1000
1200
1400
1600
1800
Raman Shift (cm-1)

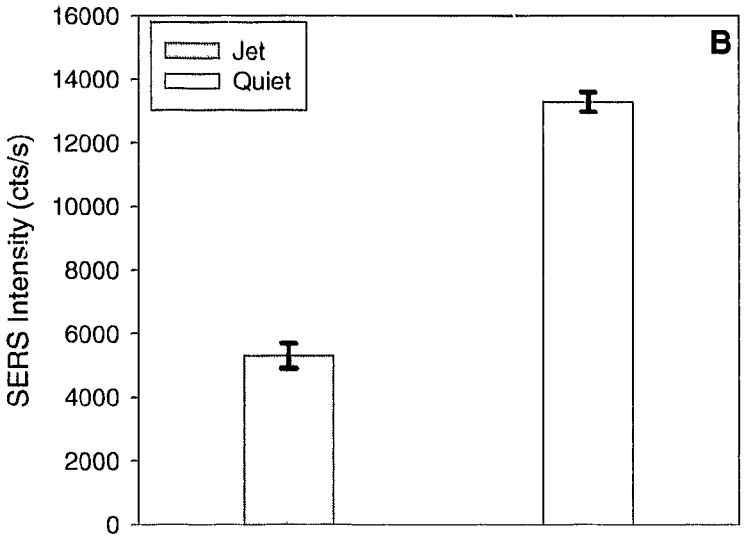
Jet
Quiet
B
SERS Intensity (cts/s)
16000
14000
12000
10000
8000
6000
4000
2000
0

Figure 2

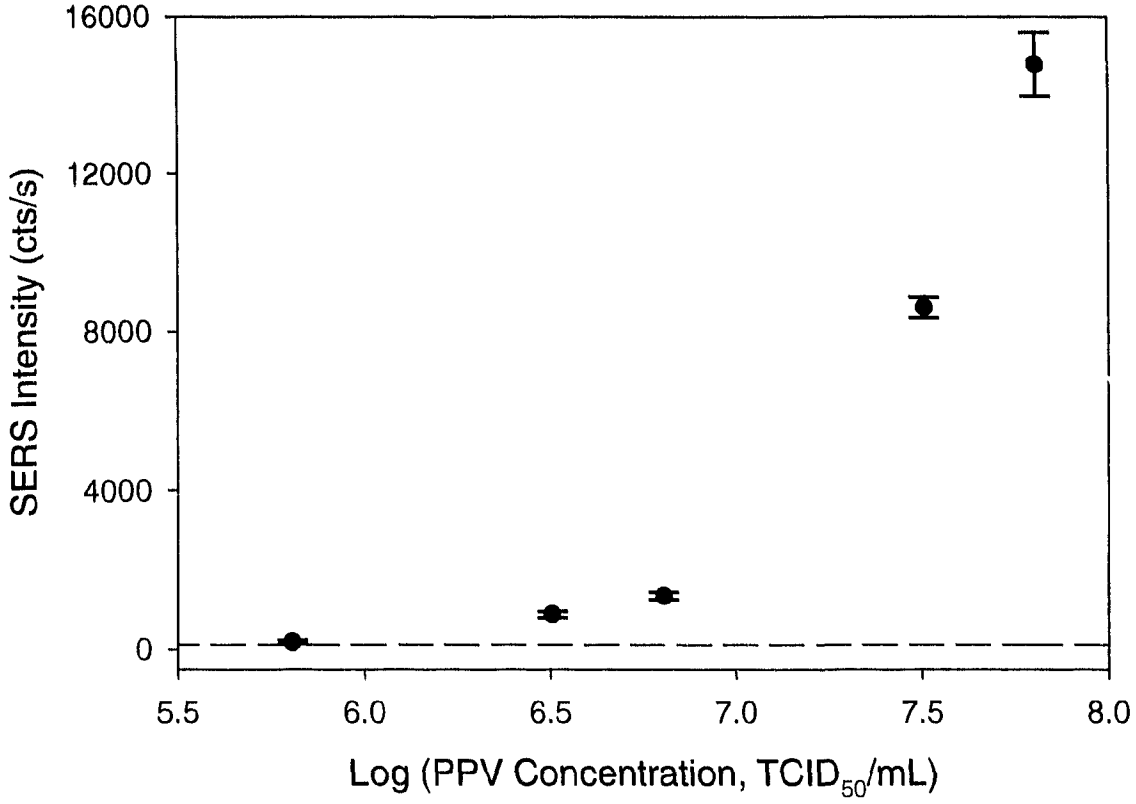
16000
12000
8000
4000
0
SERS Intensity (cts/s)
5.5
6.0
6.5
7.0
7.5
8.0
Log (PPV Concentration, TCID50/mL)

Figure 3

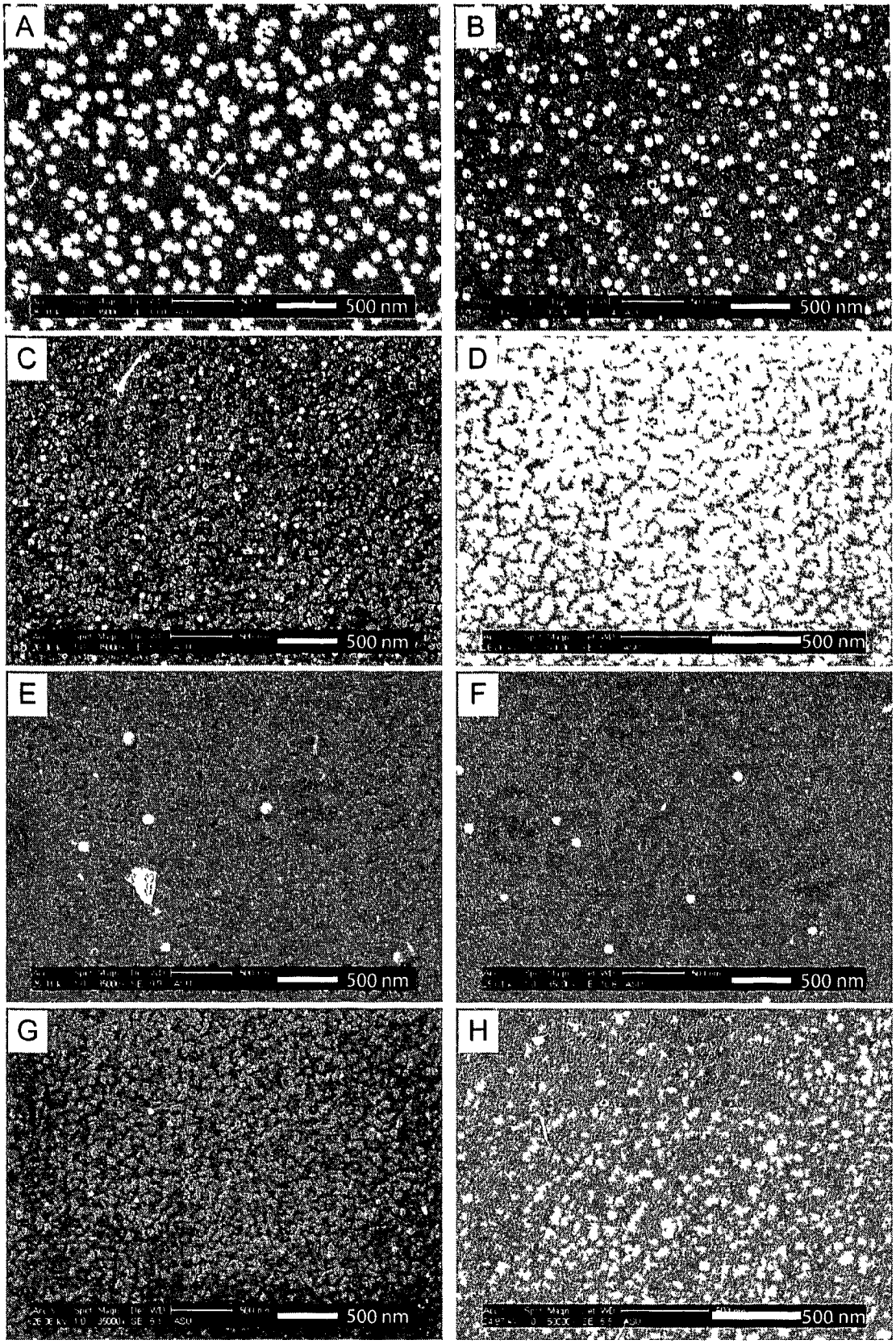

Figure 4

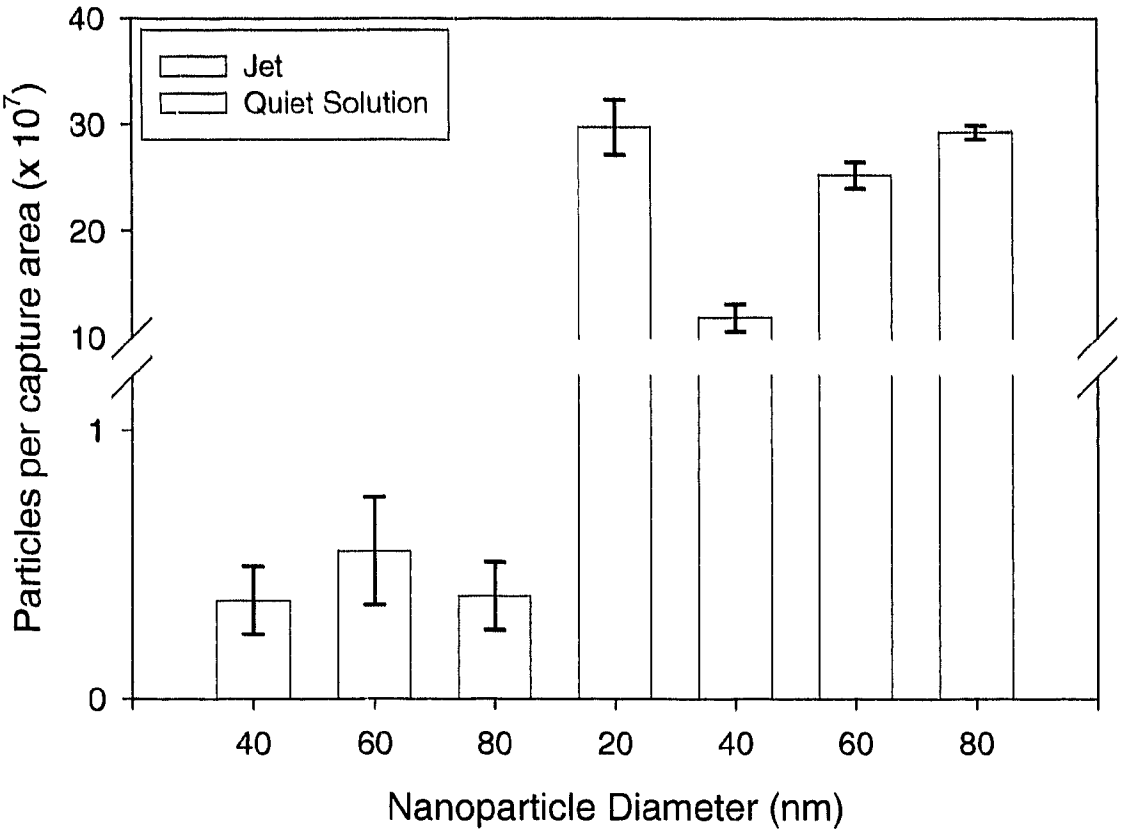
Jet
Quiet Solution
Particles per capture area (x 10^7)
40
30
20
10
1
0
40
60
80
20
40
60
80
Nanoparticle Diameter (nm)

Figure 5

CHAPTER 5: LOW-LEVEL DETECTION OF SHED PROTEIN FROM PATHOGENIC BACTERIA WITH FREE LIQUID JET SAMPLE INCUBATION AND SERS READOUT

A manuscript in preparation for submission to *Analytical Chemistry*

Jill M. Uhlenkamp[1,2] and Marc D. Porter[1,*]

[1]Center for Combinatorial Sciences, the Biodesign Institute, and the Department of Chemistry and Biochemistry, Arizona State University, Tempe, AZ 85287-6401

[2]Institute for Combinatorial Discovery, Departments of Chemistry and Chemical and Biological Engineering, Ames Laboratory-U.S. DOE, Iowa State University, Ames, Iowa 50011-3020

Abstract

A sensitive and rapid heterogeneous sandwich-type immunoassay with free liquid jet sample incubation and SERS readout is applied to the detection of heat-killed *E. coli* O157:H7. Free liquid jet incubation is extremely rapid as a consequence of the development of a very thin (e.g., 1-2 μm) diffusion layer, resulting in increased sample accumulation at the substrate surface. Free liquid jet incubation for 3 s at 10.0 mL/min with 500-μL samples was compared to 8-h quiet solution-based exposure of 20.0-μL sample. The limit of detection

(LOD) for the quiet solution assay was 10^5 cells/mL, while that for the assay employing free liquid jet was less than 1 cell/mL. Evidence for the detection of free protein, shed by the bacteria, is presented and accounts for the very low LOD achieved by free liquid jet sample incubation.

Introduction

The infectious dose of *E. coli* O157:H7 is exceedingly low, about 10-100 cells.[1] *E. coli* O157:H7 produce toxins that damage the intestinal lining and can lead to a life-threatening condition known as hemolytic uremic syndrome (HUS), highlighting the need for rapid, sensitive detection methods for this and numerous other pathogens. The current diagnostic standard for *E. coli* and many other bacteria-based infections is stool culturing, a sensitive but time consuming technique.[2] Outbreaks of *E. coli* O157:H7 infection can also be triggered by consumption of contaminated water, and, while typically problematic in developing countries, have also recently occurred in Canada, and caused six deaths and illness to thousands.[3] The development of sensitive and accurate pathogen detection is therefore requisite for the effective monitoring of water, wastewater, and environmental samples.[4]

Many of the direct, whole organism detection modes that have been developed, however, often lack sensitivity, involve complicated sample preparation, require sophisticated instrumentation, or long assay times. These include potentiometric biosensors,[5, 6] flow injection immunoanalysis,[7] fluorescent nanoparticle labeling,[8] and enzyme-based methods.[9] These techniques often require several hours or have high LODs (e.g., 5×10^7 cfu/ml). There are also several reports on the use of polymerase chain reaction (PCR) for

measurement of *E. coli* O157:H7 and other bacterial pathogens.[10-13] While extremely powerful, the routine use of PCR can be complicated by the occurrence of false positives due to contamination, high cost, and lengthy sample extraction and purification steps.[14] There is, therefore, still a strong need, therefore, for the development of an effective technology that incorporates speed, sensitivity, low cost, and accuracy for disease diagnosis and wastewater treatment monitoring.

Herein, we describe a method to achieve extremely low limits of detection (LOD) for *E. coli* through the use of a heterogeneous sandwich immunoassay with rapid incubation of sample using a free liquid jet and surface-enhanced Raman scattering (SERS)-based detection. This work extends our recent efforts on the use of free liquid jet for sample and, in one case, label delivery,[15-17] which we applied to the detection of IgG, ovalbumin, and porcine parvovirus (PPV) with total assay incubation times (i.e., both sample and label) as short as 6 s and little or no compromise in LOD.

The more common use of free liquid jets has been in cooling in metal and plastics manufacturing, lasers, and electronic equipment.[18-21] Liquid jets have been employed in investigations of heterogeneous electron-transfer reactions.[22-24] In applying a free liquid jet to incubation of sample or label in immunoassays, a hydrodynamic boundary layer is formed at the substrate surface with thickness δ_{hyd} (Figure 1). The thickness of the diffusion layer, δ_{diff}, depends on δ_{hyd} and is greatly reduced from that of quiet solution (e.g. by a factor of ~500). In this way, mass transport is increased, opening a pathway for reductions in incubation times.

The detection of 500-μL samples of heat-killed *E. coli* O157:H7 with free liquid jet incubation was accomplished via SERS readout of extrinsic Raman labels (ERLSs), resulting

in an LOD of less than 1 cell/mL, a 3-s sample incubation step, and a total assay time of ~16 h. ERLs consist of a gold nanoparticle modified with a layer of a Raman reporter molecule, which also forms covalent links to monoclonal or polyclonal antibodies as specific recognition elements. As a basis of comparison to the results from the free liquid jet-based assay, an assay for *E. coli* O157:H7 was performed with 8-h quiet solution incubation of 20.0-μL samples and 24-h total incubation time and resulted in an LOD of 10^5 cells/mL. Evidence is also provided for an enhancement mechanism, in the form of the detection of protein shed from the bacteria, which accounts for the improvement in LOD of over 10^5 via the use of free liquid jet sample delivery.

Experimental Section

Reagents. Gold colloids with 60-nm diameter (2.6×10^{10} particles/mL) were purchased from Ted Pella. Octadecanethiol (ODT), dithiobis(succinimidyl propionate) (DSP), and phosphate buffered saline (PBS) packs (10 mM, pH 7.2) were obtained from Sigma. SuperBlock and BupH Borate Buffer Packs (50 mM, pH 8.5) were acquired from Pierce. All buffers were passed through Steri-Cup GP Filter Units (Millipore).

Polyclonal goat anti-*E. coli* O157:H7 antibody was procured from US Biological as a liquid in PBS and, prior to receipt, was purified by affinity chromatography. Heat killed *E. coli* O157:H7 (10^8 cells/mL in PBS) was generously provided by Nancy Cornick of the Department of Veterinary Microbiology and Preventive Medicine at Iowa State University.

Capture Substrate Preparation. Assay capture substrates were constructed from 1 x 1 cm glass squares, cleaned with Contrad 70 (Decon Labs), coated with thin layers of chromium and gold, and modified with proteins linked by coupling through a DSP-derived

monolayer. First, ~10 nm of chromium was resistively evaporated onto the glass squares at 0.1 nm/s using an Edwards 306A resistive evaporator. Next, ~300 nm of 99.9% pure gold was evaporated at the same rate. An ODT-derived monolayer was then created for the localization of immunoassay reagents. A microcontact printing stamp[25-27] was fabricated from poly(dimethyl siloxane) (PDMS, Dow Corning) with a 3-mm hole cut in its center. The PDMS stamp was soaked in 1 mM ODT for ~1 min, dried under a stream of high purity nitrogen, and exposed for 20 s to a gold-coated glass chip. The substrates were then rinsed with ethanol, dried under a stream of high purity nitrogen, and immersed in a 0.1 mM ethanolic solution of DSP for 12 h to create a DSP-derived monolayer in the bare gold center. The succinimidyl esters at the terminus of the monolayer act to immobilize polyclonal capture antibodies via an amide linkage that forms from the reaction with primary amines of the protein. To this end, 20.0 μL of goat anti-*E. coli* O157:H7, diluted to 100 μg/mL with 50 mM aqueous borate buffer (pH 8.5), was pipetted onto the substrate and allowed to react for 8-12 h in a humidity chamber at room temperature. The substrate was next washed three times by brief immersions in 2 mL of fresh 10 mM PBS. After rinsing, 20.0 μL of SuperBlock buffer was pipetted onto the capture surface to block any unreacted succinimidyl groups. After 12 h, the substrate was again rinsed using the procedure described above.

SERS Label Preparation. ERLs have been designed to give large Raman signals and immunospecificity and as such, were optimized in previous works.[28, 29] ERLs therefore incorporate a DSNB-derived reporter, which has an intrinsically strong Raman scatterer in the form of a symmetric nitro stretch, $\nu_s(NO_2)$. The DSNB-based moiety also serves to couple monoclonal or polyclonal antibodies through succinimidyl ester chemistry, which imparts molecular specificity toward the antigen.

The first step in the assembly of ERLs is to alter the pH of a 1.0-mL suspension of 60-nm gold nanoparticles to 8.5 by the addition of 40.0 μL of 50 mM aqueous borate buffer. This step will deprotonate the primary amines of antibodies added later, which facilitates the reaction with the succinimidyl ester of DSNB. Next, an ~8-h incubation with 10.0 μL of 1.0 mM DSNB is carried out. Subsequently, 20 μg of goat anti-*E. coli* O157:H7 was added to the suspension and allowed to react for ~12 h. The subsequent step adds 100.0 μL of 10% (w/v) BSA in 2 mM aqueous borate buffer to block unreacted succinimidyl ester groups. After ~5 h, the suspension was centrifuged at 2000*g* for 10 min to remove supernatant containing unreacted DSNB and antibody. The ERLs were resuspended in 1.0 mL of 2 mM aqueous borate buffer containing 1% (w/v) BSA. This process was repeated two more times, with the final volume for resuspension adjusted to give a final ERL concentration of 5.2×10^{10} particles/mL. Finally, 100.0 μL of 1.5 M NaCl in water was added to bring the final salt concentration to 150 mM in order to mimic physiological conditions, with the suspension then passed through a syringe tip filter (0.22-μm pore size, Costar) to remove aggregates.

Protocol for Quiet Assay. For assays carried out in quiet solution, 20.0-μL aliquots of varied concentrations of heat killed *E. coli*, diluted in PBS, were exposed to capture substrates for 8 h. Next, the substrates were rinsed by three brief immersions in 2 mL of fresh 2 mM aqueous borate buffer with 150 mM NaCl. Finally, 20.0 μL of ERLs was pipetted onto each substrate. Following a 16-h incubation, the rinsing procedure described above was repeated.

Protocol for Jet Assay. Free liquid jet delivery of *E. coli* was performed with 500-μL samples delivered by jet at 10.0 mL/min. Rinsing and quiet exposure of ERLs (16 h) were accomplished as described above for the quiet assay. The jet nozzle, held 3 mm from

the sample surface, was defined by 0.5-mm internal diameter PEEK tubing (Upchurch Scientific) that was attached to the end of a syringe by standard fluidic adapters. As depicted in Figure 1, the jet was directed normal to the substrate surface and the flow was driven by a PHD2000 Programmable syringe pump from Harvard Apparatus.

Instrumentation. (i) SERS Measurements. A NanoRaman I, equipped with a 30 mW, 632.8-nm He-Ne laser, a spectrograph consisting of a modified Czerny-Turner imaging spectrometer with a resolution of 6-8 cm^{-1}, and a thermoelectrically cooled (0 °C) Kodak 0401E CCD, was used to collect all Raman spectra. The laser light, with normal incidence, is focused to a 25-μm diameter spot (2-3 mW) by an objective with a numerical aperture of 0.68. All spectra were collected with an integration time of 1 s.

(ii) Scanning Electron Microscopy (SEM). A Philips FEI XL30 ESEM FEG Environmental scanning electron microscope was used to acquire all SEM images. Prior to imaging, samples were sputter coated with a thin (~100 Å) layer of gold. Images were collected from secondary electrons and an accelerating voltage of ~25 kV was used.

Results and Discussion

Comparison of quiet and jet-based assays. Assays for *E. coli*, performed with quiet solution and free liquid jet incubation, were compared. *E. coli* samples were diluted with PBS from a stock concentration of 10^8 cells/mL to a range of concentrations from 10^3 to 10^7 cells/mL, and mixed by vortexing for ~3 s. The quiet solution assay used 20.0-μL samples, incubated for 8 h. The free liquid jet assay employed 500-μL samples, delivered by jet at 10.0 mL/min for a sample incubation time of 3 s. Labeling for both assays was carried out with quiet solution exposure of ERLs for 16 h. The results from these assays are presented in

Figure 2. Shown in Figure 2A are representative spectra, including the blank, from both the quiet solution and free liquid jet assays. These spectra have features characteristic of the DSNB-derived adlayer on the ERLs, most notably $\nu_s(NO_2)$, at 1336 cm^{-1}. The intensities of $\nu_s(NO_2)$ for the samples from both assays are plotted against the log of the sample concentration in Figure 2B. Concentrations of 10^8, 10^7, 10^6, and 10^5 cells/mL are plotted for the quiet solution assay; lower sample concentrations did not yield SERS intensities distinguishable from the blank. Conversely, the samples of lower concentrations, 10^3, 10^4, 10^5, and 10^6 cells/mL are plotted for the free liquid jet assay as the SERS intensities leveled off for samples with higher concentrations. The error bars represent the standard deviation of five measurements taken at different locations on the substrate surface. The dashed lines represent the LOD, defined by the signal from the blank plus three times its standard deviation.

There are several important observations to note about these results. First, while the two assays have almost the same SERS intensity for the 10^6 cells/mL sample, the overall trends are much different. Moreover, the signal from the jet blank is markedly lower than that of the quiet solution assay (292 cts/s compared to 695 cts/s). As a result of the lower blank signal, the free liquid jet assay has a remarkably low LOD. The LOD for the free liquid jet assay is less than 10 cells/mL while that for the quiet solution assay is 10^5 cells/mL.

This striking difference in LOD is noteworthy, especially when determining a theoretical LOD for each assay condition. If the LOD is defined as the ability to detect the presence of one bacterium in a laser spot, and assuming every bacterium is captured from a sample, the lowest concentration that would ensure interrogation of at least one bacterium by the laser is 7×10^5 cells/mL for a 20.0 μL sample and 3×10^4 cells/mL for a 500 μL sample.

An LOD lower than that of the quiet assay is therefore expected for the free liquid jet assay. However, the LODs for both assays are much lower than predicted.

We hypothesize that the basis for the observed LODs is the detection of shed protein from the *E. coli* cells. We recently reported on an assay for the detection of *Mycobacterium avium* subspecies *paratuberculosis* (MAP), the causative agent of Johne's disease, in which the observed LOD was lower than that for a prediction based on the exhaustive removal of all the microorganisms in a sample.[30] Further experimentation showed that the lower than expected LOD originated from the presence of shed surface protein from MAP. Other recent reports have also detailed the occurrence of protein shedding from bacteria,[31, 32] demonstrating that detachment could be induced by sonication.[32]

The LODs achieved for the free liquid jet assay argue that the presence of shed protein dominates the response at low concentrations. However, the capture of whole bacteria may play a role in the response found at higher sample concentrations. To explore this issue, scanning electron microscopy was used to image both types of capture substrates. Representative results are presented for several different concentrations of *E. coli* by the micrographs exemplified in Figures 4 and 5.

The micrographs for assays for *E. coli* incubation in quiet solution are shown in Figure 4. The SEM images in Figures 4A-D are of separate locations on a capture substrate exposed to 10^8 cells/mL. Figures 4A-C were obtained at 20,000x magnification spanning an area of 25.8 μm^2, which is a factor of 19 less than the area (491 μm^2) irradiated by the focused laser source. Figure 4D, on the other hand used a 5000x magnification, imaging an area of 413 μm^2, which is 18% less than that of the laser spot. *E. coli* microorganisms, characterized by their rod shape and dimensions (~2 μm x 0.8 μm),[33] can be seen in three of

the four images. Much larger numbers of spherically shaped objects, but much smaller, are also evident in all four images. These objects are consistent with the size of the gold nanoparticles which form the cores of the ERLs, noting that there are particles in areas well beyond the footprint of the bacteria. In fact, the arc imaged in Figure 4C contains a large number of ERLs (~250), but is devoid of bacteria. In Figure 4D, which was taken at 5000x, several bacteria, along with large areas populated only by ERLs, are apparent.

A substrate exposed to 10^7 cells/mL produced the four images shown in Figure 4E-4H. Figures 4E and 4F show that bacteria can also be captured at this concentration. The larger area imaged in Figure 4H, however, reveals that while there are fewer bacteria captured at this concentration, there are still a large relative number of ERLs bound to the capture substrate.

Images from the substrate exposed to 10^6 cells/mL are given in Figures 4I and 4J. There are no microorganisms found on the substrate surface at any (>5) of the examined sample locations. Likewise, the images for the substrate exposed to PBS only (blank), shown in Figures 4K and 4L, are also devoid of observable bacteria.

The images for samples exposed to *E. coli* by jet are presented in Figure 5. These images are for substrates exposed to 10^6 cells/mL (5A and 5B), 10^5 cells/mL (5C and 5D), 10^4 cells/mL (5E and 5F), and 0 cells/mL (blank) (5G and 5H). None of these images contain footprints diagnostic of whole bacteria, a result repeated upon scanning more than a 100-μm diameter area on the substrate. The lower than expected LODs for both quiet and jet assays, along with substrate images clearly showing labeling of areas devoid of captured *E. coli*, point to protein shedding as the mechanism resulting in these observations.

To investigate whether our approach to sample handling could induce protein shedding, the free liquid jet assay was repeated by omitting the vortexing step after sample dilution. Instead, the samples were mixed more gently by manual inversion. Thus, 500-μL samples of *E. coli* in PBS, ranging in concentration from 1 cell/mL to 10^6 cells/mL were delivered by free liquid jet at 10.0 mL/min, followed by quiet solution labeling by ERLs for 16 h. The SERS intensities of the $\nu_1(NO_2)$ are plotted against the log of *E. coli* concentration in Figure 3A. There is not a strong predictive trend of SERS intensity with increasing sample concentration, which argues that sample handling plays an important role in the successful capture of *E. coli* delivered by free liquid jet.

The assay for *E. coli* with free liquid jet incubation was conducted a third time with vortexing of the sample. The assay was performed with an extended concentration range of 1 cell/mL to 10^7 cells/mL and the 500-μL samples were vortexed for ~5 s prior to delivery by free liquid jet. These data are presented in Figure 3B, plotted with the results for the first assay employing sample vortexing. As in the first assay in which vortexing was used for sample preparation, the repeated assay resulted in a linear trend with an increase in SERS intensity with increasing sample concentration. Interestingly, the two trends have very similar slopes but have very different levels of non-specific binding (i.e., signals from the blank sample, illustrated by the dashed lines, which represent the signal of the blank plus three times its standard deviation). When the level of non-specific binding is subtracted from the data for each assay, the SERS intensities from the second trial are slightly higher than those of the first trial. While these differences are small, the result is a slightly better LOD of less than 1 cell/mL.

Together, the results from the three assays with free liquid jet delivery of sample, and the micrographs presented in Figures 4 and 5, argue that sample handling (i.e., vortex mixing) causes protein shedding from the *E. coli* cells, and that it is these proteins that are captured and detected in the free liquid jet assays. Additionally, increasing the time of sample vortexing may increase the number of proteins shed by the *E. coli* as the 5-s vortexing used in the second trial resulted in slightly higher SERS intensities than the first trial, which employed 3-s vortexing. We are presently designing experiments to further investigate the relationship between sample handling procedures and the resulting SERS intensities, with the goal of ascertaining whether inducement of protein shedding can be exploited more broadly and quantitatively as a rapid and highly sensitive approach to indirect microorganism detection by increasing the level of shed protein.

Conclusions

The work herein is the first report on the use of free liquid jet sample delivery for the detection of pathogenic bacteria. It relies on the detection of protein shed from the bacteria, rather than by the direct detection of whole cells, which yielded LODs of a few bacteria per 1-mL sample. This enhancement mechanism resulted in an LOD less than 1 cell/mL with a 500-μL sample delivered by free liquid jet for 3 s. While more sample was used than that for an assay employing 8-h quiet solution exposure of 20.0-μL samples (LOD=1.4×10^5 cells/mL), the LOD and sample incubation time were improved by 400,000 and 9600 times, respectively. Thus, a basis for the rapid and extremely low level detection of *E. coli* has been developed. The LODs achieved can potentially accomplish detection at a level of the

infectious dose. We are presently exploring various pathways to harness this new and exciting capability.

Acknowledgements

This work was supported through a grant from CEROS-DARPA and by the Institute for Combinatorial Discovery of Iowa State University. The Ames Laboratory is operated for the US Department of Energy through Iowa State University under contract No.W7405-eng-82. We gratefully acknowledge the use of facilities within the Center for Solid State Science at Arizona State University.

References

(1) Ibekwe, A. M.; Watt, P. M.; Grieve, C. M.; Sharma, V. K.; Lyons, S. R. *Appl. Environ. Microbiol.* **2002**, *68*, 4853-4862.

(2) http://www.cdc.gov/ncidod/dbmd/diseaseinfo/escherichiacoli_g.htm, Centers for Disease Control and Prevention, Atlanta, 2006. Accessed on August 8, 2007.

(3) In *Canada Communicable Disease Report*; Paulson, E., Ed., 2000; Vol. 26, pp 170-173.

(4) Shannon, K. E.; Lee, D. Y.; Trevors, J. T.; Beaudette, L. A. *Sci. Total Environ.* **2007**, *382*, 121-129.

(5) Ercole, C.; Del Gallo, M.; Mosiello, L.; Baccella, S.; Lepidi, A. *Sens. Actuators, B* **2003**, *B91*, 163-168.

(6) Tu, S.-I.; Uknalis, J.; Gehring, A. *J. Rapid Methods and Automation in Microbiol.* **1999**, *7*, 69-79.

(7) Bouvrette, P.; Luong, J. H. T. *Int. J. Food Microbiol.* **1995**, *27*, 129-137.

(8) Wang, L.; Cole, K. D.; Gaigalas, A. K.; Zhang, Y.-Z. *Bioconjugate Chem.* **2005**, *16*, 194-199.

(9) Gehring, A. G.; Albin, D. M.; Irwin, P. L.; Reed, S. A.; Tu, S.-I. *J. Microbiol. Methods* **2006**, *67*, 527-533.

(10) Ibekwe, A. M.; Grieve, C. M. *J. Appl. Microbiol.* **2003**, *94*, 421-431.

(11) Imamura, O.; Arakawa, H.; Maeda, M. *Luminescence* **2003**, *18*, 107-112.

(12) Jinneman, K. C.; Yoshitomi, K. J.; Weagant, S. D. *Appl. Environ. Microbiol.* **2003**, *69*, 6327-6333.

(13) Klerks, M. M.; Zijlstra, C.; van Bruggen, A. H. C. *J. Microbiol. Methods* **2004**, *59*, 337-349.

(14) Mothershed, E. A.; Whitney, A. M. *Clin. Chim. Acta* **2006**, *363*, 206-220.

(15) Uhlenkamp, J. M.; Lipert, R. J.; Granger, M. C.; Porter, M. D. *Manuscript in preparation.*

(16) Uhlenkamp, J. M.; Lipert, R. J.; Porter, M. D. *Manuscript in preparation.*

(17) Uhlenkamp, J. M.; Porter, M. D. *Manuscript in preparation.*

(18) Baonga, J. B.; Louahlia-Gualous, H.; Imbert, M. *Appl. Therm. Eng.* **2006**, *26*, 1125-1138.

(19) Fabbri, M.; Dhir, V. K. *J. Heat Transfer* **2005**, *127*, 760-769.

(20) Incropera, F. P. *Liquid Cooling of Electronic Devices By Single-Phase Convection*; John Wiley and Sons, Inc.: New York, 1999.

(21) Lienhard, J. H. V. *Annu. Rev. Heat Transfer* **1995**, *6*, 199-270.

(22) Gunasingham, H.; Fleet, B. *Anal. Chem.* **1983**, *55*, 1409-1414.

(23) Huang, Y. L.; Khoo, S. B.; Yap, M. G. *Am. Biotechnol. Lab.* **1993**, *11*, 18-20.

(24) Laevers, P.; Hubin, A.; Terryn, H.; Vereecken, J. *J. Appl. Electrochem.* **1995**, *25*, 1017-1022.

(25) Chen, C. S.; Mrksich, M.; Huang, S.; Whitesides, G. M.; Ingber, D. E. *Biotech. Prog.* **1998**, *14*, 356-363.

(26) Kumar, A.; Whitesides, G. M. *Appl. Phys. Lett.* **1993**, *63*, 2002-2004.

(27) Libioulle, L.; Bietsch, A.; Schmid, H.; Michel, B.; Delamarche, E. *Langmuir* **1999**, *15*, 300-304.

(28) Grubisha, D. S.; Lipert, R. J.; Park, H.-Y.; Driskell, J.; Porter, M. D. *Anal. Chem.* **2003**, *75*, 5936-5943.

(29) Ni, J.; Lipert, R. J.; Dawson, G. B.; Porter, M. D. *Anal. Chem.* **1999**, *71*, 4903-4908.

(30) Yakes, B. J., Iowa State University, Ames, IA, 2007.

(31) Rhoades, E.; Hsu, F. F.; Torrelles, J. B.; Turk, J.; Chatterjee, D.; Russell, D. G. *Mol. Microbiol.* **2003**, *48*, 875-888.

(32) Speer, C. A.; Scott, M. C.; Bannantine, J. P.; Waters, W. R.; Mori, Y.; Whitlock, R. H.; Eda, S. *Clin. Vaccine Immunol.* **2006**, *13*, 535-540.

(33) Berg, H. C. *E. Coli in Motion*; Springer: New York, 2004.

Figure Captions

Figure 1. Schematic of a free liquid jet depicting the hydrodynamic properties of the jet and resulting stagnation and boundary layer regions. Adapted from reference 20.

Figure 2. (A) Representative spectra (offset for clarity) of several *E. coli* concentrations for assays with quiet solution incubation (top three spectra) and free liquid jet delivery (bottom three spectra). (B) Dose response curves for *E. coli* assays using the intensity of $\nu_s(NO_2)$. Assay with quiet solution incubation used 20.0-μL samples and 8-h incubations. Free liquid jet delivery was accomplished with 500-μL samples delivered at 10.0 mL/min for 3 s. Labeling was carried out with 16-h exposure of 20.0 μL of ERLs for 16 h in both cases. Error bars are the standard deviation of five measurements made at different locations on the substrate. The dashed lines represent the LOD defined by the signal of the blank plus three times its standard deviation.

Figure 3. (A) Dose-response curve for an *E. coli* assay performed without vortexing for mixing of samples. (B) Dose-response curve of a second trial of the free liquid jet assay for *E. coli* (500-μL samples delivered at 10.0 mL/min) using sample vortexing, plotted with the data from Figure 2B.

Figure 4. Sample scanning electron micrographs for *E. coli* assay using quiet solution sample and label incubation. (A-C) 10^8 cells/mL, 20,000x magnification; (D) 10^8 cells/mL, 5000x magnification; (E-G) 10^7 cells/mL, 20,000x magnification; (H) 10^7 cells/mL, 5000x

magnification; (I) 10^6 cells/mL, 20,000x magnification; (J) 10^6 cells/mL, 5000x magnification; (K) Blank, 20,000x magnification; (L) Blank, 5000x magnification.

Figure 5. Sample scanning electron micrographs for *E. coli* assay with sample delivery by free liquid jet and quiet solution label incubation. (A) 10^6 cells/mL, 20,000x magnification; (B) 10^6 cells/mL, 5000x magnification; (C) 10^5 cells/mL, 20,000x magnification; (D) 10^5 cells/mL, 5000x magnification; (E) 10^4 cells/mL, 20,000x magnification; (F) 10^4 cells/mL, 5000x magnification; (G) Blank, 20,000x magnification; (H) Blank, 5000x magnification.

Table 1. Values of SERS intensity per ERL for quiet solution and free liquid jet samples. Number of ERLs per laser spot calculated by enumerating ERLs in five images (20,000x; 25.80 μm^2) and extrapolating to laser spot size (490.87 μm^2).

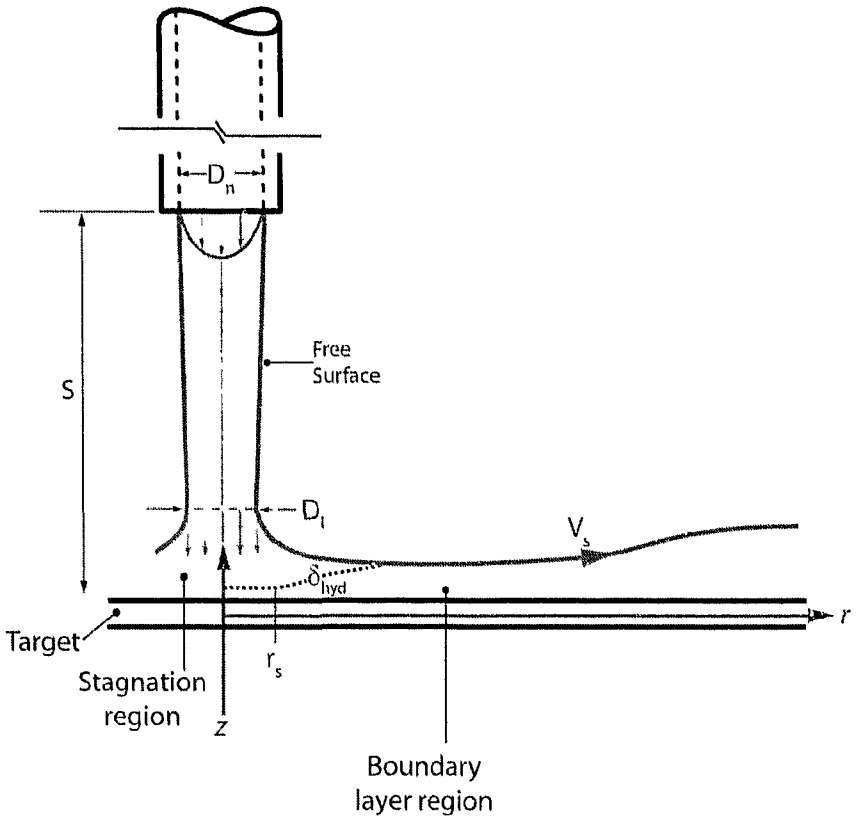
D_n
S
Free
Surface
D_j
V_s
δ_hyd
r
Target
Stagnation
region
r_s
z
Boundary
layer region

Figure 1

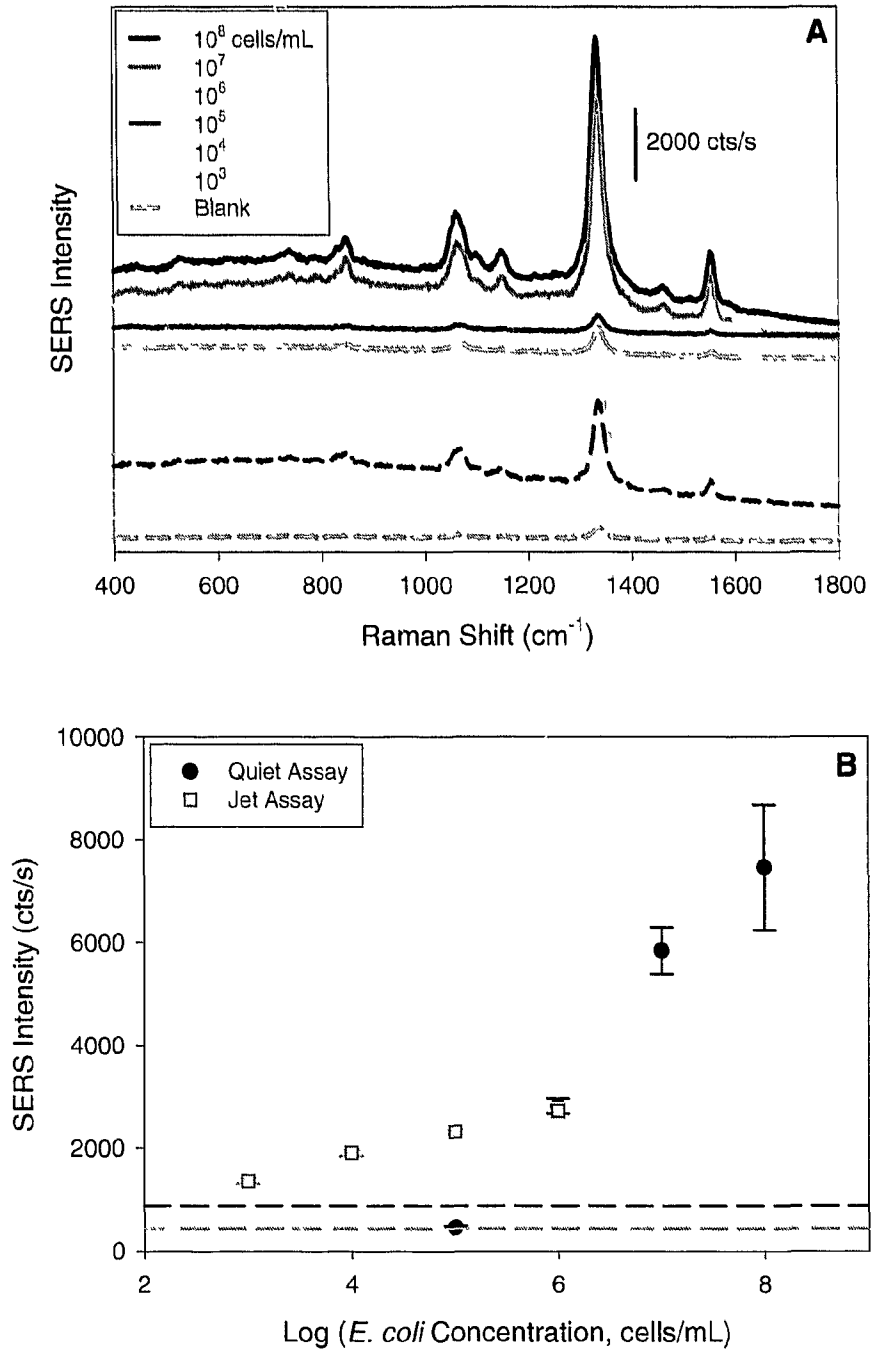
A
10^8 cells/mL
10^7
10^6
10^5
10^4
10^3
Blank
2000 cts/s
SERS Intensity
400
600
800
1000
1200
1400
1600
1800
Raman Shift (cm^{-1})
B
Quiet Assay
Jet Assay
SERS Intensity (cts/s)
10000
8000
6000
4000
2000
0
2
4
6
8
Log (*E. coli* Concentration, cells/mL)

Figure 2

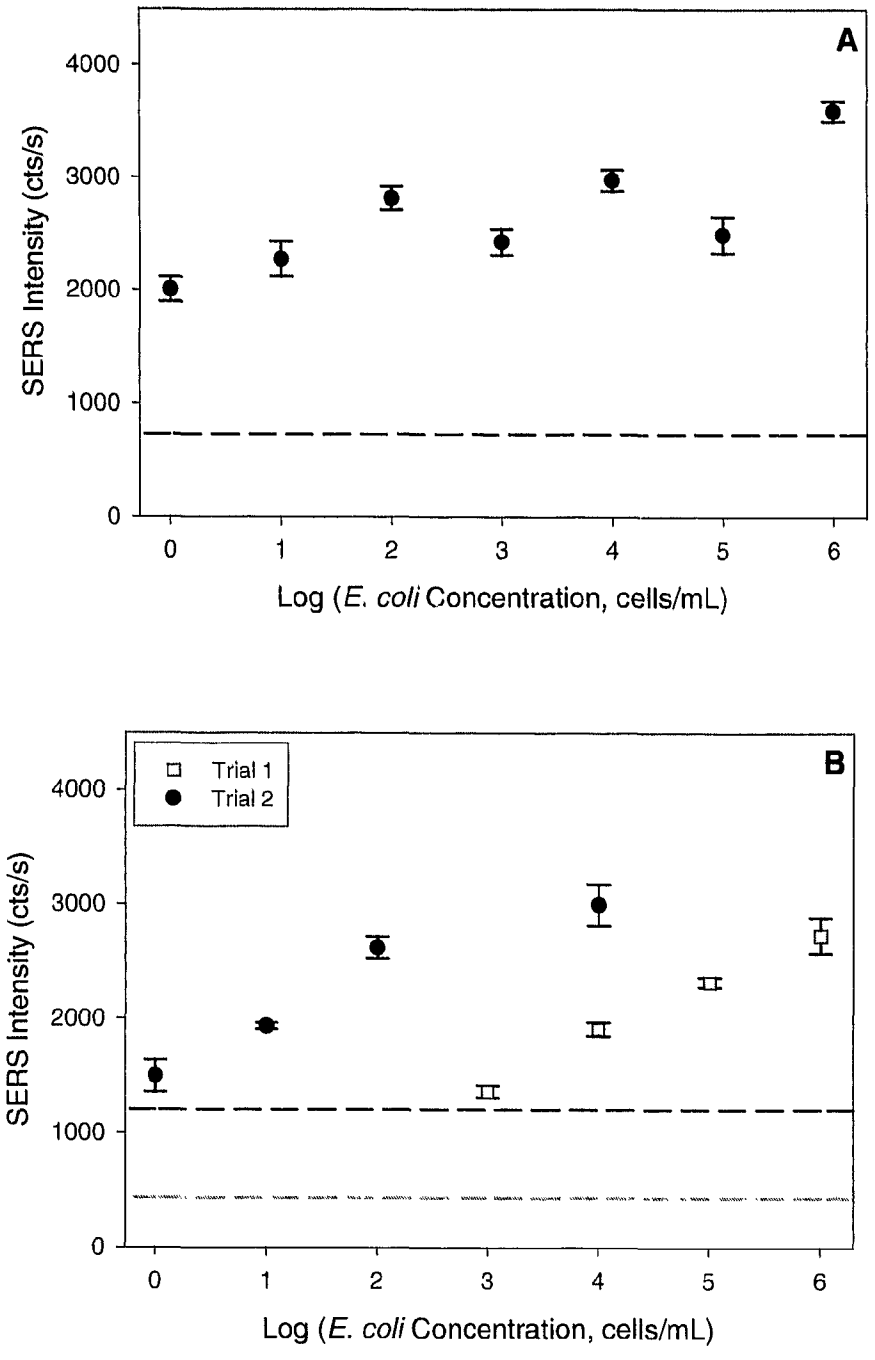
A
SERS Intensity (cts/s)
4000
3000
2000
1000
0
0
1
2
3
4
5
6
Log (E. coli Concentration, cells/mL)
B
Trial 1
Trial 2
SERS Intensity (cts/s)
4000
3000
2000
1000
0
0
1
2
3
4
5
6
Log (E. coli Concentration, cells/mL)

Figure 3

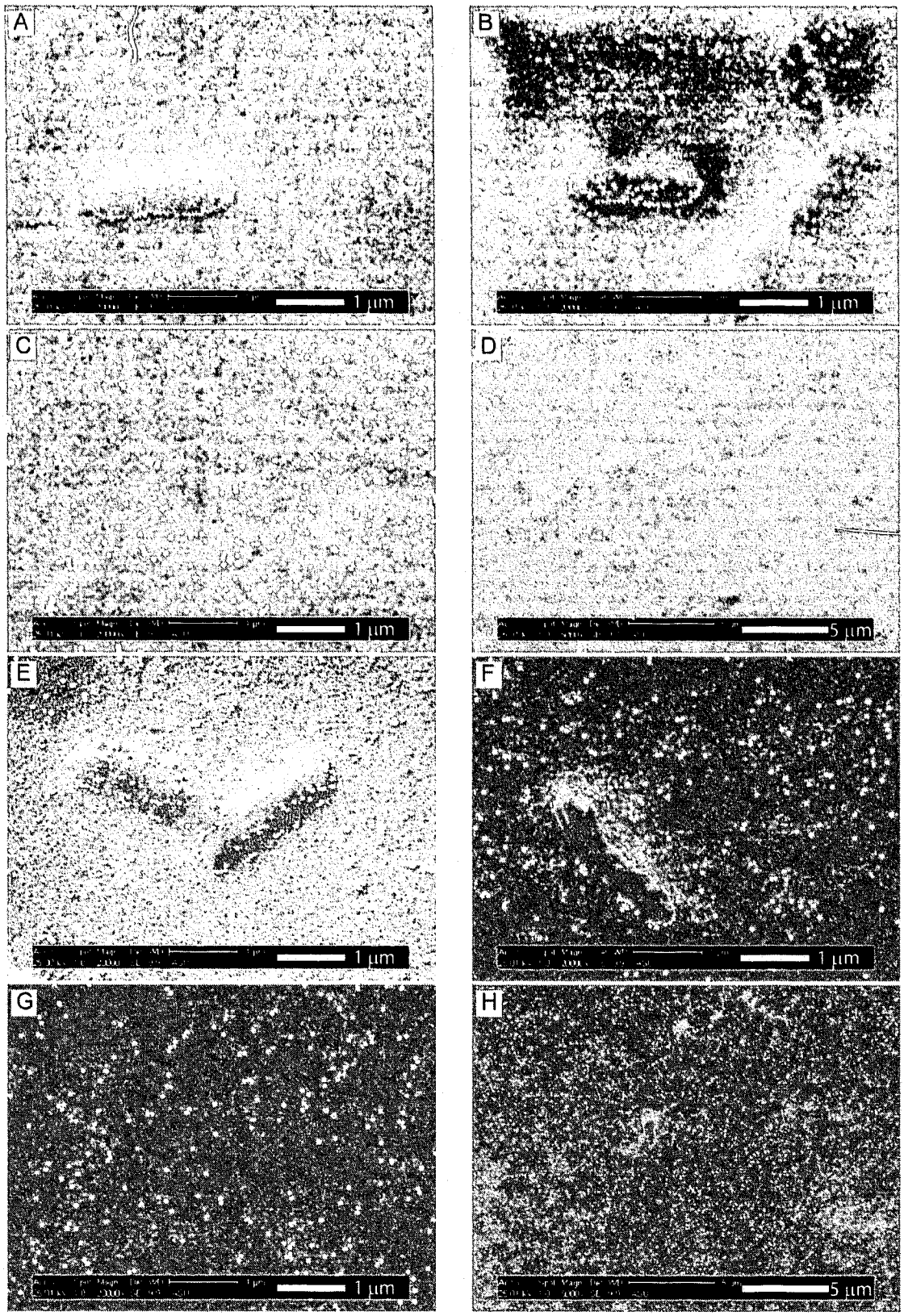

Figure 4 (continued next page)

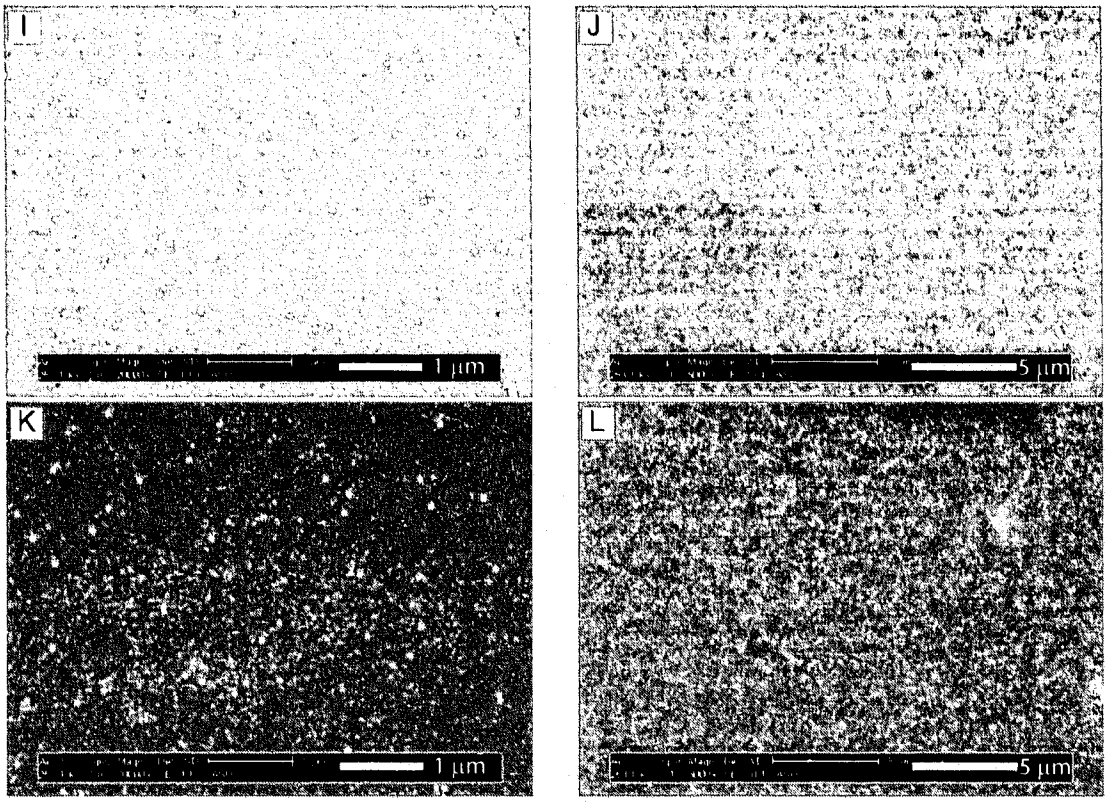

Figure 4 (continued from previous page)

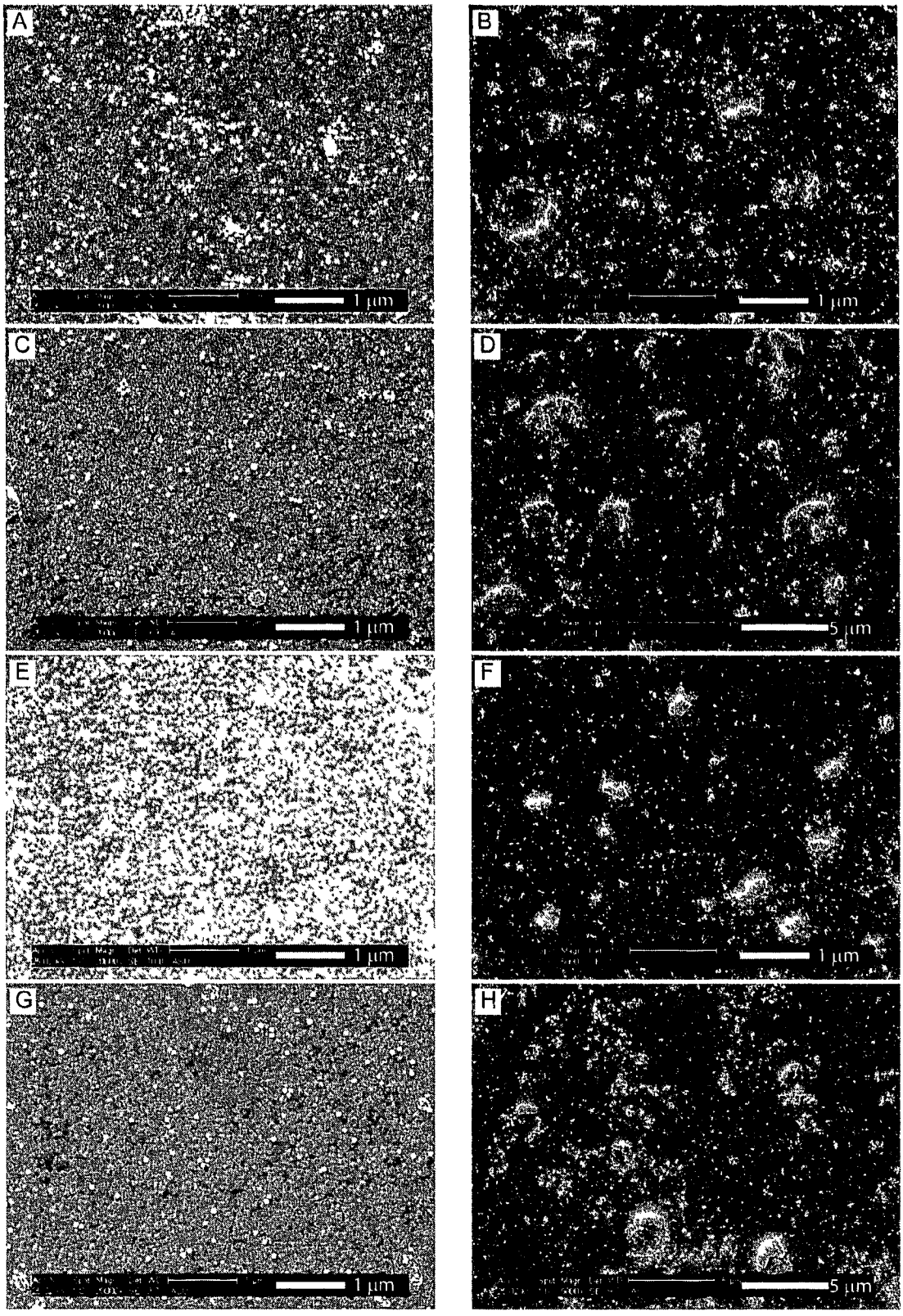

Figure 5

Supplemental Information

Evaluation of SEM images. The ERLs in each scanning electron micrograph were enumerated to ascertain the SERS intensity per bound ERL. Five images from different locations on the substrate were collected for quiet solution assay samples with concentrations of 10^8, 10^7, 10^6, and 0 cells/mL; and for free liquid jet assay samples with concentrations of 10^6, 10^5, 10^4, and 0 cells/mL. The average number of particles per imaged area (25.80 μm^2) was extrapolated to the area interrogated by the laser upon collection of SERS spectra (490.87 m2). These data, along with the average SERS intensity from five locations on the substrate, are presented in Table S1 and were used to calculate the SERS intensity per particle.

There are several noteworthy observations from these data. The first is that the SERS intensity per particle varies between and within the quiet solution and free liquid jet experiments. The substrates for which *E. coli* was incubated in quiet solution have more surface-bound ERLs than the substrates for which free liquid jet was used for *E. coli* delivery. This result is expected as it follows the data for SERS intensity. The intensity per particle within the two experiment types varies as well. This number differs more within the quiet solution data than the free liquid jet data. The intensity per particle for the free liquid jet assay is very similar for all samples except the blank, which is about five times below that of the other samples. The intensity per particle for the blank is also lower than the other samples in the quiet solution set, however the other vary to a greater extent than those with jet delivery.

This inconsistency in the samples with non-zero concentrations could be attributable to an imaging artifact. The initial aim in collecting these images was to determine whether intact bacteria are captured from the samples. Because of this, it is highly likely that these images are fully representative because captured *E. coli* tend to be more heavily labeled with ERLs than the surrounding substrate. In fact, when images taken with lower magnification (i.e., 5000x) of the substrates that were exposed to 10^8 and 10^7 cells/mL are enumerated, the intensities per particle at the two substrates are much closer in value to that for the substrate incubated with 10^6 cells/mL. The values for intensity per particle then become 2.15, 1.97, and 2.14 counts/s/particle for the 10^6, 10^7, and 10^8 cells/mL samples, respectively.

In both sets of assays, however, the difference in intensity per ERL between the blanks and the other samples remains. We suspect that this may be due to the presence of nonspecifically bound, non-active ERLs. That is, there may be a higher propensity for ERLs that were not fully coated with DSNB and antibody to non-specifically interact with the substrate surface in the absence of captured antigen. These "poorly" labeled ERLs would then be counted in the SEM images but would not contribute, or would contribute to a lesser degree, to the measured SERS intensity. Further studies are needed to support this hypothesis.

E. coli Incubation Method	Sample Concentration (cells/mL)	SERS Intensity (cts/s)	# ERLs per image (ERLs)	# ERLs per laser spot (ERLs)	Intensity per ERL (cts/s/ERL)
Quiet	10^8	7456 (±1223)	347 (±58)	6606 (±1101)	1.13
	10^7	5835 (±455)	210 (±9)	3995 (±179)	1.46
	10^6	2815 (±149)	69 (±9)	1308 (±179)	2.15
	Blank	695 (±59)	45 (±7)	856 (±128)	0.81
Jet	10^6	2727 (±157)	169 (±11)	3219 (±212)	0.85
	10^5	2319 (±44)	148 (±8)	2820 (±148)	0.82
	10^4	1909 (±59)	116 (±7)	2213 (±130)	0.86
	Blank	292 (±46)	94 (±14)	1796 (±260)	0.16

Table S1

CHAPTER 6: CONCLUSIONS

This dissertation investigated the use of free liquid jets for sample and label delivery in immunoassays, the main goal of which was to achieve rapid incubations. Chapter 2 began the work towards this goal through the development of a protocol for free liquid jet sample and label incubations. This was accomplished with the use of IgG and fluorescently-tagged anti-IgG. The effect of sample volume and label concentration on assay performance was studied and a comparison was made between assays employing quiet solution and free liquid jet incubations. While the signals obtained with the free liquid jet assay were lower than those from quiet solution samples, an extremely low blank signal was achieved and thus, a comparable limit of detection (LOD). The LODs for the quiet and free liquid jet assays were 400 and 330 pM, respectively. Additionally, while a larger sample was used for the jet experiment, incubation times for both sample and label were decreased from the 12-h steps used in the quiet assay to just 3 s each. This dramatic result achieved the goal set forth with respect to implementation of a free liquid jet. A qualitative look at the theoretical accumulation of antigen and label was also completed and begins to explain the basis for the signals observed with quiet and jet assays.

Sensitive assays with surface-enhanced Raman scattering (SERS) readout have been previously described by our laboratory. Thus, Chapter 3 extended free liquid jet assay incubations with SERS-based readout for the detection of IgG and ovalbumin, a biowarfare agent simulant. While effective delivery of SERS-based labels (modified gold nanoparticles) by jet was not immediately realized, an alternative means to decrease labeling time was

accomplished via concentrated labels. In this way, an assay for ovalbumin was performed in under 40 min with a LOD of 790 pM. Ovalbumin was also detected in a complex matrix (i.e., milk) with a lower LOD of 280 pM.

Chapter 4 furthered free liquid jet capabilities to assays for porcine parvovirus (PPV). This virus was detected with SERS readout with an LOD of 4×10^5 $TCID_{50}$/mL, which was lower than that of a quiet solution assay at 2×10^7 $TCID_{50}$/mL. This chapter also examined the use of smaller sized nanoparticles for the construction of SERS-based labels, which were used to label captured IgG by jet.

Finally, Chapter 5 focused on the detection of pathogenic bacteria, namely *E. coli* O157:H7. When a free liquid jet and quiet solution assay were compared, the LODs, while very different, were both lower than that theoretically expected. The basis for this observation was investigated using scanning electron microscopy (SEM), which argued for an enhancement mechanism by way of the detection of protein shed from the surface of bacteria. Sample handling procedures further supported this finding. In this way, free liquid jet incubation resulted in the indirect detection of *E. coli* O157:H7 with an LOD of less than 1 cell/mL.